



National Library
of Canada

Acquisitions and
Bibliographic Services Branch

395 Wellington Street
Ottawa, Ontario
K1A 0N4

Bibliothèque nationale
du Canada

Direction des acquisitions et
des services bibliographiques

395, rue Wellington
Ottawa (Ontario)
K1A 0N4

Your file: *Voire référence*

Our file: *Notre référence*

NOTICE

The quality of this microform is heavily dependent upon the quality of the original thesis submitted for microfilming. Every effort has been made to ensure the highest quality of reproduction possible.

If pages are missing, contact the university which granted the degree.

Some pages may have indistinct print especially if the original pages were typed with a poor typewriter ribbon or if the university sent us an inferior photocopy.

Reproduction in full or in part of this microform is governed by the Canadian Copyright Act, R.S.C. 1970, c. C-30, and subsequent amendments.

AVIS

La qualité de cette microforme dépend grandement de la qualité de la thèse soumise au microfilmage. Nous avons tout fait pour assurer une qualité supérieure de reproduction.

S'il manque des pages, veuillez communiquer avec l'université qui a conféré le grade.

La qualité d'impression de certaines pages peut laisser à désirer, surtout si les pages originales ont été dactylographiées à l'aide d'un ruban usé ou si l'université nous a fait parvenir une photocopie de qualité inférieure.

La reproduction, même partielle, de cette microforme est soumise à la Loi canadienne sur le droit d'auteur, SRC 1970, c. C-30, et ses amendements subséquents.

University of Alberta

**A Study of Nocturnal Drainage Flows in Relation to
Woodsmoke Pollution in a Valley**

by

Brian J. Wiens



**A thesis submitted to the Faculty of Graduate Studies and Research in partial
requirement for the degree of Master of Science.**

Department of Earth and Atmospheric Sciences

**Edmonton, Alberta
Fall 1995**



National Library
of Canada

Acquisitions and
Bibliographic Services Branch

395 Wellington Street
Ottawa, Ontario
K1A 0N4

Bibliothèque nationale
du Canada

Direction des acquisitions et
des services bibliographiques

395, rue Wellington
Ottawa (Ontario)
K1A 0N4

Your file Votre référence

Our file Notre référence

**THE AUTHOR HAS GRANTED AN
IRREVOCABLE NON-EXCLUSIVE
LICENCE ALLOWING THE NATIONAL
LIBRARY OF CANADA TO
REPRODUCE, LOAN, DISTRIBUTE OR
SELL COPIES OF HIS/HER THESIS BY
ANY MEANS AND IN ANY FORM OR
FORMAT, MAKING THIS THESIS
AVAILABLE TO INTERESTED
PERSONS.**

**L'AUTEUR A ACCORDE UNE LICENCE
IRREVOCABLE ET NON EXCLUSIVE
PERMETTANT A LA BIBLIOTHEQUE
NATIONALE DU CANADA D'E
REPRODUIRE, PRETER, DISTRIBUER
OU VENDRE DES COPIES DE SA
THESE DE QUELQUE MANIERE ET
SOUS QUELQUE FORME QUE CE SOIT
POUR METTRE DES EXEMPLAIRES DE
CETTE THESE A LA DISPOSITION DES
PERSONNE INTERESSEES.**

**THE AUTHOR RETAINS OWNERSHIP
OF THE COPYRIGHT IN HIS/HER
THESIS. NEITHER THE THESIS NOR
SUBSTANTIAL EXTRACTS FROM IT
MAY BE PRINTED OR OTHERWISE
REPRODUCED WITHOUT HIS/HER
PERMISSION.**

**L'AUTEUR CONSERVE LA PROPRIETE
DU DROIT D'AUTEUR QUI PROTEGE
SA THESE. NI LA THESE NI DES
EXTRAITS SUBSTANTIELS DE CELLE-
CI NE DOIVENT ETRE IMPRIMES OU
AUTREMENT REPRODUITS SANS SON
AUTORISATION.**

ISBN 0-612-06555-3

Canada

University of Alberta

Library Release Form

Name of Author: Brian J. Wiens

Title of Thesis: **A Study of Nocturnal Drainage Flows in Relation to
Woodsmoke Pollution in a Valley**

Degree: Master of Science

Year this Degree Granted: 1995

Permission is hereby granted to the University of Alberta Library to reproduce single copies of this thesis and to lend or sell such copies for private, scholarly, or scientific purposes only.

The author reserves all other publication and other rights in association with the copyright in the thesis, and except as hereinbefore provided, neither the thesis nor any substantial portion thereof may be printed or otherwise reproduced in any material from whatever without the author's prior written permission.

A handwritten signature in black ink, appearing to read 'Brian J. Wiens', is written over a horizontal line.

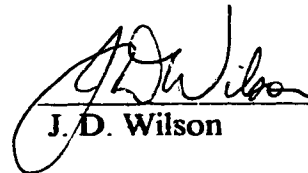
Brian J. Wiens
3615-117A Street
Edmonton, Alberta
T6J 1V3

31 July 1995

University of Alberta

Faculty of Graduate Studies and Research

The undersigned certify that they have read, and recommend to the faculty of Graduate Studies and Research for acceptance, a thesis entitled "A Study of Nocturnal Drainage Flows in Relation to Woodsmoke Pollution in a Valley" by Brian J. Wiens in partial fulfilment of the requirements for the degree of Master of Science.



J. D. Wilson



E. P. Lozowski



D. P. Wiens

June 1995

Abstract

The river valley at Whitehorse frequently experiences elevated levels of total suspended particulate from wintertime wood burning. We infer the dominant influence on wood smoke pollution is dispersion by wind and turbulence and focus our investigation on small scale nocturnal flow in a valley.

We survey observations and numerical investigations of drainage flows and attempt to form some discriminators between flow regimes. This serves as background for two nocturnal simulations with the Mesoscale Community Compressible Model (MC2).

We conclude that since drainage flows are frequently of substantial force and scale, they are quite effective for pollutant dispersion. This implies that conditions which are ideal for drainage flows (i.e. clear skies, light winds and a dry atmosphere) need not coincide with conditions that lead to the highest accumulation of airborne pollutants in a valley. We tentatively propose, that the highest pollution levels will develop in a valley when a light synoptic flow occurs in conjunction with conditions that inhibit drainage flow.

Acknowledgement

Special thanks to my wife, Kelly, and my three children, Alexander, Jocelyn and Amelia who have lovingly supported me through my course of studies. They patiently endured a husband and father who has spent countless hours physically cloistered with computers and books, and mentally sequestered for many of the remaining hours of the past two years.

Thanks to my thesis advisor, J. D. Wilson, for his expertise and commitment to science. His guidance and knowledge helped shape and focus my course of study. His attention to scientific detail remains a model for me.

Thanks also to Environment Canada who provided a leave of absence and funding for this period of studies. Special thanks to the Arctic Weather Centre for use of computing equipment and to Ron Goodson for his hours setting up and maintaining my computer resources.

And finally, thanks to Pierre-Jean Robiquet, whose contributions to science were frequently crucial to my completion of this task.

1 Introduction	
1.1 Motivation	
1.2 Wood Smoke	2
1.2.1 History at Whitehorse	2
1.2.2 Wood burning	4
1.2.3 Health Impacts	4
1.2.4 Other locations.	5
1.3 Climate and Geographical Regime at Whitehorse	6
1.4 Combustion Characteristics	11
1.5 Regression Analysis of TSP in Riverdale	13
1.6 Present Strategy	14
1.7 Implications	15
1.8 Methodology of this Study	16
2 Mathematical Flow Description	18
2.1 Forces Acting on a Fluid Element	18
2.1.1 Shear and Normal Forces - Stresses and Strains	19
2.1.2 Newton's Second Law	20
2.1.3 Continuum Hypothesis	21
2.1.4 The Problem of Closure	22
2.1.5 Reynolds Averaging	22
2.2 Closure Schemes	25
2.2.1 First Order Closure or K theory	25
2.2.2 E- Theory: One and a half order Closure	26
2.2.3 Higher Order Closure	27
2.3 Casting the Equations into a Rotating Frame of Reference	27
2.4 Introducing Topographic Information into the Equations	29
2.4.1 Pressure Ratio as the Vertical Co-ordinate	30
2.4.2 Transformed Height Co-ordinates	31
2.4.3 Implications of the Transformation	31
2.5 Conclusions	32
3 General Valley Flows	33
3.1 Definition of Valley Shape Parameters	33
3.2 Conceptual Model of Nocturnal Valley Flows	35
3.3 Observations of Drainage Flows	38
3.3.1 Case of a Uniform Sloping Plain	38

3.3.2	Valley Winds	39
3.3.3	Laboratory Models of Flows Across Valley	41
3.4	Interaction of Valley Winds with Large Scale Flows	42
3.4.1	Large Scale Pressure Gradient/Wind	42
3.4.2	Stratification / Gravity Waves	43
3.4.3	Shear Interactions with the Large-Scale Wind	44
3.4.4	Clouds and Moisture Profile	45
3.5	Interactions Between the Valley and Adjacent Geography	46
3.5.1	Downstream Blocking	46
3.6	Local Forcing Within the Valley	46
3.6.1	Radiational Variation along the Valley	46
3.6.2	Sidewall and Tributary Contributions	48
3.7	Conclusions	49
4	Exploratory Dimensional Analysis of Nocturnal Drainage Flows (2D Symmetry)	51
4.1	Dimensional Analysis of Buoyancy Flows	53
4.1.1	One-Dimensional Treatment	53
4.1.2	Buoyant Interactions with Large-Scale Wind	54
4.2	Shear Interactions with the Large-Scale Wind	58
4.3	Radiational Influences on Drainage Flows	62
4.4	Conclusions	64
5	Numerical Modelling	65
5.1	Mass-Consistent Models of Flow in Complex Terrain	65
5.2	Two-Dimensional Models	66
5.3	Three-Dimensional Valley Flow Models	69
5.4	Conclusions	73
6	Numerical Experiments	75
6.1	Numerical Experimental Method	75
6.2	Overview of the Mesoscale Compressible Community Model (MC2)	77
6.2.1	Model Equations and Co-ordinates	77
6.2.2	Pre-processor Module	79
6.2.3	Integration Module	79
6.2.4	Model Physics	80
6.2.5	Nesting and Boundary Conditions	82
6.2.6	Post-Processing of Data	84

6.2.7 Summary	84
6.3 Drainage Flow Experiments	85
6.3.1 Idealised Atmosphere	85
6.3.2 Development of a Nocturnal Boundary Layer over a Flat Plain	88
6.3.3 Development of a Nocturnal Boundary Layer with MC2	91
6.3.4 Development of the Nocturnal Boundary Layer in a Valley with MC2	97
6.4 Conclusions	112
7 Conclusion	114
7.1 Goals of the Study	114
7.2 Original Hypothesis	114
7.3 Summary of Nocturnal Evolution	114
7.4 Implications of Nocturnal Evolution	115
7.5 Directions for Further Investigation	116
7.6 Revised Hypothesis	117
7.7 Summary	117
Bibliography	118

List of Tables

1.1 Emission from typical residential combustion	10
1.2 Calculated annual emissions for Riverdale.	10
2.1 Scale analysis of terms in geostrophic equations	28
4.1 Summary of variables and discriminators for drainage flow	64
6.1 Summary of boundary values for idealised atmosphere	87
6.2 Summary of initial variables and dimensionless parameters for MC2 over sinusoidal valley	98

List of Figures

1.1 Typical equivalent size distribution for woodsmoke particulate	3
1.2 Topographical map of Whitehorse	8
2.1 Top face of fluid element	19
2.2 Sigma co-ordinates	29
2.3 Gal-chen co-ordinates	30
3.1 Fundamental valley dimensions	33
3.2 Representation of two-dimensional Topographic Amplification Factor	34
3.3 Evening drainage pattern (after Defant 1949)	35
3.4 Late evening drainage pattern (after Defant 1949)	36
3.5 Drainage flow decreases on slopes (after Defant 1949)	37
3.6 Drainage flows on exposed slope (after Preston-Whyte and Tyson 1972)	38
3.7 Calculated and observed wind profiles in a valley (after Defant 1949)	39
4.1 Four idealised extremes of nocturnal valley flow	51
4.2 One-dimensional buoyancy	52
4.3 Possible gravity wave flow regimes	55
4.4 Influences on buoyant interaction between a valley and external flow	56
4.5 Possible gravity wave flow trajectories	58
4.6 Principal influences on shear interaction between a valley and external flow	59
4.7 Shear ratio for varying openness of a valley	60
4.8 Shear ratio for varying wind speed across a valley	61
6.1 Weighting function for boundary nesting	83
6.2 Temperature profile for idealised atmosphere	85
6.3 Profiles of potential temperature (after Delage 1974)	89

6.4 Wind structure (after Delage 1974)	89
6.5 Vertical profiles of Turbulent Kinetic Energy (TKE) (after Delage 1974)	90
6.6 Evolution of potential temperature over flat plain from MC2	92
6.7 Spatially averaged wind profiles over flat plain from MC2	93
6.8 Sub-grid TKE over flat plain from MC2	94
6.9 Spatially resolved TKE over flat plain from MC2	95
6.10 Net surface IR radiation over valley from MC2 at one hour	99
6.11 Mean sea level pressure over valley from MC2 at four hours	100
6.12 Anemometer height wind field over valley from MC2 at four hours	101
6.13 Winds at first calculation level over valley from MC2 at four hours	102
6.14 Vertical profile of U at West ridge from MC2 at four hours	103
6.15 Vertical profile of I on West slope (elevation 1800 metres) from MC2	103
6.16 Vertical profile of U on West slope (elevation 1200 metres) from MC2	104
6.17 Vertical profile of U on West slope (elevation 600 metres) from MC2	104
6.18 Vertical profile of U at valley centre from MC2	105
6.19 Vertical profile of U on East slope (elevation 1200 metres) from MC2	105
6.20 Vertical profile of U on East slope (elevation 1800 metres) from MC2	106
6.21 Vertical profile of V in the southern valley centre from MC2	107
6.22 Vertical profile of V in the northern valley centre from MC2	107
6.23 Cross section through valley of V from MC2	108
6.24 Profile of temperature on West slope from MC2	110
6.25 Profile of temperature at valley centre from MC2	110
6.26 Profile of temperature on East slope from MC2	111

Variable List

f	Horizontal coriolis parameter	$2\Omega \sin \varphi$	1/s
	Vertical coriolis parameter	$2\Omega \cos \varphi$	1/s
g	Acceleration of gravity		m/s ²
l	Turbulent length scale/ mixing length		m
m	Map scale factor for polar stereo graphic	$\left(\frac{1+\sin \varphi_0}{1+\sin \varphi}\right)$	-
q	Pressure ratio	$\left(\ln \left(\frac{p}{p_0}\right)\right)$	-
t	Time		s
u _*	Friction velocity		m/s
z	Vertical coordinate perpendicular to X and Y		m
z ₀	Roughness length		m
A	Area of a valley cross-section		m ²
B	Moisture Sinks		kg/s
C	Liquid Water Content		kg/kg
C _p	Specific heat of air at constant pressure		J/kgK
D	Ridge to valley floor depth		m
E	Sources of Moisture		kg/s
F _R	Froude Number	$\frac{U}{NL}$	-
F _{X,Y,Z}	Sources or Sinks of momentum		m/s ²
H _s	Sensible Heat Flux		W/m ²
K	Eddy Viscosity		m ² /s
K _E	Specific pseudo kinetic energy	$\frac{U^2+I^2}{2}$	m ² /s ²
L	Heat Sources or Sinks		J/s
M	Humidity		%
N	Brunt-Vaisala Frequency	$\sqrt{\frac{g}{\theta} \frac{\partial \theta}{\partial z}}$	1/s
O	Openness Paramater	$\frac{W_V}{D}$	-
Q	Heat (subscript denotes source)		J
R	Gas Constant for dry air		J/kgK
Ri	Richardson Number		-

S	Metric projection term		m²
T	Temperature		°K or °C
U	Horizontal Mean Wind in the X direction		m/s
U_s	Slope Flow		m/s
V	Horizontal Mean Wind in the Y direction		m/s
W	Vertical velocity in transformed co-ordinate		m/s
W_R	Ridge cross-sectional width		m
W_V	Ridgetop valley width		m
X	Horizontal x coordinate in polar stereographic projection		m
Y	Horizontal y coordinate in polar stereographic projection		m
Z	Transformed vertical coordinate		m
α	Ratio for exponent in potential temperature equation	$\frac{R}{C_p}$	-
γ	Lapse rate	$\frac{\Delta T}{\Delta z}$	K/m
ε	TKE dissipation rate		m²/s³
η	Kolmogorov length scale	$\left(\frac{v^3}{\epsilon}\right)^{\frac{1}{4}}$	metres
ν	kinematic viscosity		m²/s
σ_ψ	Standard deviation for a variable ψ		[ψ]
φ	Geographical Latitude		degrees
φ_ψ	Stability Function for ψ		-
ψ	Generic variable of the flow		

1

Introduction

"Learn by trying to understand simple things - always honestly and directly. What keeps the clouds up ... Then when you have learned what an explanation really is, you can go on to more subtle questions" (Richard Feynman)

1.1 Motivation

This study is motivated by a desire to better understand wintertime conditions of light wind and limited vertical mixing in the river valley at Whitehorse, which frequently cause high levels of particulate woodsmoke pollution. Concentration of any pollutant is controlled by its rate of emission, transforming reactions, and physical dispersion by wind and turbulence. Woodsmoke is chemically non-reactive over the span of several days and is emitted at similar rates at Whitehorse for varying dispersion conditions. Therefore, concentration of woodsmoke pollution at Whitehorse is principally controlled by dispersion, which can be described if a wind and turbulence field can be defined. This reduces the core of the pollution question to a small scale flow problem. A reliable determination of wind and turbulence in the valley, in combination with given rates of emissions, will permit calculation of pollutant concentration.

A valley flow is influenced by external pressure gradients, large scale atmospheric stratification, turbulent shear stress imposed by the overlying flow, and gradients of pressure and temperature within and outside the valley driven by differential radiational cooling or warming. At Whitehorse there is a broad valley with complex variations of terrain and cover, that yields a flow highly variable in

both time and space. This suggests a simplified version of conditions at Whitehorse be examined, to begin to isolate causes and effects.

1.2 Wood Smoke

"It was icy cold, but the hot sweat rolled down my cheeks,
and I don't know why;
And the greasy smoke in an inky cloak went streaking down
the sky."

(Cremation of Sam McGee - Robert Service)

1.2.1 History at Whitehorse

In the latter part of 1980, Environmental Protection Service (EPS) a division of Environment Canada (EC), began receiving complaints about wood smoke pollution in the Riverdale subdivision of Whitehorse. A sampling program was implemented in response, and has continued in various configurations until the present (1995). In general the concentrations of total suspended particulate (TSP) at Whitehorse are low, but the first winter of monitoring in Riverdale (McCandless 1984) recorded values up to $72 \mu\text{g}/\text{m}^3$ ($120 \mu\text{g}/\text{m}^3$ is considered the maximum acceptable level).

Between November 1981 and February 1982 there were eight episodes where TSP exceeded $100 \mu\text{g}/\text{m}^3$ (SENES 1983). Meteorological data indicate that the winter of 1981-1982 had lower temperatures than 1980-1981, which partially explains the increased emissions. Monitoring the following year exhibited 14 days with TSP over $100 \mu\text{g}/\text{m}^3$. In the early 1980's Energy and Natural Resources (ENR) operated an incentive program, for installing woodburning appliances to convert or supplement domestic heating from heating oil. This led to a substantial increase in the number of wood fired heaters in use, which is a likely contributor to the increasing incidence of episodes of high TSP.

Dichotomous sampling with fine and coarse filters showed that over 95 percent of the TSP in Whitehorse was smaller than $2.5 \mu m$ (McCandless 1984), consistent with other studies (Mullbaier 1982) of woodsmoke particulates. Known background levels of TSP from downtown Whitehorse, in combination with the particulate size distribution, gave a high degree of confidence that the increase was due to wood burning.

Carbon monoxide (CO) is another potentially harmful emission from wood combustion but fairly low concentrations have been observed. Comparisons between CO concentrations in Riverdale and in the downtown area (across the river) from December 1982 to mid-March 1983, yielded similar average CO levels downtown and in Riverdale (near 2 ppm). Riverdale exhibited lower maximum values and less hourly variation.

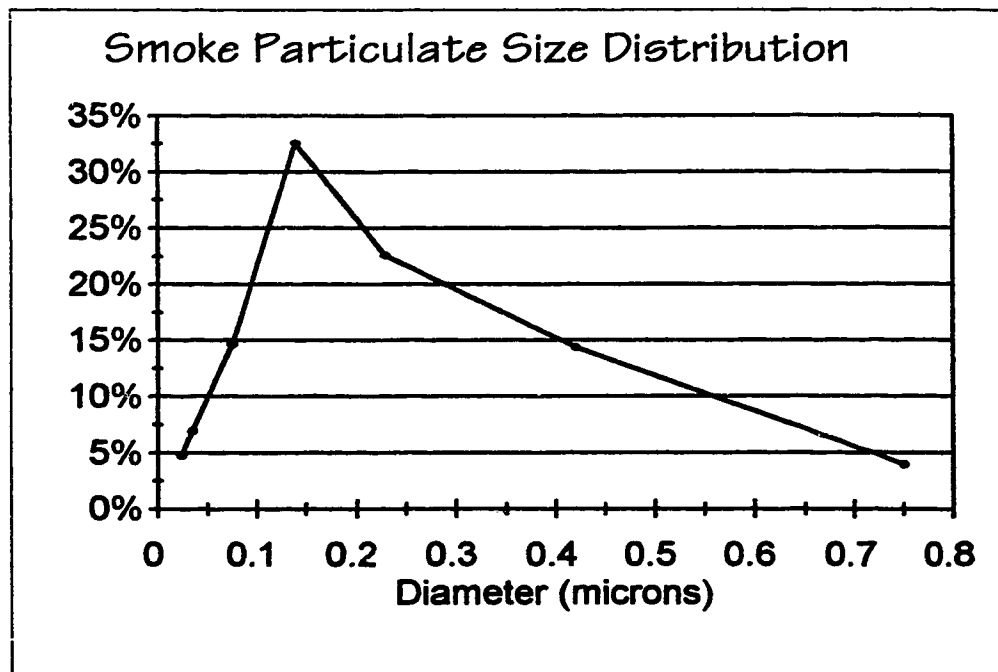


Figure (1.1) Typical equivalent size distribution for woodsmoke particulate. Plotted points are from discrete sampling bins. The mode size is 0.14 microns. (after Mullbaier 1982)

1.2.2 Wood burning

Wood energy constitutes a small percentage of Canada's energy consumption on a national average, but in some localities such as Whitehorse, wood forms a substantial contribution. Woodsmoke releases particulate emissions which are nearly 99 percent fine (smaller than $2.5 \mu m$), see Figure (1.1), as well as carbon monoxide, hydrocarbons and a diverse mixture of gaseous toxic organic compounds (Stuart 1983). The particulate emissions of woodsmoke are 60 percent Elemental Carbon, with the remainder being mostly organic carbon compounds. This combination of emissions presents a negative health effect where and when poor atmospheric dispersion allows high concentrations to accumulate

1.2.3 Health Impacts

Health impacts are difficult to assess, but the distribution of particulate matter in woodsmoke coincides closely with the ideal size for settling in the lungs (Figure 1.1). The optimum size is near 0.5 microns since smaller particles are more likely to be exhaled again, and larger particles are less likely to enter the lungs (Stuart 1983). Woodsmoke contains known and suspected carcinogens in both gaseous and particulate form. Jacobs (1982) estimates that each increase of $1 \mu g/m^3$ average annual suspended woodsmoke particulate, translates to a 0.041/10,000 increase in mortality rate. Whitehorse, with a population just over 20,000, would only require an increase in the mean annual particulate of $12 \mu g/m^3$ to attribute one death per year to woodsmoke (for a single neighbourhood the increase would need to be greater). There is certainly

substantial discomfort during an elevated pollution period, particularly to persons with respiratory ailments.

1.2.4 Other locations.

In Juneau, Alaska, a receptor modelling study used measurements of pollutants and apportioned the emissions to potential sources (Cooper et al 1984). The primary goal of this study was to ascertain the role of woodsmoke contributions to airborne pollutants, with no effort directed to prediction or meteorological analysis. Juneau is located on the east shore of Gastineau Channel in the Alaska panhandle with the residential areas extending East into the Mendenhall valley. Winter is marked by frequent temperature inversions. A series of sampling filters allowed measurement of particulate size, and chemical species distributions. Regression analysis was done on these data versus known distributions for road dust, woodsmoke, and marine salts. Not surprisingly, there was site dependency on pollutant contribution; but in residential areas, wood smoke contributed about 80 percent of the fine particle (less than $2.5 \mu m$) TSP. The conclusion was that wood smoke from residential heating was a substantial contributor to air pollution in Juneau. It was noted that the fine nature of the particulate matter constituting wood smoke makes it more hazardous to health than particulates from road dust or marine sources.

A receptor modelling approach was also used at Fairbanks, located in east central Alaska about 300 miles inland from the Gulf of Alaska. The climate is

strongly continental and the city is located in the Chena river valley. The goals and conclusions were similar to the Juneau study.

Studies have been conducted for various valleys in mainland United States and all reach similar conclusions (Allwine 1982, Carlson 1982, DeCesar 1982). Wood burning releases proportionately large amounts of particulate and other pollutants compared with similar heat output from fluid fossil fuels. The locations which seem to suffer the worst problems are valley locations under thermal inversions with light flow. Some areas have introduced legislation in response to smoke problems, to prohibit wood burning during stagnant conditions. Most regions have also identified that the emission levels are dependant on the design and operation of the stove as well as the nature of the fuel(Kowalczyk et al 1982, Mullbaier 1982) . National regulations are being tightened in both Canada and the United States for the maximum allowable rate of pollutant release from wood burning appliances.

1.3 Climate and Geographical Regime at Whitehorse

Whitehorse is geographically and climatologically mid-way between the distinctly continental arctic climate of Fairbanks, and the maritime climate of Juneau. Whitehorse is located in southern Yukon at a latitude of 60° 43' North and longitude of 135° 04' West. Inland canals of the Pacific Ocean lie 120 kilometres to the south, the St Elias Mountains lie 200 kilometres to the West, and several smaller mountain ranges lie North and East. The vegetation is boreal forest, primarily evergreen species with local stands of deciduous trees. The Yukon River

flows Northwest through Whitehorse from its headwaters at Marsh lake 20 kilometres to the Southeast. The river at Whitehorse is at an elevation of about 617 metres, with the airport on an escarpment above the river at an elevation of 703 metres. Whitehorse lies in one of numerous deep parallel valleys generally oriented from Southeast to Northwest. Mountains rise to up to 2000 metres nearby.

Whitehorse is one of the windiest locations in the Yukon with about ten percent of hourly winds at the airport exceeding 30 km/h (Wahl et al, 1987) and the highest frequency of strong winds occurring in the period November through February. Wind has a directional preference with 52.5 percent of observations with winds from South to Southeast, 20 percent from Northwest to north, 12 percent with no measurable wind (calm) and the remainder scattered around the compass (Environment Canada 1982b).

The mean annual temperature is -1.7°C at Whitehorse with a mean daily minimum temperature of -25°C in January, and a mean daily maximum of 20°C in July (EC 1982a). Winter is frequently marked by a temperature inversion and the mean lapse rate (i.e. decrease of temperature with increasing height) from the surface to 850 mb at Whitehorse in January is $\frac{\Delta T}{\Delta z} = -0.39^{\circ}\text{C}/100\text{m}$ (Wahl et al 1987). The average daily range of surface temperatures is near 9 degrees for the winter months.

The presence of mountains, upstream in typical atmospheric flows, tends to put the Whitehorse area in a rain shadow, and the precipitation regime is considered semi-arid, with a mean annual precipitation near 275 mm. Slightly less



Figure (1.2) Topographical Map of Whitehorse. Riverdale subdivision is marked as is the current site for pollutant monitoring. The area shaded is anecdotally reported to have higher smoke concentrations.

than half of this amount falls in the winter months as snow. Snow tends to fall in storm events with several snowfalls of five to ten centimetres per year. Early winter is frequently marked by shallow stratiform cloud layers with light snow and little accumulation. Later winter tends to be colder with decreasing cloud cover. Cold spells are frequently accompanied by the formation of ice fog which typically lasts eight to ten hours, but can blanket the valley for several days.

Overall the winter climatology of the Whitehorse area is dominated by continental arctic airmasses, with accompanying cold temperatures and an arctic inversion. There are frequent intrusions of mild maritime air from the Gulf of Alaska that will raise temperatures to near or above the freezing mark. Much of the winter is fairly windy, which weakens the temperature inversion and moderates temperatures. Under clear skies and light winds, Whitehorse can become bitterly cold with a strong temperature inversion. Clear and cold events typically last only several days before either cloud or wind intervenes to moderate conditions, but occasionally cold outbreaks last well over a week.

The relatively high latitude of Whitehorse, combined with high albedo due to snow cover, leads to little net insolation during the winter under clear conditions (Clark 1972), and negative net radiation (i.e. net loss) from October through March on average (Wahl et al 1987).

Whitehorse is situated in a SSE to NNW river valley with the valley floor sloping gently to the north (Figure 1.2). The ridges along either side of the valley

have mean heights of 1400 metres above sea level, with numerous peaks over 1700 metres. The ridge lines are about 30 kilometres apart perpendicular to the valley.

Riverdale subdivision is located on the east bank of the Yukon River which flows northward along the centre of the valley. Urban heat island effects are considered to be small and climate records of average monthly minimum temperature show that from November to February, Riverdale is one half to one degree cooler overnight than the airport (EC 1984a). This difference is primarily due to a drainage flow from surrounding slopes. Riverdale is located in a steep sided bowl which opens for about 45 degrees of arc westward to the river (Figure

	Wood	Oil
Particulates	220	32
CO	2,200	240
HC	30	40
NO _x	14	430

Table 1.1 Emission in ng/J from typical residential combustion.
(After Mullbaier 1982)

Contaminant	Annual Emissions from Wood Burning (kg)	Annual Emissions from Oil Burning (kg)
Particulate	28,612	899
NO _x	2,508	6,670
CO	532,875	4,830
PAH	929	348

Table 1.2 Calculated annual emissions for Riverdale for the 1981-1982 heating season (After SENES 1983)

1.2). On the west side of the river, about 3000 metres away an 85 metre escarpment rises to the airport.

Whitehorse has a small population spread over a large area in several subdivisions widely spaced in the valley. The Riverdale area has been the principal district with pronounced woodsmoke problems, but since 1992 there also have been concerns raised in other subdivisions prompting Environmental Protection Service (EPS) to conduct trial sampling at several locations. The population of Riverdale was 3300 in the 1981 census with 1211 single family dwellings. Approximately 75 percent of the residents are in single family homes and the remainder in townhouses or low-rise apartment buildings. In 1983 approximately 60 percent of the private homes used wood fuel as primary or supplementary domestic heating. The average annual consumption is five cords (128 ft³ per cord) of wood per home, with annual consumption in Riverdale of between 3500 and 4000 cords of wood (1981 to 1984).

1.4 Combustion Characteristics

The wood used at Whitehorse is mostly fire-killed lodgepole pine with about half burned in airtight stoves. Appliances with little air control such as fireplaces or Franklin type stoves, produce TSP emissions similar to airtight units, but airtight units tend to produce much higher CO and PAH's due to the lower combustion temperature and limited oxygen supply. Oil is the other principal heating fuel with estimated annual consumption for Riverdale being 2.9×10^6 litres.

Tables 1.1 and 1.2 show typical values for emission products and the estimated rates of their emission for Riverdale. These values will vary over time with changes in total consumption and the character of the appliances used. Between 1982 and 1983 a 20 percent increase in use of airtight stoves was estimated, which should translate into increased CO emissions. Interestingly, CO levels in the Riverdale subdivision have shown little variation. (McCandless 1984).

Spherical particles under one μm radius (such as dust) have a terminal fall velocity on the order of 10^{-5} m/s (W_g). A typical chimney exit is about five metres above ground and if the plume rises for another five metres before entrainment eliminates buoyancy, the mean height of particle injection into the atmosphere can be approximated as ten metres (h_0), with a vertical velocity of zero and horizontal velocity in equilibrium with the ambient flow. Neglecting removal by turbulent impaction on the ground, the particle size considered hazardous would have a suspension time (T_s) of about 36 days before it settled out (i.e. $T_s = h_0/W_g$). By comparison snowflakes tend to fall about 1.0 ms^{-1} and ice crystals at about 0.5 ms^{-1} (Rogers 1979).

Soot particles from woodburning appliances are initially hydrophobic (Wolff and Klimisch 1982) and would typically remain inert for several days until coagulation with other particles occurs. The hexagonal shape of particulate elemental carbon, which is the primary constituent of soot, may be conducive to deposition (they may act as an ice nuclei), but no corroborating studies were found.

1.5 Regression Analysis of TSP in Riverdale

SENES (1983) calculated regression statistics of average TSP versus average daily windspeed at the airport based on one year of monitoring at three sites in Riverdale. They calibrated relationships, for the three monitoring stations, between windspeed at the airport (predictor) and TSP at the stations (predictand), of the form

$$TSP = Ae^{-Bu} \quad (1.1)$$

A and B are the calibration constants and u is the 24 hour mean windspeed measured at the airport. At the three sites A varied from 155 to 246, and B varied from 0.095 to 0.139 with correlation coefficients (r) between 0.76 to 0.866.

The usefulness of this study is marginal and there are substantial flaws in the methodology. TSP exhibits large variation over a period of several hours, and so a 24 hour averaged value will filter out most of the variation. Furthermore, the critical values of TSP are the extremes when TSP rises to harmful levels for a period of several hours.

Wind speed at the airport and in Riverdale will not have uniform correlation with TSP under varying speed regimes, wind directions, and thermal stratification. If local windspeed is believed to be the principal influence on TSP, then a study should begin by establishing the relationship between local winds and TSP. The next step is to establish relations between the Riverdale wind and the airport wind. One of the goals of the SENES study was to establish a relation which could be used for prediction. The variable (u) chosen as a predictor is one which cannot currently be forecast with any degree of reliability, nor does it make

much sense as sole predictor in view of the many factors that dispersion theory reveals as relevant. A significant improvement should be possible by stratifying the data by wind direction, background thermal stratification and potential speed (pressure gradient), but to date this has not been done.

There is a substantial body of anecdotes describing the variation in smoke concentration in Riverdale. The density of objective measurement has not been sufficient to prove any conclusions as to the regional distribution but it can be reliably stated that there are areas of Riverdale which are more prone to high wood smoke pollution concentrations. These areas tend to be near the edges of the subdivision along Alsek road (shaded in Figure 1.2) and primarily along the Northeast boundary just below the escarpment. The monitoring site is located in the Southwest area of Riverdale.

1.6 Present Strategy

The development of strong thermal inversions, with associated shallow mixing and light winds, is reliably anticipated in Whitehorse by the forecast office, but not all episodes lead to high pollutant levels. Legislation exists to temporarily prohibit use of wood burning appliances in Riverdale (a "no burn" order), but this is generally done in reaction rather than anticipation. Emissions continue for several hours until the wood in the heaters is consumed. A "no burn" is issued by a smoke control officer who disseminates the order through local radio stations. This order is usually issued in response to rising TSP levels from the monitoring tower. There is no established objective method to issue the order in advance.

The precursors to smoke episodes are well known to most Whitehorse residents: clear skies, light winds and (usually) an established arctic airmass. The smoke control officer consults with the local weather forecasters (located at the Whitehorse airport) for predictions of wind and cloud. This input is used in conjunction with TSP levels to decide if a no-burn order should be issued.

1.7 Implications

The preceding discussion allows several conclusions relative to this study. There can be a high level of confidence that increase in TSP monitored at the Riverdale site is due to increased use of wood as a residential heating fuel. This has potential health hazards which might be ameliorated by better understanding of conditions which lead to high levels of TSP. Currently it is not possible to reliably predict onset or termination of increased levels of TSP. One study has identified correlations but they rely on a predictor which is hard to predict.

The inert nature and small size of wood smoke particulate allows treatment as a non-reactive, neutrally-buoyant tracer. Hence, transport and dispersion is the primary mechanism to eliminate pollutants. Dispersion and transport are relatively easy to model, given a reliable flow field.

All documented cases of high pollution levels at Whitehorse are a result of poor dispersion, although there is certainly some variation in emission. Emission rates of TSP per kilogram of fuel have been shown to decrease with increased rate of burn in a given appliance (Barnett and Shea 1982). This suggests that there should be little overall increase in emission rates from domestic heating with lower

temperatures, and variation in emission will be assumed to have much less significant impact on TSP, than variation in dispersion by the wind.

This focuses the investigation at Whitehorse on the flow conditions which lead to the beginning and end of smoke episodes. If the flow can be described and predicted, it should be relatively simple to describe the distribution and concentration of pollutants from wood smoke emissions.

In the study that follows, we will attempt to develop principles which will aid in understanding wind in broad, thermally stratified valleys, with a width on the order of tens of kilometres and a depth on the order of 1000 metres, with the goal of achieving sufficient description to allow pollutant dispersion calculations of greater skill than was formerly possible. Synoptic scale (on the order of 1000 km horizontally and 10 km vertically) atmospheric conditions generate the external environment or boundary conditions for such a valley flow. Valleys channel flow, and individual valley geometry contributes substantially to the character of the flow. Pollutant concentrations primarily become a problem in conditions of stable thermal stratification where light flows allow high concentrations to accumulate. The change from stable to neutral (or unstable) stratification is usually marked by increasing wind speeds and deeper vertical mixing that will decrease the local concentrations of pollutants.

1.8 Methodology of this Study

The Yukon river valley at Whitehorse generates a topographically modified wind and thermal regime. In winter, cold air settling down slopes (katabatic

settling) frequently strengthens the background temperature inversion associated with an overlying arctic airmass. This leads to a highly stratified thermal structure in the valley and results in light winds, limited vertical mixing and a general decoupling of the valley from the upper atmospheric flow.

Numerous studies have examined valley wind flow under varying atmospheric conditions. These include periods of intensive measurement with comprehensive grids of sophisticated sensors, long term statistical studies, qualitative flow visualisation with visible tracers, wind tunnel and water channel studies, and numerical simulations. The body of studies has established some common features of valley flows, as well as specific structures in given atmospheric conditions and valley characteristics.

A comprehensive understanding of the wind at high resolution (on the order of 100 metres) in the valley at Whitehorse is beyond the scope of this thesis, and possibly (in view of the terrain complexity) beyond the capabilities of current understanding of disturbed turbulent windflows. We will content ourselves with a coarse resolution (on the order of 1 kilometre in the horizontal), in an idealised valley.

A review of observational, statistical and numerical studies in various valleys will examine fundamental concepts to help explain some observed atmospheric behaviour. A sophisticated three-dimensional mesoscale model will simulate the development of a nocturnal boundary layer over flat terrain, and over a sinusoidal valley with similar dimensions to the valley at Whitehorse.

2

Mathematical Flow Description

"...when you can measure what you are speaking about and express it in numbers, you know something about it; but when you cannot express it in numbers your knowledge is of a meagre and unsatisfactory kind; it may be the beginning of knowledge, but you have scarcely in your thoughts advanced to the state of science, whatever the matter may be." (Lord Kelvin)

The equations describing compressible fluid flow were first derived by M. Navier in 1827 and by S. D. Poisson in 1831 based on intermolecular force considerations. These equations were also derived by B. de Saint Venant in 1853 and by G. G. Stokes in 1845. The latter two derivations were based on the assumption that shear and normal stresses are linear functions of the velocity gradient tensor. The equations have become known as the Navier-Stokes equations and form the foundation for mathematical and numerical description of fluid flows. An abbreviated derivation of the equations follows, based on Schlichting (1970) and Rajaratnam (1987), to demonstrate the inherent assumptions and form a basis from which simplifications are commonly made. A bias will be taken to atmospheric considerations.

2.1 Forces Acting on a Fluid Element

Consider an element of fluid of dimension dx , dy , dz and having a mass of $\rho dx dy dz$. Forces which act throughout the mass of a fluid element are body forces, such as gravitational force, and are given by external conditions. We can describe these forces:

$$\vec{F}_B = \hat{i}F_X + \hat{j}F_Y + \hat{k}F_Z \quad (2.1)$$

Surface forces, such as pressure or friction, act at the boundaries of the fluid element and are considered a function of the rate at which the fluid is strained.

Formally we write

$$\vec{P} = \hat{i}P_x + \hat{j}P_y + \hat{k}P_z \quad (2.2)$$

For this discussion an isotropic Newtonian fluid is assumed, which includes all gases and some liquids (e.g. water). An isotropic fluid implies that the relation between components of stress and the rate of strain is the same in all directions. A Newtonian Fluid is one which obeys Stokes law of friction: stress is linearly proportional to strain.

2.1.1 Shear and Normal Forces - Stresses and Strains

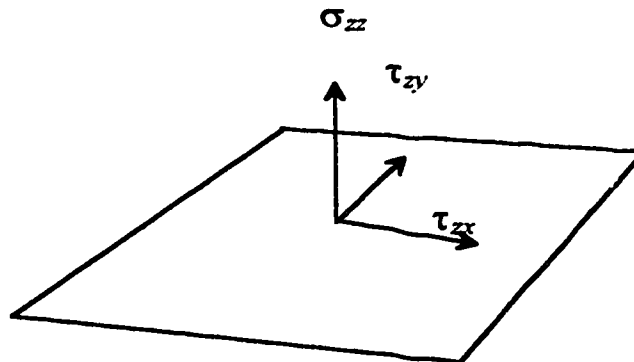


Figure (2.1) Top face of cubic fluid element with shearing and normal stresses

On each face of a cubic fluid element there are stresses parallel and perpendicular to each face. Consider the top face as in Figure (2.1). The first subscript refers to the face the force acts on, and the second the direction the force acts in. In notation for the normal stresses, σ , it is usual to drop the repeated subscript. The stress vector on face x (y,z) is

$$\vec{P}_x = \hat{i}\sigma_x + \hat{j}\tau_{xy} + \hat{k}\tau_{xz} \quad (2.3)$$

$$\vec{P}_y = \hat{i}\tau_{yx} + \hat{j}\sigma_y + \hat{k}\tau_{yz} \quad (2.4)$$

$$\vec{P}_z = \hat{i}\tau_{zx} + \hat{j}\tau_{zy} + \hat{k}\sigma_z \quad (2.5)$$

which can be expressed in matrix notation and is known as the stress tensor

$$\Pi = \begin{pmatrix} \sigma_x & \tau_{xy} & \tau_{xz} \\ \tau_{yx} & \sigma_y & \tau_{yz} \\ \tau_{zx} & \tau_{zy} & \sigma_x \end{pmatrix} \quad (2.6)$$

Taking the gradient gives three force vectors.

$$F_x = \frac{\partial}{\partial x}\sigma_x + \frac{\partial}{\partial y}\tau_{yx} + \frac{\partial}{\partial z}\tau_{zx} \quad (2.7)$$

$$F_y = \frac{\partial}{\partial x}\tau_{xy} + \frac{\partial}{\partial y}\sigma_y + \frac{\partial}{\partial z}\tau_{zy} \quad (2.8)$$

$$F_z = \frac{\partial}{\partial x}\tau_{xz} + \frac{\partial}{\partial y}\tau_{yz} + \frac{\partial}{\partial z}\sigma_z \quad (2.9)$$

2.1.2 Newton's Second Law

Newton's second law, can be expressed as

$$\rho \frac{D\vec{W}}{Dt} = \vec{F} + \vec{F}_B \quad (2.10)$$

where

$$\frac{D\vec{W}}{Dt} = \frac{\partial \vec{W}}{\partial t} + \vec{W} \bullet \nabla \vec{W} \quad (2.11)$$

and \vec{W} is the complete velocity vector. Stokes hypothesis relates the components of the stress tensor to the velocity gradient, so that in tensor notation

$$\sigma_{ij} = -p\delta_{ij} + \mu \left(\frac{\partial u_i}{\partial x_j} + \frac{\partial u_j}{\partial x_i} - \frac{2}{3}\delta_{ij} \frac{\partial u_k}{\partial x_k} \right) \quad (i, j, k = 1, 2, 3) \quad (2.12)$$

This can be substituted into the surface force vectors and combined with the body force vectors to complete Newton's second law.

$$\frac{\partial u_i}{\partial t} + u_j \frac{\partial u_i}{\partial x_j} = \frac{1}{\rho} F_{Bi} - \frac{1}{\rho} \frac{\partial p}{\partial x_i} + \nu \left[\frac{\partial}{\partial x_i} \left(\frac{\partial u_j}{\partial x_j} \right) + \frac{\partial^2 u_i}{\partial x_j^2} - \frac{2}{3} \frac{\partial}{\partial x_i} \left(\frac{\partial u_j}{\partial x_j} \right) \right] \quad (2.13)$$

These equations (Navier-Stokes equations) are generally combined with the continuity equation,

$$\frac{\partial p}{\partial t} + \nabla \cdot (\rho \vec{W}) = 0 \quad (2.14)$$

and supplemented by the equation of state for an ideal gas

$$p = \rho RT \quad (2.15)$$

by an empirical relationship for viscosity (primarily a function of temperature), and

an energy equation,

$$\frac{DT}{Dt} = \frac{1}{\rho C_p} \left[Q + \frac{Dp}{Dt} \right] + R \quad (2.16)$$

where Q is the heat transfer and R is the radiation term. This provides a set of seven equations for the seven unknowns of u, v, w, p, ρ, T, μ and allows a complete description of the flow if boundary and initial conditions can be imposed.

Simplifications are often introduced to the equation set. The first is to eliminate the compressibility of the flow, $\frac{D\rho}{Dt} = 0$. The second is to assume that viscous forces of the flow are negligible, $\nu = 0$. This inviscid incompressible set of equations is known as Euler's equations, in vector notation:

$$\frac{D\vec{W}}{Dt} = \frac{1}{\rho} \left(\vec{F}_B - \nabla \vec{p} \right) \quad (2.17)$$

$$\nabla \cdot \vec{W} = 0 \quad (2.18)$$

2.1.3 Continuum Hypothesis

Within the atmosphere there is a wide spectrum of scales of motion ranging from molecular to planetary. It is not possible to fully describe all scales of motion and in most cases only a small spectrum is of interest. The continuum hypothesis models the fluid without microscale structure and assumes that all distinguishing properties (i.e. density, viscosity) are averaged over many molecules and thus continuous in the fluid. This means that considered motions are much larger than

the mean free path of the molecules; physical properties at a point are averaged over a finite volume, and are continuous and relatively smooth in space.

Kolmogorov theory suggests that the smallest scales of motion existing in a flow are a function of the fluid viscosity (ν), and the rate of dissipation of turbulent kinetic energy (ϵ), giving a length scale characteristic of the smallest scales

$$\eta = \left(\frac{\nu^3}{\epsilon} \right)^{\frac{1}{4}} \quad (2.19)$$

Typical values for η in air are on the order of 10^{-4} m, which is much larger than the mean free path of molecules for most of the atmosphere. The continuum hypothesis is not valid in the very high atmosphere with low molecular density and high molecular energy, or in a shock wave with abrupt discontinuities.

2.1.4 The Problem of Closure

In any description of the flow some scales of time and space remain unresolved. In the simplest cases, (e.g. large scale laminar flow high above the ground) this unresolved portion can be ignored with limited impact on the solution, but in most cases, particularly near the ground, the unresolved flow has a substantial effect on the resolved portion of the flow. This demands some method to describe the unresolved portion of the flow.

2.1.5 Reynolds Averaging

To clarify or distinguish the resolved and unresolved scales, each of the variables of the flow can be written as

$$\xi = \langle \xi \rangle + \xi' \quad (2.20)$$

where the brackets $\langle \rangle$ refer to the resolved portion, and imply either a time or spatial average, while $'$ indicates an unresolved or fluctuating motion. This

decomposition can be introduced to the variables in the Navier-Stokes equations and to any ancillary equations needed to describe the flow.

Typical averaging operators are

$$\langle \xi \rangle = \frac{1}{T} \int_{t_0}^{t_0+T} \xi(x, y, z, t) dt \quad (2.21)$$

$$\langle \xi \rangle = \frac{1}{XYZ} \iiint_{x-\frac{X}{2} \ y-\frac{Y}{2} \ z-\frac{Z}{2}}^{x+\frac{X}{2} \ y+\frac{Y}{2} \ z+\frac{Z}{2}} \xi(x, y, z, t) dx dy dz \quad (2.22)$$

The function $\langle \xi \rangle$ remains a field variable, a function of x, y, z, t , but is much smoother than ξ . Based on the averaging operator some definitions of averaging

need to be introduced. Using two arbitrary variables of the flow, f and g

$$f = \langle f \rangle + f' \quad g = \langle g \rangle + g' \quad (2.23)$$

The averaging operation satisfies:

$$\langle f + g \rangle = \langle f \rangle + \langle g \rangle \quad (2.24)$$

$$\langle \alpha f \rangle = \alpha \langle f \rangle \quad \text{where } \alpha = \text{constant} \quad (2.25)$$

and if T is sufficiently long will satisfy

$$\left\langle \frac{\partial f}{\partial s} \right\rangle = \frac{\partial \langle f \rangle}{\partial s} \quad \text{for } s = x_i \text{ or } t \quad (2.26)$$

$$\langle \langle f \rangle g \rangle = \langle f \rangle \langle g \rangle \quad (2.27)$$

These relations imply

$$\langle \langle f \rangle \rangle = \langle f \rangle \quad (2.28)$$

$$\langle f' \rangle = 0 \quad (2.29)$$

$$\langle \langle f \rangle \langle g \rangle \rangle = \langle f \rangle \langle g \rangle \quad (2.30)$$

$$\langle \langle f \rangle g' \rangle = 0 \quad (2.31)$$

Splitting the variables into resolved and unresolved portions, and applying these rules of averaging generates a set of equations known as Reynolds equations. As an example consider the x direction equation of motion in an incompressible flow

$$\frac{\partial u}{\partial t} + \frac{\partial}{\partial x}(u^2) + \frac{\partial}{\partial y}(uv) + \frac{\partial}{\partial z}(uw) = -\frac{1}{\rho} \frac{\partial p}{\partial x} + \nu \left[\frac{\partial^2 u}{\partial x^2} + \frac{\partial^2 u}{\partial y^2} + \frac{\partial^2 u}{\partial z^2} \right] \quad (2.32)$$

substituting decomposed u and p yields

$$\begin{aligned} & \frac{\partial}{\partial t}(\langle u \rangle + u') + \frac{\partial}{\partial x}(\langle u \rangle + u')^2 + \frac{\partial}{\partial y}(\langle u \rangle + u')(\langle v \rangle + v') + \frac{\partial}{\partial z}(\langle u \rangle + u')(\langle w \rangle + w') \\ & = -\frac{1}{\rho} \frac{\partial}{\partial x}(\langle p \rangle + p') + \nu \left[\frac{\partial^2}{\partial x^2}(\langle u \rangle + u') + \frac{\partial^2}{\partial y^2}(\langle u \rangle + u') + \frac{\partial^2}{\partial z^2}(\langle u \rangle + u') \right] \end{aligned} \quad (2.33)$$

Using a time average of the result, and assuming a steady state flow and constant viscosity the equation becomes

$$\begin{aligned} \frac{\partial \langle u \rangle^2}{\partial x} + \frac{\partial \langle u \rangle \langle v \rangle}{\partial y} + \frac{\partial \langle u \rangle \langle w \rangle}{\partial z} & = -\frac{1}{\rho} \frac{\partial \langle p \rangle}{\partial x} + \nu \left[\frac{\partial^2 \langle u \rangle}{\partial x^2} + \frac{\partial^2 \langle u \rangle}{\partial y^2} + \frac{\partial^2 \langle u \rangle}{\partial z^2} \right] \\ & - \left[\frac{\partial \langle u'^2 \rangle}{\partial x} + \frac{\partial \langle u'v' \rangle}{\partial y} + \frac{\partial \langle u'w' \rangle}{\partial z} \right] \end{aligned} \quad (2.34)$$

giving a time averaged x component of the Navier-Stokes equations. Similar relations can be obtained for the y and z directions, which expressed in tensor notation are

$$\frac{\partial \langle u_i \rangle}{\partial t} + \langle u_j \rangle \bullet \frac{\partial \langle u_i \rangle}{\partial x_j} = -\frac{1}{\rho} \frac{\partial \langle p \rangle}{\partial x_i} + \frac{\partial}{\partial x_j} \left[\tau_{ij}^{\text{viscous}} + \tau_{ij}^{\text{turbulent}} \right] \quad (2.35)$$

where the stresses have been expressed as viscous and turbulent tensors so that

$$\tau_{ij}^{\text{turbulent}} = -\langle u'_i u'_j \rangle \quad (2.36)$$

Including the continuity equation this yields four equations but we cast up six additional unknowns: $\langle u'^2 \rangle$, $\langle v'^2 \rangle$, $\langle w'^2 \rangle$, $\langle u'v' \rangle$, $\langle u'w' \rangle$, and $\langle v'w' \rangle$. This step of explicit averaging is necessary to obtain governing equations for the resolved flow, but leaves an unclosed set of equations. Equations of state and thermodynamic equations are usually required to describe a given flow and averaging each equation adds more unknown variables. To satisfy the need for additional equations, various models have been introduced to represent the extra

unknowns. These models are not physically rigorous but introduce empirical or semi-empirical equations to close the set .

2.2 Closure Schemes

2.2.1 First Order Closure or K theory

Permitting ourselves to be a little loose in our terminology (we now include ρ), the Reynolds stress tensor (equation 2.36) in matrix representation is

$$\tau_{ij}^{turbulent} = \rho \begin{bmatrix} \langle u'^2 \rangle & \langle u'v' \rangle & \langle u'w' \rangle \\ \langle u'v' \rangle & \langle v'^2 \rangle & \langle v'w' \rangle \\ \langle u'w' \rangle & \langle v'w' \rangle & \langle w'^2 \rangle \end{bmatrix} \quad (2.37)$$

The terms on the diagonal are the Reynolds normal stresses and the other terms are Reynolds shear stresses. If the assumption is made that the Reynolds stresses are fixed by the shear in the resolved flow then a gradient transfer model, known as first order closure or K-theory, can be used to express unresolved terms such as

$$\langle u'w' \rangle = -K \frac{\partial \langle u \rangle}{\partial z} \quad (2.38)$$

Here K is the Eddy Viscosity (in m^2/s), which can be considered analogous to molecular viscosity except the scale of motion is on the order of typical turbulent motions or eddies, and the mechanism is not molecular but related to the kinetic energy of the motion. This expression begs a specification for K . In the simplest case K might be assumed constant through the layer of interest and prescribed from experimental data. A more sophisticated approach is to express K as a function of position and atmospheric state, with an empirical function determined from relevant experimental data. The "success" of K-theory hinges to a large degree on the calibration of K, usually from the flow to which the model will be

applied. In some ways this is simply a curve fitting exercise. To alleviate this problem one may attempt to diagnose K from a theoretical perspective.

2.2.2 E- ϵ Theory: One and a half order Closure

Here we still use a gradient transfer model with a physically more realistic equation for K such as

$$K = c_0 l \sqrt{E} \quad (2.39)$$

where

$$E = \frac{(\langle u'^2 \rangle + \langle v'^2 \rangle + \langle w'^2 \rangle)}{2} \quad (2.40)$$

is the turbulent kinetic energy, l is a turbulence length scale or mixing length and c_0 is a proportionality constant. A prognostic equation for E can be derived

$$\frac{\partial E}{\partial t} = -\langle u_i \rangle \frac{\partial E}{\partial x_i} - \langle u'w' \rangle \frac{\partial \langle u \rangle}{\partial z} + \frac{g}{\theta_0} \langle w'\theta' \rangle - \frac{\partial}{\partial z} \left[\left(\frac{\langle w'p' \rangle}{\rho} \right) + \langle w'E \rangle \right] - \epsilon \quad (2.41)$$

where the first term on the right is the advection term (zero in horizontally homogenous turbulence), the second term is shear production, the third is buoyant production (which may also be a sink), the fourth term is the vertical transport term and the final term is the dissipation rate of turbulent kinetic energy. ϵ is typically modelled

$$\epsilon = c_\epsilon \frac{E^{\frac{3}{2}}}{l} \quad (2.42)$$

where c_ϵ is a constant and l is a length scale as above. This set of relations can be solved to obtain an eddy viscosity, K, that responds implicitly to flow disturbances. It still requires that the constants be tuned by comparison with observed flows, but this method generally gives better results than a simple algebraic prescription of K.

2.2.3 Higher Order Closure

It is possible to derive conservation equations for higher order moments such as $\langle w'^2 T' \rangle$, that will appear in the budget equations for lower order moments such as $\langle w' T' \rangle$. This again introduces more unknowns than equations and requires a model to describe the new variables. Higher order closure has a high computational cost with the additional variables and equations, and has not demonstrated substantial improvement. Pielke (1984) suggests that the primary function of higher order closure is to direct improvement in lower order schemes.

2.3 Casting the Equations into a Rotating Frame of Reference

The equations considered so far have all been represented in a fixed Cartesian frame of reference. Atmospheric flows occur on the rotating earth and some modification of the equations is needed to include this rotation. It can be shown (e.g. Holton 1979) that the equation of motion in a rotating frame considering only pressure, gravitation and rotational forces is

$$\frac{DU}{Dt} = -2\Omega \times U - \frac{1}{\rho} \nabla p + g \quad (2.43)$$

where Ω is the angular velocity of the frame of reference.

If a steady state flow (and a low Rossby number) is assumed then this equation simplifies to the geostrophic wind equations where the only forces considered are pressure and Coriolis forces. The geostrophic equations in their complete form are

$$-\frac{uv \tan \phi}{a} + \frac{uw}{a} = -\frac{1}{\rho} \frac{\partial p}{\partial x} + 2\Omega v \sin \phi - 2\Omega w \cos \phi \quad (2.44)$$

$$\frac{u^2 \tan \phi}{a} + \frac{vw}{a} = -\frac{1}{\rho} \frac{\partial p}{\partial y} - 2\Omega u \sin \phi \quad (2.45)$$

$$-\frac{u^2 + v^2}{a} = -\frac{1}{\rho} \frac{\partial p}{\partial z} - g + 2\Omega u \cos \phi \quad (2.46)$$

Here a is the distance to the earth's center (radius at sea level plus elevation) and φ is the latitude. The terms divided by " a " arise from the conversion from spherical into Cartesian co-ordinates. For large scale flow at mid-latitudes, a scale analysis suggests it is valid to ignore the terms involving a and w , as they are two, or greater, orders of magnitude smaller (Holton 1979) than the remaining terms. In flow through substantial terrain (or in strong convective motions), w is often of a similar order of magnitude to u , and these simplifications are not valid. A scale analysis which assumes $u \approx 10 \text{ m/s}$, $w \approx 1 \text{ m/s}$, $\frac{\partial p}{\partial x} \approx 10^{-3} \text{ Pa/m}$, $2\Omega \sin \varphi \approx 2\Omega \cos \varphi \approx 10^{-4} \text{ s}^{-1}$, $\frac{\partial p}{\partial z} \approx 10 \text{ Pa/m}$, and $a \approx 10^7 \text{ m}$, suggests a different set of terms (Table 2.1).

Term Description	Equation
terms of horizontal velocity products over the earth's radius	$\frac{uv}{a} = \frac{10^2}{10^7} \approx 10^{-5}$
terms of vertical with horizontal velocity products over the earth's radius	$\frac{uw}{a} = \frac{10}{10^7} \approx 10^{-6}$
Coriolis terms with horizontal velocity	$2\Omega u \sin \varphi = 10^{-4} \times 10 \approx 10^{-3}$
Coriolis terms with vertical velocity	$2\Omega w \cos \varphi = 10^{-4} \times 1 \approx 10^{-4}$
horizontal pressure gradient	$\frac{\partial p}{\partial x} \approx 10^{-3}$
vertical pressure gradient	$\frac{\partial p}{\partial z} \approx 10$

Table 2.1 Scale analysis of terms in geostrophic equations under assumptions described in text .

Under these conditions the equations can be simplified if the terms of the two highest orders of magnitude are retained. Equation (2.43) then becomes

$$\frac{1}{2\Omega\rho} \frac{\partial p}{\partial x} = v \sin \varphi - w \cos \varphi \quad (2.47)$$

Equation (2.45) becomes the familiar geostrophic equation for u

$$-\frac{1}{2\Omega\rho} \frac{\partial p}{\partial y} = u \sin \varphi \quad (2.48)$$

Similarly equation (2.46) reduces to

$$\frac{1}{\rho} \frac{\partial p}{\partial z} = -g \text{ or } \frac{\partial p}{\partial z} = -\rho g \quad (2.49)$$

which is the hydrostatic approximation.

The inclusion of rotational effects can be applied to more complete forms of the flow equations which adds Coriolis terms and slightly modifies the value of the acceleration of gravity due to centrifugal effects. The horizontal and vertical components of the Coriolis parameter are defined as

$$f = 2\Omega \sin \varphi \quad (2.50)$$

$$\hat{f} = 2\Omega \cos \varphi \quad (2.51)$$

In most applications the horizontal component "f," is the only parameter included.

2.4 Introducing Topographic Information into the Equations

Topography can be treated by a transformation of the vertical co-ordinate. The goal of the transform is for the ground to correspond to a constant level in the new co-ordinate system (i.e. the ground transforms to a plain in the new co-ordinate).

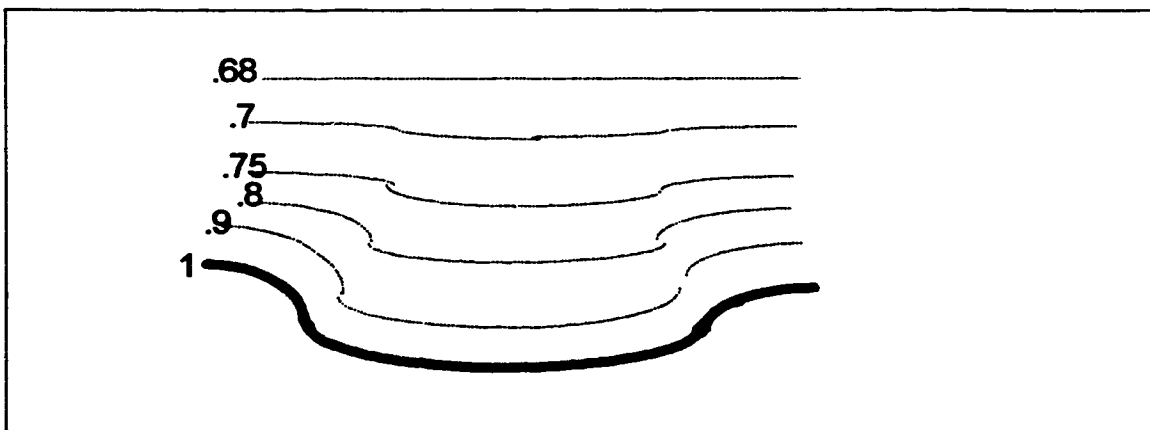


Figure (2.2) Sigma Co-ordinates. Sigma 1 at ground decreasing upward

2.4.1 Pressure Ratio as the Vertical Co-ordinate

The most common transformation is to convert the vertical co-ordinate of height, in real or geopotential metres, into pressure. In this way the highest value is at the surface with decreasing values with increasing height (Figure 2.2). A ratio of pressure at a given level with surface pressure gives the sigma co-ordinate which is terrain-following at the surface

$$\sigma = \frac{p(z)}{p_0} \quad (2.52)$$

Here p_0 is the surface pressure so at ground level σ is 1 and falls to 0 at a height of ∞ . The only weakness of this system is that the levels are arbitrary and have no intrinsic relation to meteorological processes.

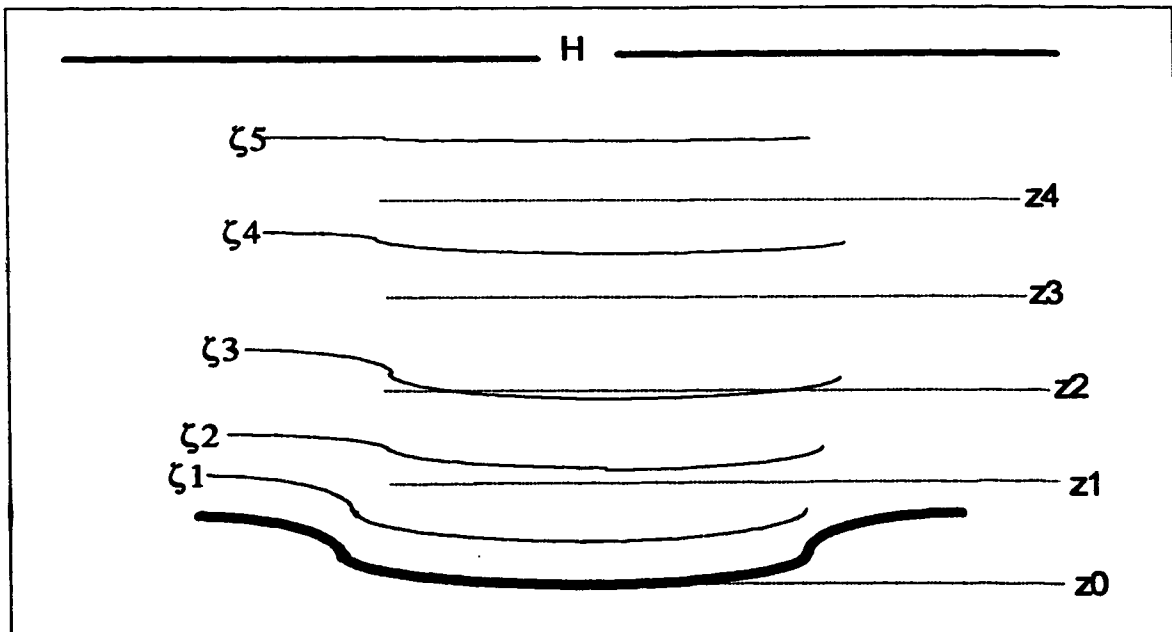


Figure (2.3) Gal-Chen Co-ordinate. z_0 to z_4 heights in geopotential metres. ζ_0 to ζ_5 heights in Gal-Chen metres. H is the model top; the same in geopotential and Gal-Chen metres.

2.4.2 Transformed Height Co-ordinates

Another alternative is to directly transform the height co-ordinate to respond to topography. One such method is the Gal-Chen co-ordinate

$$\zeta(X, Y, z) = \left[\frac{z-h_0(X,Y)}{H-h_0(X,Y)} \right] H \quad (2.53)$$

where X, Y, z are the local co-ordinates, h_0 is the function for topography (i.e. local ground height) and H is the imposed top of the atmosphere. Then $\zeta = 0$ at the surface and $\zeta = H$ at the top (Figure 2.3). The unit of vertical length will vary with, and hence respond to, the underlying topography. In numerical models the vertical levels are chosen and placed arbitrarily and do not respond to atmospheric conditions. The use of a fixed lid makes this scheme ideal for use in a nesting numerical model with boundary conditions imposed by either a larger scale model or a series of (historical) analyses.

2.4.3 Implications of the Transformation

The most obvious implication of a co-ordinate transformation is that co-ordinate lines do not necessarily intersect at right angles or even constant angles (non-orthogonal co-ordinate system). Extra terms arise in the governing equations. This generally requires that variables be transformed back to a simple Cartesian co-ordinate system for examination.

The other significant consequence is that motion along a fixed vertical co-ordinate surface (i.e. constant ζ in Figure 2.3) is not necessarily horizontal. This implies that the use of the horizontal Coriolis parameter, f , will introduce error where the slope of the X or Y surface departs substantially from horizontal. In atmospheric applications this is only significant near the surface of steeply

sloping terrain. It should also be noted that the horizontal and vertical Coriolis parameters are of similar magnitude for mid-latitudes and only differ substantially toward either the pole or equator.

2.5 Conclusions

This chapter has briefly introduced the fundamental flow equations and their decomposition into some common simplifications. A portion of the flow remains unresolved. The influence of this unresolved flow on the resolved flow can be parameterized by models determined through a combination of theory and empiricism, commonly referred to as the physics of a numerical model. The resolved flow, or dynamics, is profoundly affected in most cases by unresolved scales so great attention is required for parameterizations.

The co-ordinate system for flow equations in the atmosphere must take into account the inertial effects of the earth's rotation. This introduces some modifications to the flow equations with additional terms but no additional unknowns. Most of these additional terms can be ignored for many atmospheric flows. A scale analysis reveals that some commonly neglected terms can be significant in portions of the flow near the surface of steeply sloping terrain, where the vertical velocity component can be comparable to the horizontal components.

The model equations can be transformed along the vertical co-ordinate to include topography. These transformations allow the set of differential equations to respond to the lower topographic boundary conditions.

General Valley Flows

"No! There's the land (Have you seen it?)
 It's the cusseddest land that I know.
 From the big, dizzy mountains that screen it,
 To the deep, deathlike valleys below."
 (Robert Service, The Spell of the Yukon)

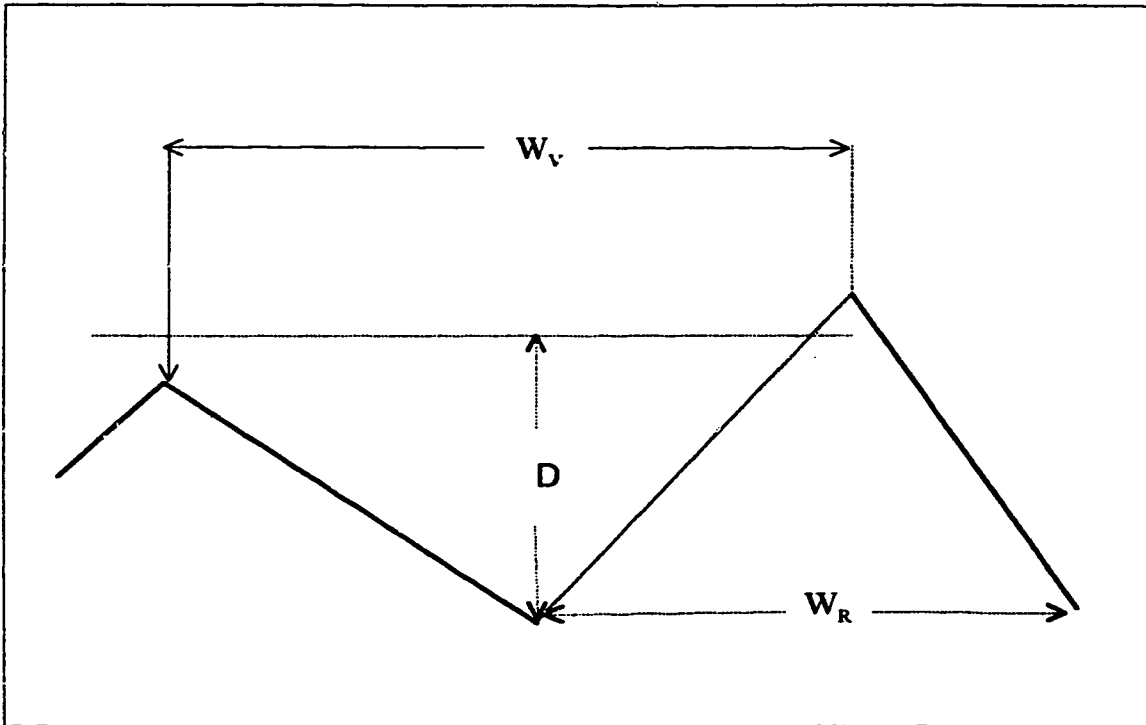


Figure (3.1) Fundamental valley dimensions of ridgetop width (W_v), ridge width at the base (W_R) and average valley depth (D).

3.1 Definition of Valley Shape Parameters

A set of shape parameters is helpful for a discussion of differing valleys.

The first ratio is the openness parameter

$$O = \frac{W_v}{D} \quad (3.1)$$

where W_v is the ridgetop width of the valley and D is average ridge to floor depth (Figure 3.1). This ratio provides a simple indicator of the gross characteristics of a valley but without further description implies a triangular valley shape.

Whiteman (1990) describes the topographic amplification factor (TAF) to explain the increased diurnal temperature variation in a valley. This was defined as a ratio of the volume of air below a reference height over a plain, versus the volume of air contained beneath the same height in a valley. In two dimensions,

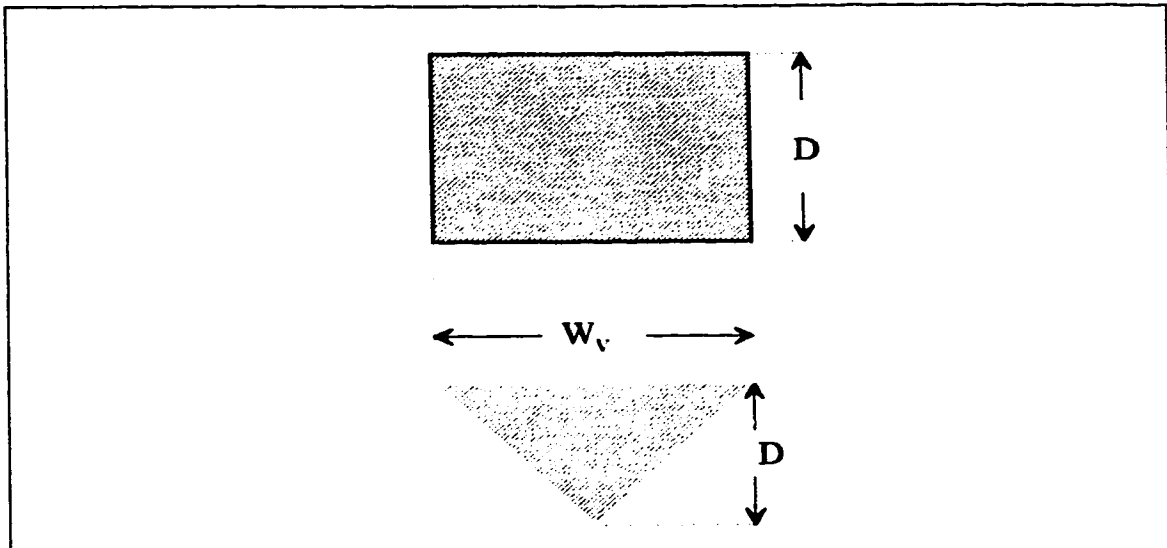


Figure (3.2) Representation of the two-dimensional Topographic Amplification Factor (TAF) which is a ratio of the volume of air over a plain versus the volume of air within a valley with similar width (W_v) and depth (D). In the case shown the $A_{\text{valley}} = 1/2 W_v D$ which implies $TAF = 2$.

considering a unit length of the valley, as in Figure (3.2),

$$TAF = \frac{W_v \cdot D}{A_{\text{valley}}} \quad (3.2)$$

where A is the area of a valley cross section. TAF is a geometrical factor which describes valley shape and will be near one for a wide open valley and will be large for a narrow valley with convex sides. In general TAF will vary along the length of a valley. If along valley symmetry can be assumed, a TAF can be chosen for a typical cross section. The TAF can be considered as a cooling or heating efficiency factor since a TAF of 2 implies that a valley will be twice as effective at cooling the enclosed air than a layer of air of similar depth over a plain of similar

width (although this neglects altered radiation geometry). In a valley the smaller volume of air (than over a plain of similar width and depth) is enclosed by sloped walls which makes radiation, conduction and convection more efficient at transporting energy.

The slope of the valley floor is a third descriptive factor expressed in degrees from the horizontal. The valley shape can be described as "U or V" shaped to provide an easily visualised description of a cross-section of the valley (a U shaped valley will have a smaller TAF, than a V shape). At Whitehorse there is an openness (O) of 36, a TAF of 1.5, the valley tends toward a V shape, and slopes to the Northwest at an angle of about 1 degree.

3.2 Conceptual Model of Nocturnal Valley Flows

The conceptual model of Defant (1949) is a helpful starting point for the case where large-scale flows are weak enough to permit slope flows to dominate.

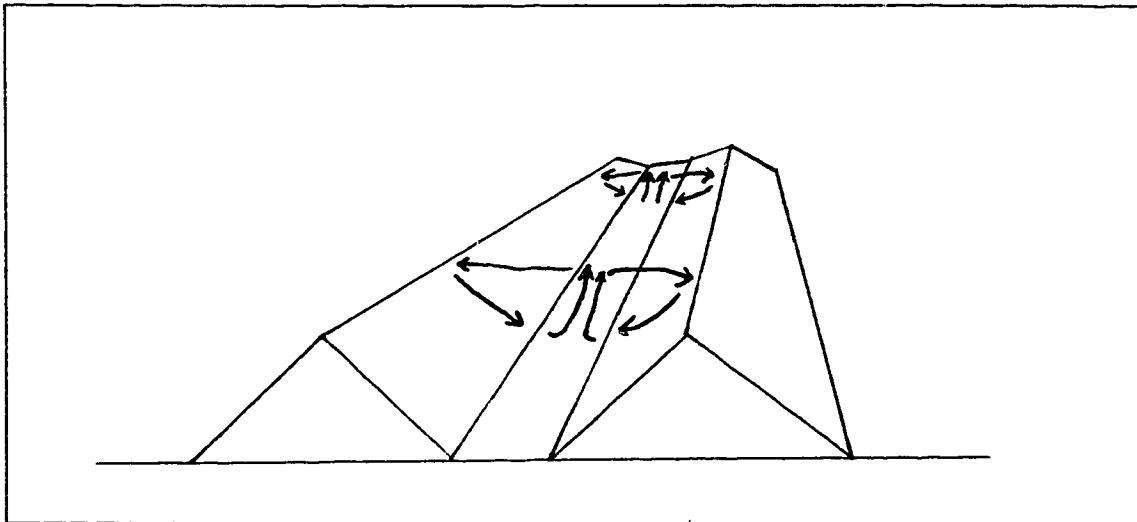


Figure (3.3) Evening drainage pattern in a valley where the valley-plain temperature difference is negligible and slope drainage has developed. (after Defant, 1949)

The nocturnal portion of Defant's discussion forms the basis for the following model.

During the evening there comes a brief state of quasi-equilibrium when the winds in the valley are light and the temperature difference between the valley and the plain is negligible. The drainage down the sidewalls of the valley develops into the two dimensional circulation as in Figure (3.3) which allows the valley to cool more efficiently than the plain. A valley-plain pressure difference develops (valley pressure is higher) since the average temperature of a column of air in valley is cooler than a column over the plain. The effect of the pressure difference may be enhanced by drainage along the slope of the valley floor as an along valley flow begins to develop (Figure 3.4). This along valley flow will be strongest near the mid point of the valley, where the drainage flows converge. As the downvalley

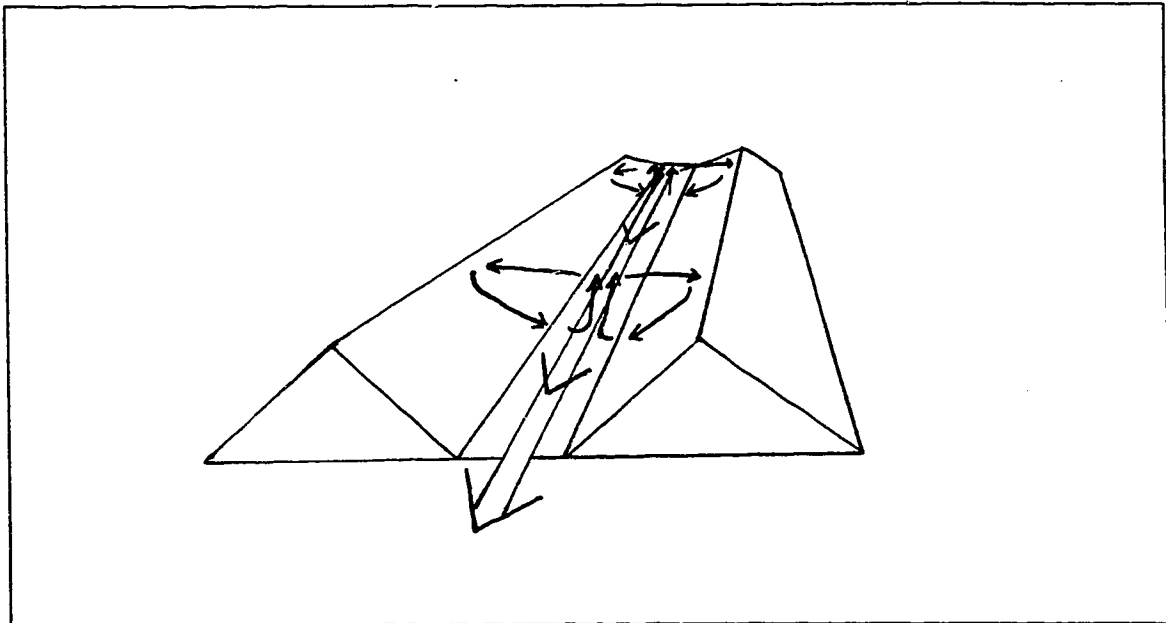


Figure (3.4) In the late evening a temperature and pressure difference between the valley and the plain causes an along valley flow to develop (after Defant, 1949)

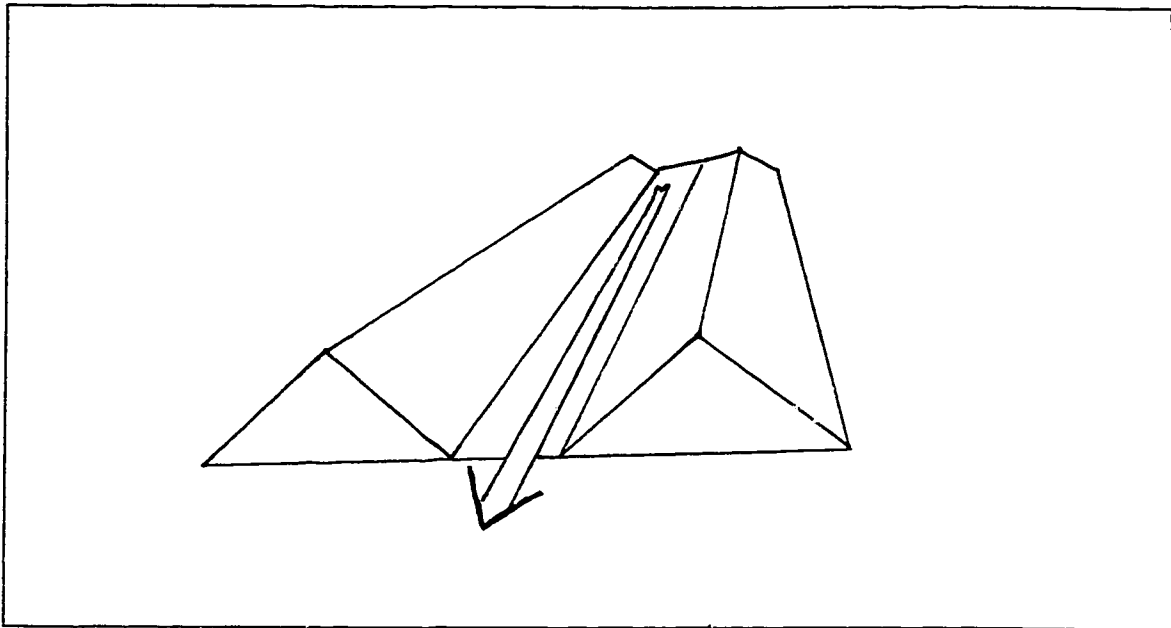


Figure (3.5) As the valley approaches its minimum temperature, the sidewall drainage decreases and the principal flow is the valley flow. (after Defant, 1949)

flow develops, the upward vertical motion above the convergence zone will tend to decrease, as the mass begins to drain along the valley. Defant (1949) reasoned that as the valley approached its minimum temperature and the rate of cooling decreased, the drainage flow down the slopes would also diminish and the principal flow would be the valley flow (Figure 3.5).

The conceptual extension of two-dimensional flow into three dimensions has also been suggested by others (Stovel 1983, Wong 1985). Two-dimensional flow will be distorted by the imposition of an along valley background flow, driven by shear stress and/or pressure gradient. The result would be maintenance of a pair of mirrored, cross-valley solenoids, but the background flow would tend to elongate the cross valley circulation into a helical pattern. The conceptual model

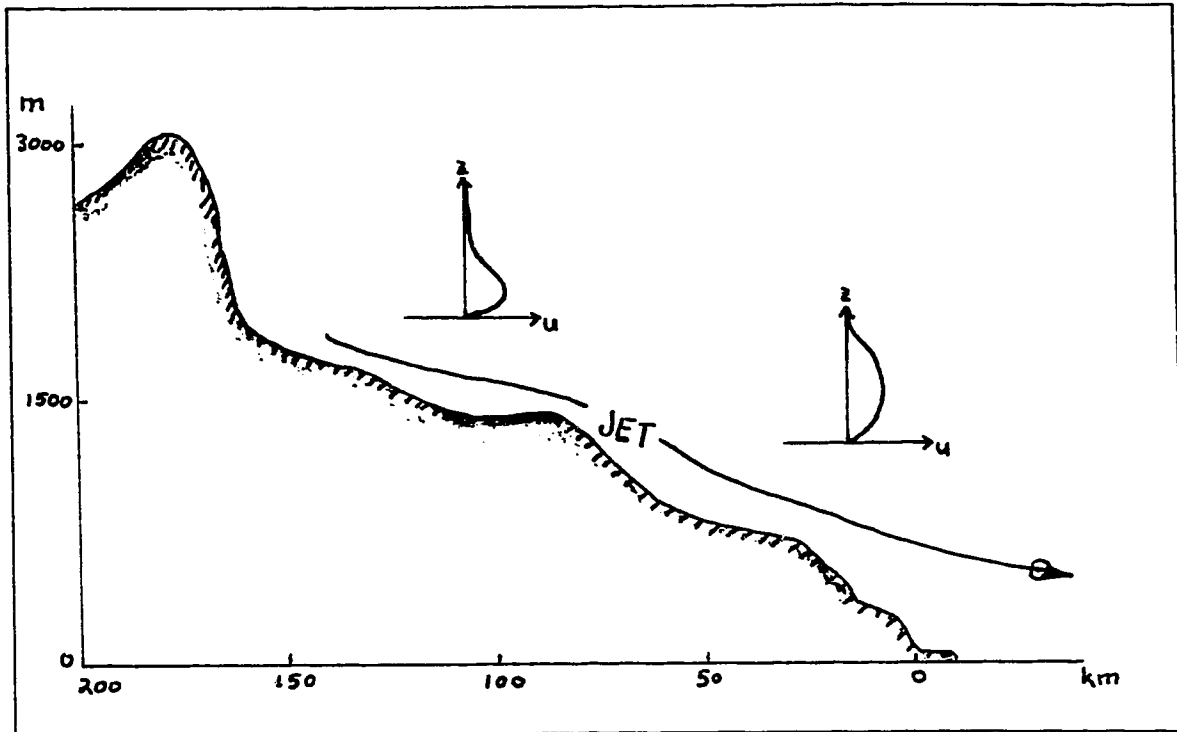


Figure (3.6) Drainage flows on an extensive exposed slope in Natal Province. Horizontal scale of 180 kilometres and elevation change of 3000 metres with an overall gradient of about 1:65 (modified from Tyson and Preston-Whyte 1972)

progresses very quickly beyond simple comprehension and is only useful to consider qualitatively, portions of the flow.

3.3 Observations of Drainage Flows

3.3.1 Case of a Uniform Sloping Plain

Tyson and Preston-Whyte (1972) presented observations of nocturnal drainage flows taken in Natal province (1964-1970) on an extensive slope, showing a drainage depth of about 300 metres, with a wind maximum in the middle of this layer (Figure 3.6). The location of the drainage wind maximum (jet) increased in height above the terrain, with increasing distance down the slope.

3.3.2 Valley Winds

Valley winds have been studied quite extensively, primarily due to the frequent siting of towns and cities on or near rivers which tend to be in valleys. Most studies focus on the diurnal trend of downvalley flow at night and upvalley flow by day. The mechanism of both flows is quite similar, but the following discussion will be limited to drainage.

An early investigator, Wagner (1938) recognised that valley winds occurred in valleys of varying sizes and cross-sections. The principal mechanism was seen as the pressure difference that resulted between the valley and the surrounding plain below or the plateau above the valley due to radiational differences. Nocturnal cooling (through radiational heat loss) will be more efficient in the smaller volume of air in the valley, and it will become colder than

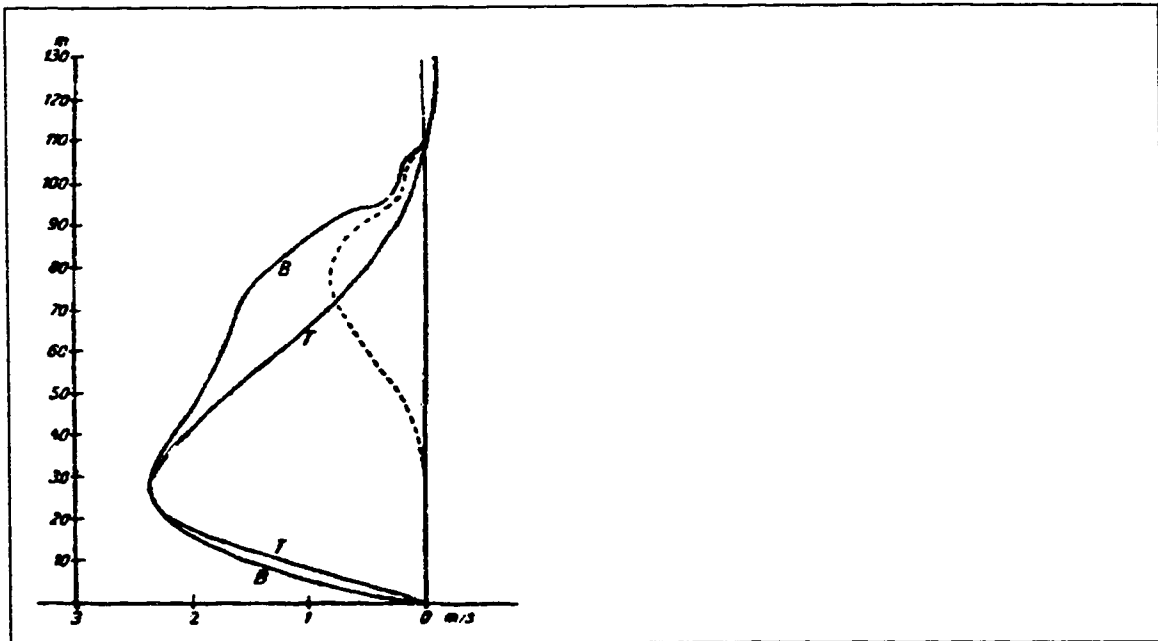


Figure (3.7) Calculated and observed nocturnal wind profiles in a valley. T is the theoretical curve; B is the measured curve and the dashed curve is the difference. Vertical axis in metres and horizontal in m/s.(after Defant 1949)

air over an adjacent plain. This will result in a pressure difference, due to the difference in the average temperature of a column of air. Air will then flow from the higher pressure valley to the lower pressure plain.

Wagner inferred that the depth of valley flows was typically below the ridge heights and depressed in the middle of the valley. Several years later Defant (1949) presented some typical wind profiles (Figure 3.7). These profiles show a wind maximum at about 27 metres above the surface under drainage conditions.

One of the most comprehensive observational studies of valley flows took place from 17 September to 07 October 1984 under Atmospheric Studies in Complex Terrain (ASCOT) described by Clements et al (1989). This project worked in Brush Creek, a 25 kilometre long valley located about 50 km north of Grand Junction, Colorado. The floor of Brush Creek valley has a slope of approximately 1.5° and the ridgetop is about 300 metres wide at the mid-point, opening to about 700 metres wide at the mouth. The valley is about 600 metres deep, with sidewall slopes of $35-40^\circ$, and an upvalley compass direction of 320° . Brush Creek is one of a series of parallel valleys, which opens into a wider valley, with a mid-point openness ratio, $O \approx 6$ and a $TAF \approx 2$. The observation nights were selected for ideal drainage conditions of clear skies and light overlying winds, to minimize the influence of external conditions. Numerous articles describe in detail the features of the flow measured in Brush Creek.

One of the features which was observed was the development of a nocturnal jet, which meandered along the valley about 100 metres above the floor. The jet was higher above the valley floor in the narrower portions of the valley

and the width of the jet increased as the valley widened. In the lower part of the valley the jet rose higher above the valley floor as the night progressed.

3.3.3 Laboratory Models of Flows Across Valley

Lee et al. (1987) conducted flow visualisation experiments in a saline stratified water tank. They towed valleys of varying steepness and ridge separation (perpendicular to the tow direction), and varied the Froude number

$$F_R = \frac{U}{D \sqrt{\frac{g}{\rho_0} \frac{d\rho}{dz}}} \quad (3.3)$$

(where D is hill height, ρ is the fluid density) with differing tow speeds, U . To describe the behaviour of the flow, they suggest a characteristic non-dimensional ratio

$$C_R = \frac{\lambda}{W_V} \quad (3.4)$$

where

$$\lambda = 2\pi D F_R \quad (3.5)$$

and W_V is the valley width at ridgetop. They found that the deepest penetration of the flow into the valley occurs when $C_R=1$, which is when the flow follows the valley contour. For values less than 0.75 the valley becomes stagnant. With $C_R=2$, the flow separates near the ridge and develops a highly turbulent recirculating flow. Lee et al. also identified the ridge shape as influential, and so they considered the ratio

$$\frac{W_V}{W_R} \quad (3.6)$$

where W_R is the ridge width. They observed that separation occurred for values of $1 \leq \frac{W_I}{W_R} \leq 3$, but was otherwise unlikely. Overall they concluded, C_R is the fundamental parameter determining penetration of external flows.

Bell and Thomson (1980) also conducted towing tank experiments using a sawtooth valley shape, and found that a Froude number of 1.3 was the maximum value for the occurrence of stagnant flows (i.e. no valley penetration by external flows).

3.4 Interaction of Valley Winds with Large Scale Flows

3.4.1 Large Scale Pressure Gradient/Wind

Purves (1979) conducted a study at Baden-Sollingen in the Rhine Valley ($O \approx 150, TAF \approx 3$) using 800 mean sea level (MSL) pressure charts to determine geostrophic wind. The winds were along the valley axis in 90% of the observations, with strongest valley winds occurring when the geostrophic wind was perpendicular to the valley; so that the valley wind flowed from high to low pressure (cross-isobar flow). Purves found that the valley wind was weak, with a high directional variability, when the geostrophic wind approached alignment with the valley. This relationship held for stability conditions ranging from distinct inversions to unstable. The magnitude of the wind was seven times greater under unstable conditions than with a temperature inversion.

A similar effect was identified by Overland and Bernard (1981) in the Juan de Fuca Strait, with winds generally channelled along the strait; by Whiteman and Doran (1993) in a Tennessee valley; and by Higgs (1990) in the Georgia Strait.

Thus the primary force, which drives along-valley wind in large open valleys, is pressure gradient along the valley floor. Variation within the valley of the direction and strength of the pressure gradient is the primary determinant of airflow. The effects of shear stress imposed by the overlying flow cannot be entirely ignored, but even in unstable conditions with moderate to strong flows, these studies suggest that the along-valley pressure gradient effect is dominant. Under stable conditions this effect is generally more pronounced.

3.4.2 Stratification / Gravity Waves

Thermal stratification is a fundamental control on shear interaction between the valley wind and the overlying free atmosphere wind. Increasingly stable stratification inhibits vertical coupling via turbulent transport of momentum, but on the other hand permits development of gravity waves, which can develop into a strong invasive flow into the valley.

Vertical disturbances due to flow over terrain will generate periodic vertical motion in a stably stratified flow known as gravity waves, where buoyancy is the restoring vertical force for a displacement. The strength of these waves is determined by the thermal stratification, the energy (velocity) of the flow and the magnitude of the imposed disturbance.

The amplitude of the wave will be equal to the vertical extent of the disturbance if shear and frictional dissipation of energy are ignored. The character of the resultant wave will also be influenced by the shape of the topography. The vertical displacement of the flow will be a function of the upstream topography. If

an isolated ridge initiates the disturbance the magnitude of the wave can be expected to be greater than if the ridge is one in a series of parallel ridges and valleys. Similarly the effect on the flow will be different if the ridge of interest is in the centre or at the end of a series of parallel ridges.

3.4.3 Shear Interactions with the Large-Scale Wind

Barr and Orgill (1989) suggest that valley winds are seldom completely decoupled from the flow in the free atmosphere. Strong winds external to the valley and the resultant turbulence, will overpower local circulations. Given ideal conditions of clear skies and light external winds, differential radiational cooling develops pressure gradients on the order of moderate synoptic or mesoscale gradients. There exists a continuum between calm clear conditions in which the valley flow is maximally decoupled, and cloudy and/or strong flow conditions in which the locally driven circulation is overwhelmed by the external flow.

Barr and Orgill note that Jaffe (1958) related the geostrophic wind to valley flows based on studies in three closed Vermont valleys. Jaffe found that an upvalley geostrophic wind of greater than 14 metres/second eliminated drainage flow. Cross-valley geostrophic winds of greater than 9 metres/second altered the drainage but did not eliminate it. Ideal conditions for a drainage flow were found when the pressure gradient supported a geostrophic wind less than 6 m/s.

Barr and Orgill (1989) found lighter ridgetop windspeeds allowed a deeper drainage layer to form in Brush Creek. The data also indicate that in the absence of a ridge top wind the flow will tend to fill the valley. Their data

exhibited a fair degree of scatter which suggests that ridge top speed is not sufficient to describe drainage depth (or volume flux).

3.4.4 Clouds and Moisture Profile

The moisture profile has an influence on the radiation balance. The strongest factor is cloud which is a highly effective emitter and absorber of long wave radiation. The presence of cloud will hamper the net loss of radiation, and hence reduce the surface cooling.

Even in the absence of cloud, moisture alters the transparency of the atmosphere to long wave radiation and raise the emissivity of moist layers for radiating long wave energy. Most cases in the atmosphere have some combination of layers of liquid and gaseous water which will have a strong influence on the radiation budget. No attempt will be made to explore the nature of the radiation balance beyond stating that the presence of moisture in the atmosphere will reduce radiational loss, particularly when manifest as cloud.

The other aspect of moisture which bears consideration is the formation of cloud and the resultant change in heat budget by latent heat processes. Bossert et al. (1989) examined terrain-induced flow using mountain top observations from the Rocky Mountain Peaks Experiment (ROMPEX) from the summers of 1984 to 1987. They found a substantial impact on the flow from the release of latent heat from convective cloud development. This alteration in the thermal and pressure gradient led to abrupt transitions from daytime inflow to nocturnal outflow. The vertical structure also showed variation with pronounced decoupling of the

regional and surface nocturnal flow in dry radiative conditions (i.e. no convective cloud and an otherwise dry atmosphere to permit radiative heat loss). It was more uniform in situations with convective cloud.

3.5 Interactions Between the Valley and Adjacent Geography

3.5.1 Downstream Blocking

Neff and King (1989) examined the flow downstream from Brush Creek when Doppler LIDAR data from ASCOT 1984 suggested downstream flow blockage. Brush Creek drains into the Roan Creek which drains through De Beque Canyon cut through the Book Cliffs escarpment about 50 km downstream.

This area provides a basin which would allow cool drainage flows to pool until the air overflowed the escarpment. The drainage flow in Brush Creek was observed to elevate during the night into a low level jet. Neff and King used measurements at several points to infer that this elevation of the jet may be a result of the down valley flow riding on top of the pool of cold air in the drainage basin. Their significant conclusion was that investigating valley flow needs to consider the effects of surrounding terrain beyond the domain of principal interest.

3.6 Local Forcing Within the Valley

3.6.1 Radiational Variation along the Valley

By considering a bulk energy balance for the volume of air contained below ridgetop in a triangular valley; assuming a dry system, and that this volume is (convectively) decoupled from the overlying atmosphere where winds are light

(negligible advection), one may show that (McKee and O'Neal, 1989),

approximately

$$\frac{\partial \bar{T}}{\partial t} \approx \frac{1}{\rho C_p} \frac{W_V}{A} Q_* + \Delta \quad (3.7)$$

where \bar{T} is the bulk mean air temperature in a valley cross section of unit along valley length, Q_* is the mean net radiation at the level of the ridgetop and Δ represents changes in ground heat storage. If we ignore changes in density (or assume that density (ρ) is approximately constant) along x (the x -direction aligned along the valley) then from the derivative of the ideal gas law with respect to x

$$\frac{\partial p}{\partial x} \approx R\rho \frac{\partial T}{\partial x} \quad (3.8)$$

If we integrate equation (3.7) with respect to time, and assume a short enough period that Q_* can be assumed constant and that ground storage is negligible, we can write

$$T \approx T_0 + \frac{1}{\rho C_p} \frac{W_V}{A} Q_* t \quad (3.9)$$

and by taking the derivative with respect to x of equation (3.9) and substituting back into equation (3.8)

$$\frac{\partial p}{\partial x} \approx \frac{RQ_* t}{\rho C_p} \frac{\partial}{\partial x} \left(\frac{W_V}{A} \right) \quad (3.10)$$

During the night-time, Q_* is negative and hence if the ratio $\frac{W_V}{A}$ increases with x then pressure should decrease with x , and vice versa. This derivation is not rigorous, but the result is qualitatively correct.

McKee and O'Neal (1989) estimate that for Brush Creek, during drainage flows, the differential radiation along the valley will develop pressure gradients approximately three times the strength of the pressure gradient due to the valley slope. They also report that observations in valleys where the ratio $\frac{W_V}{A}$ decreases

toward the mouth, provide evidence of pooling and inhibition of along valley drainage

3.6.2 Sidewall and Tributary Contributions

Porch et al (1989) investigated the relative contributions of sidewall and tributary flows using data from Doppler acoustic sounders and cross-path optical anemometers. They observed a temporal oscillatory behaviour for flux down the main valley and from tributaries. They also noted that versus the sidewalls the tributaries had a disproportionate contribution to the total volume flux of the drainage flow. One explanation is that the radiational shape alters the cooling rate in the tributary, in keeping with the work of McKee and O'Neal (1989). A negative correlation was observed between tributary mass flux and the flux in the main valley which was seen as indicative of an interaction between the main flow and the tributary inflow. The relation may be diagnostic in that the tributaries are more efficient radiational cooling sites, or causative in that the main flow interacts with the sheltered tributaries to improve the cooling efficiency through turbulent mixing. Porch et al. emphasise the importance of the parameterization of sub-grid tributary flux in numerical models as separate from and larger than slope flows.

Coulter et al. (1989) examined tributary fluxes into Brush Creek from Pack Canyon which itself has three tributaries. They found substantial variation within the valleys with differing shape and radiational shielding. During morning transition they found that Pack Creek, which remained shaded, continued to drain after the upslope flow had begun in Brush Creek. They also observed that the

ambient flow interacted with drainage depending on direction, location in the valley and time of day. They estimated that in certain conditions exterior winds formed a recirculation in the upper portions of Pack Creek which enhanced the drainage by about 20% over the estimates derived by cooling and surface area arguments.

Shinn et al (1989) examined TKE data which showed the highest values near the sidewall surface with a shallower turbulent layer than the main valley. The sidewall also showed a greater variation in the intensity of the TKE. This was speculated to be related to a meandering core of strong valley winds, further supported by a lack of a similar trend in narrow tributary canyons.

3.7 Conclusions

The ideal conditions for drainage winds are clear skies, low humidities and light ambient winds. Cloud and humidity change the radiation balance which is a function of surface and air (cloud) temperature, effective emissivity and layer opacity. Wind changes the turbulent mixing and heat transfer within the air, and between the air and ground. The ambient wind varies with large-scale pressure gradients, upstream topography and regional scale thermal variations (e.g. ocean breeze).

The valley topography is also important. The width, depth, length and shape of the valley, the slope of the sidewalls, and likely vegetative cover. There appears to be a substantial contribution to the flow from tributary drainage. The character of the upstream topography, the external flow, and thermal stratification

determine wave interaction with the valley. The topography at the valley mouth and in adjoining valleys can also affect drainage flow as the cool air pools or interacts with other drainage flows.

The resultant flow in a valley exhibits a number of features which can be explained by simplified models. A two-dimensional solenoidal cross valley circulation is often evident in observations. A low-level jet along a slope and a downvalley jet are usually observed. Observations of drainage flows also show that the interaction of the various influences is complex. It is not generally possible to describe the resultant flows in terms of simplified models, but elements of the simple models seem helpful.

The final conclusion is that it is possible to learn a great deal about the mechanisms and interaction of valley flows by examining simplified cases or individual forcings. A comprehensive analysis of drainage flows will require a method to describe the interaction and derive the resultant flow.

4 Exploratory Dimensional Analysis of Nocturnal Drainage Flows (2D Symmetry)

In the numerical study, described in Chapter six, we attempted to set up a flow having symmetry along the North-South axis with a weak westerly flow in the free atmosphere (i.e. we studied a weak transverse flow across an idealised valley section). Even in so simple a case, we can envisage several types of flow that might develop, depending on valley geometry and the relative importance of several (potentially) dominating factors, which in this chapter we quantify in the most schematic terms:

1. U_E ; the strength of the "external" or background wind (a measure of the overlying flow, which to repeat, we consider to be perpendicular to the valley axis). We neglect background shear and assume negligible along valley pressure gradient.
2. $\frac{\partial \theta}{\partial z}$; the stratification of the background flow.

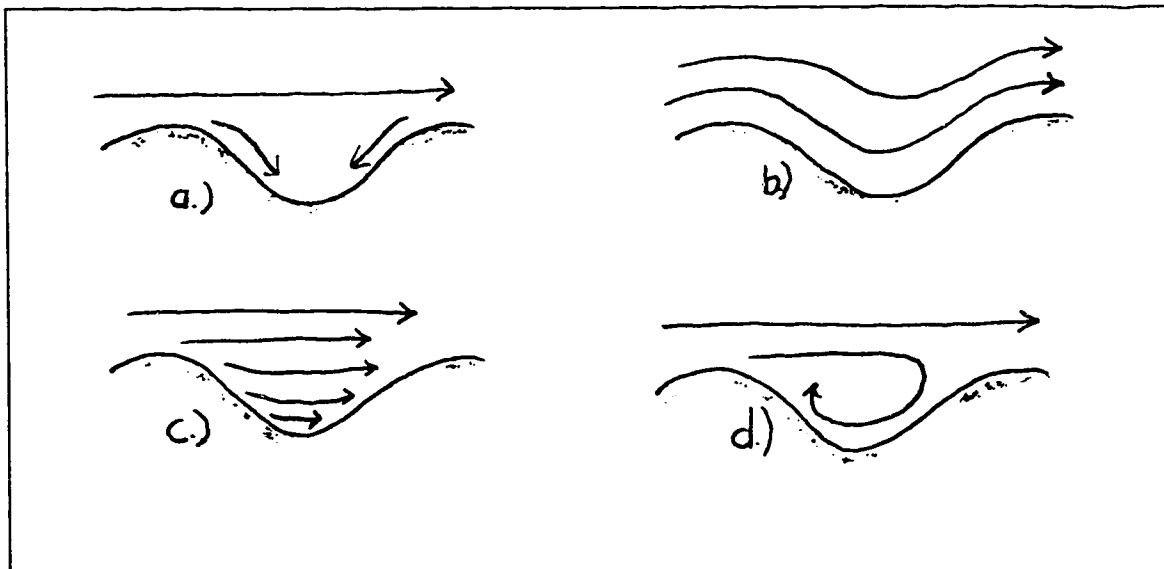


Figure (4.1) Four idealised extremes of a nocturnal valley flow dominated by; a) buoyant drainage; b) gravity waves; c) shear (flushing flow); d) turbulent wake.

3. Q_{H0} ; the strength of the nocturnal surface cooling generally expressed in terms of the net heat flux at ground (negative into the ground), $\langle w'\theta' \rangle_G$.
4. D ; the valley height.
5. W_v ; the valley ridgetop width

Figure (4.1) sketches several idealised extremes of the nocturnal valley flow we consider possible, and we might classify these as drainage dominated (Figure 4.1a), gravity wave dominated (Figure 4.1b), shear dominated (or flushing flow) (Figure 4.1c) and wake dominated (Figure 4.1d).

In any case of a complex system, it is a good idea to consider whether dimensional analysis can help to organise our understanding. Here we use dimensional analysis, in an exploratory manner, to see whether we might arrive at a set of characteristic (non-dimensional) parameters that could permit distinction of the above-mentioned flow categories. This was intended to permit us to anticipate the nature of the flow we might "create" with the numerical model from a given initial state.

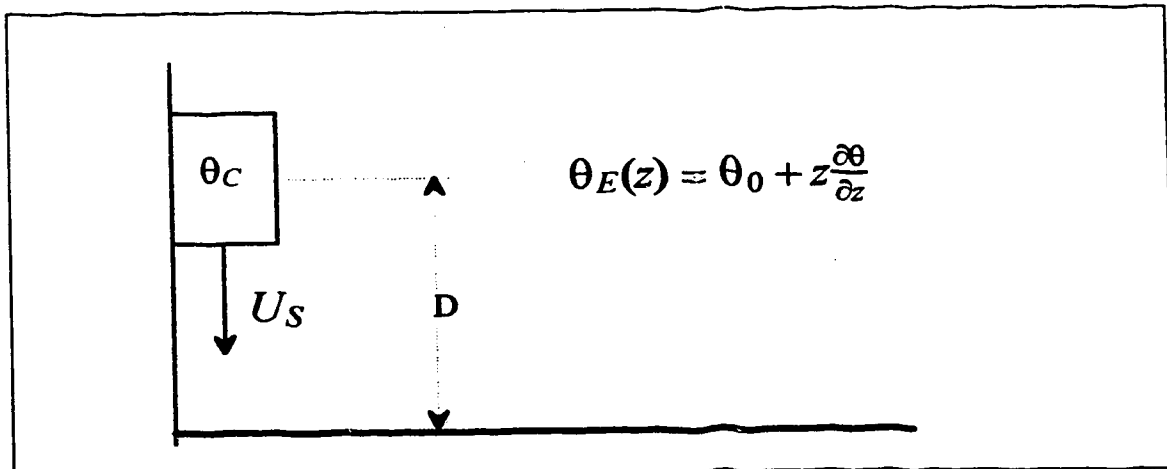


Figure (4.2) One-dimensional buoyancy driven motion with environmental potential temperature a linear function of height, and showing a parcel some distance, D , above the ground being cooler than the environment. These combine to produce the slope or buoyancy velocity (U_s).

4.1 Dimensional Analysis of Buoyancy Flows

If an equation in n variables is dimensionally homogeneous with respect to m fundamental dimensions, it can be expressed as a relation between $n-m$ independent dimensionless groups. (Buckingham Pi Theorem)

4.1.1 One-Dimensional Treatment

Consider a stably stratified atmosphere (Figure 4.2) where $\frac{\partial\theta}{\partial z} > 0$, which implies that for any $z > 0$, $\theta_E > \theta_0$. Let the parcel temperature $\theta_C = \theta_0$ for simplicity. Forcing which arises from friction and sensible or latent heat transfer is ignored. This simple picture gives rise to five variables involving three fundamental dimensions.

1. U_s , the resultant buoyancy driven velocity [m/s].
2. D , the initial height of the parcel [m].
3. g , the acceleration of gravity [m/s²].
4. θ_0 the parcel potential temperature (equalling the potential temperature at ground level) [°K].
5. $\frac{\partial\theta}{\partial z}$ the background temperature stratification, assumed constant [K/m].

Two dimensionless ratios can be formed:

1. $\frac{U_s^2}{Dg}$, a ratio of the kinetic energy (per unit mass) of the parcel to the initial gravitational potential energy (per unit mass) of the parcel. This is the square of a Froude number in common use in oceanography.
2. $\frac{D}{\theta_0} \frac{\partial\theta}{\partial z}$, a ratio of the temperature difference between the parcel and the environment, to the parcel potential temperature (environment potential temperature at the surface).

Thus the equation for the buoyant velocity will take the form

$$U_s^2 = Dg F\left(\frac{D}{\theta_0} \frac{\partial\theta}{\partial z}\right) \quad (4.1)$$

where F denotes an unknown function of its argument. This implies a greater buoyant velocity for larger D or g , and leaves the relationship with temperature gradient indefinite.

Consider, by comparison, an equation applicable to buoyant convective motion, such as that of Weismann and Klemp (1989)

$$B = g \int_{z_0}^Z \frac{\theta - \theta_0}{\theta_0} dz \quad (4.2)$$

where B is the buoyant energy per unit mass [m^2s^{-2}]. If shear forces are neglected

$$U_{S(\max)} = \sqrt{2B} \quad (4.3)$$

If we write

$$\theta = \theta_0 + z \frac{\partial \theta}{\partial z} \quad (4.4)$$

and substitute into Equation (4.2),

$$B = g \int_0^D \left[\frac{\theta_0}{\theta_0} + \frac{z}{\theta_0} \frac{\partial \theta}{\partial z} - \frac{\theta_0}{\theta_0} \right] dz = \frac{g}{\theta_0} \frac{\partial \theta}{\partial z} \frac{D^2}{2} \quad (4.5)$$

Substituting into Equation (4.3)

$$U_S^2 = \frac{gD^2}{\theta_0} \frac{\partial \theta}{\partial z} \quad (4.6)$$

This equation is consistent with Equation (4.1) if $F(x)=x$.

4.1.2 Buoyant Interactions with Large-Scale Wind

Four general flow regimes can be identified for the gravity-wave coupling between a valley and a stably stratified external flow (Figure 4.3). A minimal set of variables which describe the flow are shown in Figure (4.4).

1. the external flow U_E which can be taken as the upstream free atmosphere flow near the ridge top level.

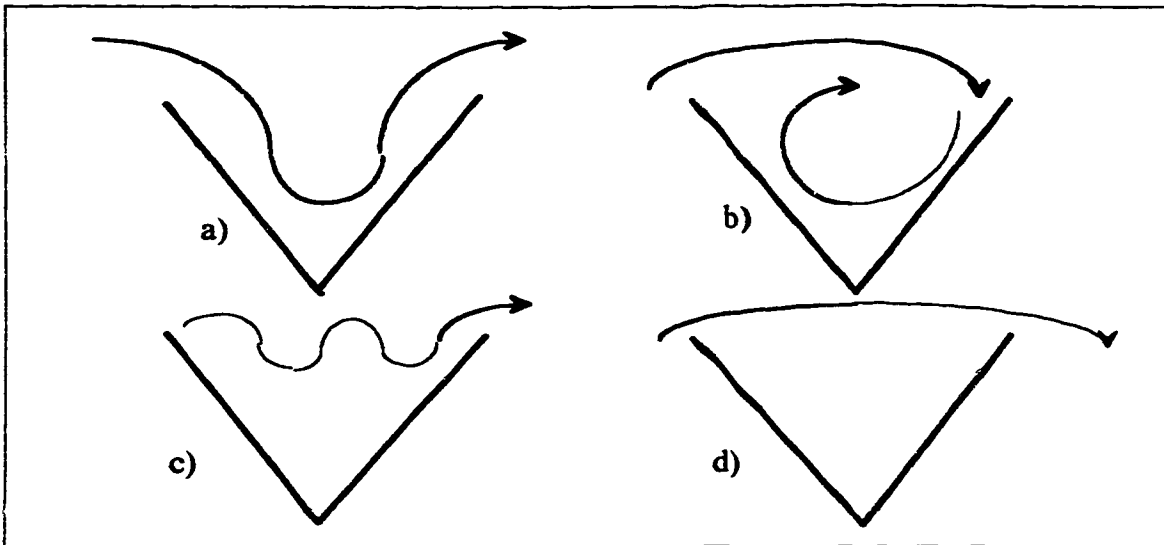


Figure (4.3) Possible flow regimes for gravity waves in a cross valley flow. a) the wavelength is similar to the valley and flushes through. b) the wavelength sets up a standing eddy and a reverse flow. c) the wavelength is short and the waves ripple across the top leaving stagnation in the valley. d) the wavelength is long and skips over the valley.

2. the invasive flow forced by gravity waves U_s . This value will tend to be on the order of zero or U_E .
3. the valley width W_v .
4. the valley depth D from the ridge top level to the valley floor. This will also be considered as the magnitude of the vertical displacement of an impinging flow (for most situations an exaggeration since upstream topography will reduce the amount of vertical displacement).
5. the external stratification $\frac{\partial \theta}{\partial z}$ of the upstream flow (we do not consider the temperature structure within the valley).
6. the acceleration of gravity g .
7. the mean upstream potential temperature θ .

These variables imply the following four dimensionless parameters describe the flow

1. $\frac{W_v}{D} = O$, the openness ratio of the valley.

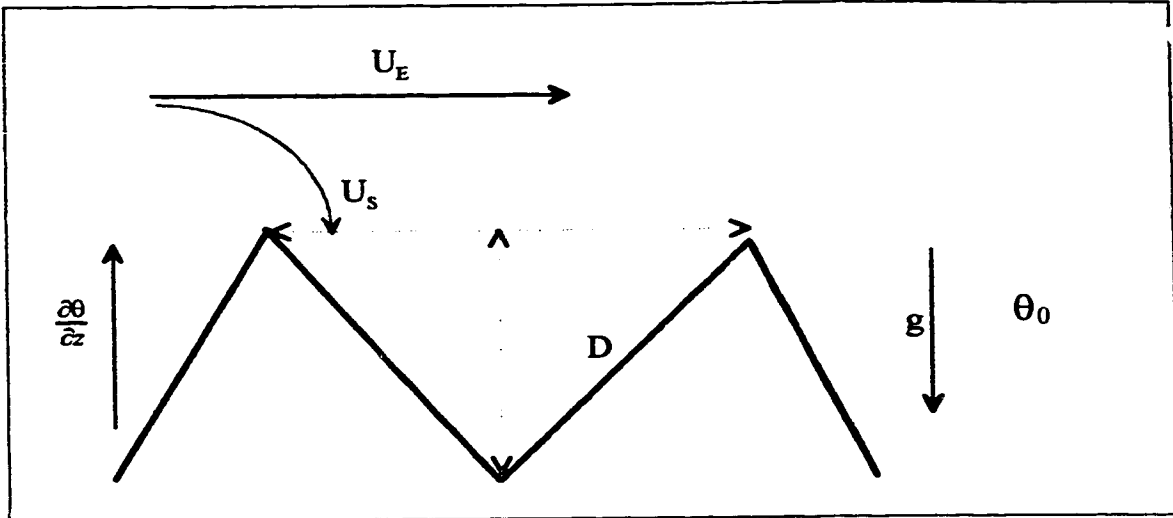


Figure (4.4) Influences on the buoyant interaction between a valley and the external wind (U). U_s is the downslope flow, U_E is the flushing wind, D is the ridge to floor valley depth, W_v is the ridge top width, g is the acceleration of gravity and the atmospheric stratification is described by $\frac{\partial \theta}{\partial z}$

2. $\frac{\partial \theta}{\partial z} \frac{D}{\theta_0}$, a large scale stratification parameter, the ratio of the total variation in potential temperature over the valley depth, to the background potential temperature.
3. $\frac{U_E^2}{gD}$, a ratio of the kinetic energy per unit mass of the external flow to the gravitational potential energy per unit mass contained in the depth of the flow (a Froude number squared).
4. $\frac{U_S}{U_E}$, a ratio of the invasive flow versus the external flow. This ratio will be near unity for a gravity wave which follows the terrain; it will be near minus one at valley bottom for a standing eddy situation; and near zero for other cases.

A relation can be formed from the these four ratios which should describe the strength of the invasive flow

$$U_S = U_E \left(\begin{array}{c} \frac{W_v}{D}, \frac{D}{\theta_0} \frac{\partial \theta}{\partial z}, \frac{U_E^2}{gD} \\ \{n1\} \quad \{n2\} \quad \{n3\} \end{array} \right) \quad (4.7)$$

The nature of the function F is indefinite but manipulating its arguments may provide clues;

The square of the buoyant Froude number arises as n^3/n^2 ,

$$F_R^2 = \frac{U_E^2}{D \frac{g}{\theta_0} \frac{\partial \theta}{\partial z}} = \frac{U_E^2}{D^2 \frac{g}{\theta_0} \frac{\partial \theta}{\partial z}} \quad (4.8)$$

This is the ratio of the horizontal kinetic energy of the external flow to the buoyant energy of the atmosphere. The Froude number is not defined for unstable stratification (i.e. $\frac{\partial \theta}{\partial z} < 0$), and is infinite under neutral conditions. Under stable conditions the Froude number provides a measure of the damping effect of stratification on vertical motions induced by topography.

The wavelength of the gravity waves induced by a disturbance to the flow can be written

$$\lambda = \frac{2\pi U}{N} = 2\pi D F_R \quad (4.9)$$

where N is the Brunt-Väisälä frequency. This can be compared with the valley width to form a characteristic ratio of the flow (Barr and Orgill, 1989)

$$C_R = \frac{\lambda}{W_V} \quad (4.10)$$

This ratio is implicitly "contained" as one of the arguments of our F():

$$C_R^2 = \frac{n^3}{n^2(n^1)^2} 4\pi^2 = \frac{U_E^2 \theta_0 4\pi^2}{W_V^2 g \frac{\partial \theta}{\partial z}} \quad (4.11)$$

When $C_R \approx 1$, the flow will tend to follow the contours of the terrain, which will result in a cross valley flushing much like case (a) in Figure 4.4. If C_R differs substantially from unity then either case (c) or (d) will develop. Case (b) is likely to develop when $C_R \approx 2$, and the impact of the flow on the opposite valley wall

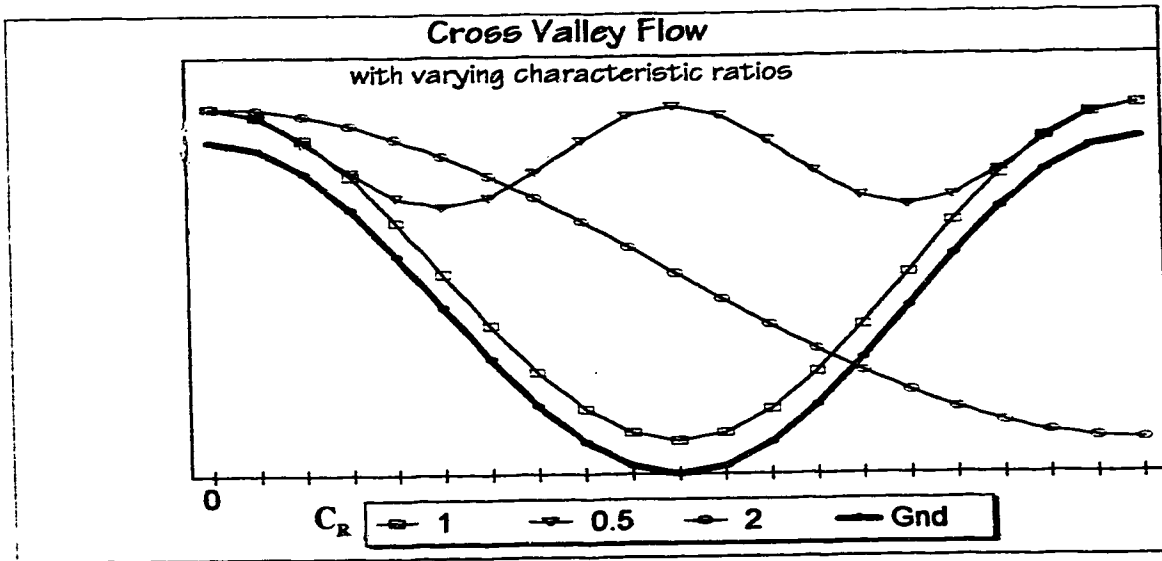


Figure (4.5) Possible flow trajectories of gravity waves for differing internal wavelengths expressed as C_R , a ratio of the wavelength versus the valley width. $C_R=0.5$ has a reduced amplitude for diagram clarity.

causes a recirculating eddy to form. Figure 4.5 presents some possible trajectory curves for different C_R . With a characteristic ratio of 2.0 the flow would impact the opposite valley wall at nearly a right angle. From this diagram it is easy to envision a divergent recirculation developing on the slope with one branch flushing through the valley in the opposite direction to the free wind and the upper slope with wind parallel to the free wind.

4.2 Shear Interactions with the Large-Scale Wind

Consider a two-dimensional valley set into a flat plain (Figure 4.6). The slope angle is shallow and it is assumed that the slope flow is approximately horizontal with vertical velocities much less than the horizontal. Figure (4.6) is a representation of seven possible fundamental influences in this valley. From these variables four dimensionless parameters can be formed

1. $\frac{U_E^2}{gD}$, a ratio of the kinetic energy per unit mass in the external flow to the potential energy per unit mass in the column of air in the valley center (a Froude number).
2. $\frac{\theta_E - \theta_V}{\theta_E} = \frac{\Delta\theta}{\theta_E}$, a stability parameter; negative in unstable stratification, zero for neutral conditions, and positive for stable.
3. $\frac{U_E - U_S}{U_E} = \frac{\Delta U}{U_E}$, a wind shear ratio that would be one if the shear driven wind were zero. This ratio will be near zero if the shear driven wind is similar to the external wind. This can be considered as an index of the degree to which the valley flow is shear (turbulence) decoupled from the external flow.
4. $\frac{W_V}{D} = O$, the openness parameter which represents the shape of the valley in terms of a triangular shape. If O is very small than the horizontal distance over which shear can act may not be sufficient to transfer momentum to the valley floor. If O is large than there is a large horizontal distance for shear to transfer momentum downward and it is more likely that effect will reach the valley floor.

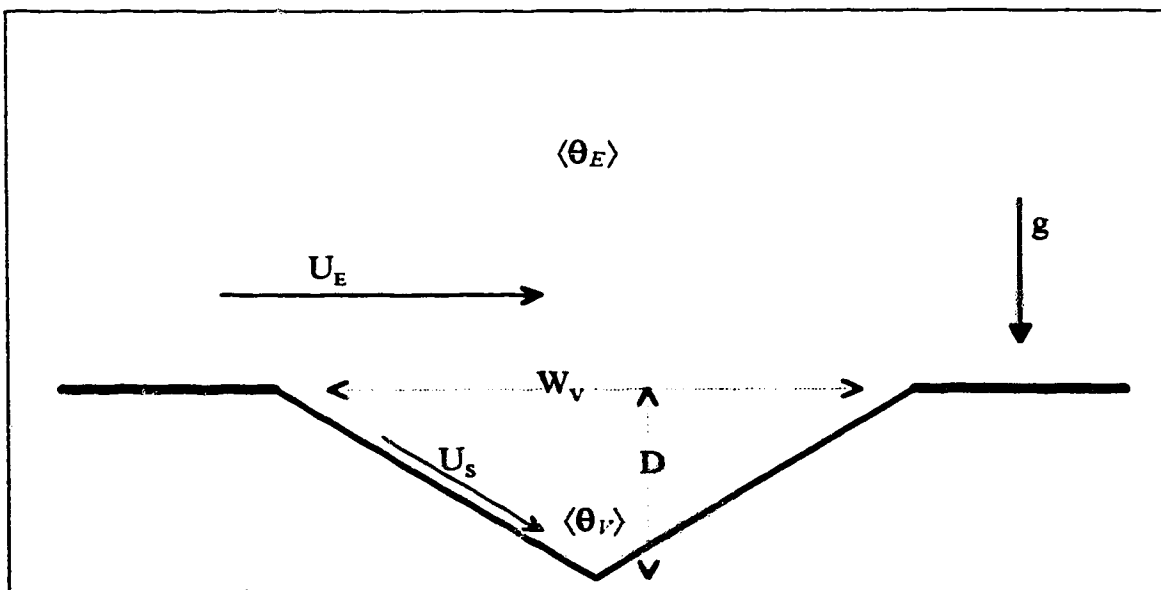


Figure (4.7) Principal influences on shear interaction between a valley and the free atmosphere. U_E is the external or ambient wind, U_S is the shear (turbulence) driven flow, g is the acceleration of gravity, W_V is the valley width, D is the valley depth, and the valley and external mean potential temperatures are $\langle\theta_V\rangle$ and $\langle\theta_E\rangle$

Suppose that

$$\Delta U^2 = U_E^2 F\left(\frac{U_E^2}{gD}, \frac{\Delta\theta}{\theta_E}, \frac{w_v}{D}\right) \quad (4.12)$$

Intuition suggests that difference in the flow between the valley and the free atmosphere should be inversely proportional to the first and third terms of the function, and proportional to the second. If we assume a linear dependence on each argument, then

$$(\Delta U)^2 = (U_E)^2 \left(\frac{gD}{U_E^2}\right) \left(\frac{\Delta\theta}{\theta_E}\right) \left(\frac{D}{w_v}\right) = \frac{gD^2 \Delta\theta}{w_v \theta_E} \quad (4.13)$$

which is in the form of a quotient of a gradient Richardson number with the openness parameter.

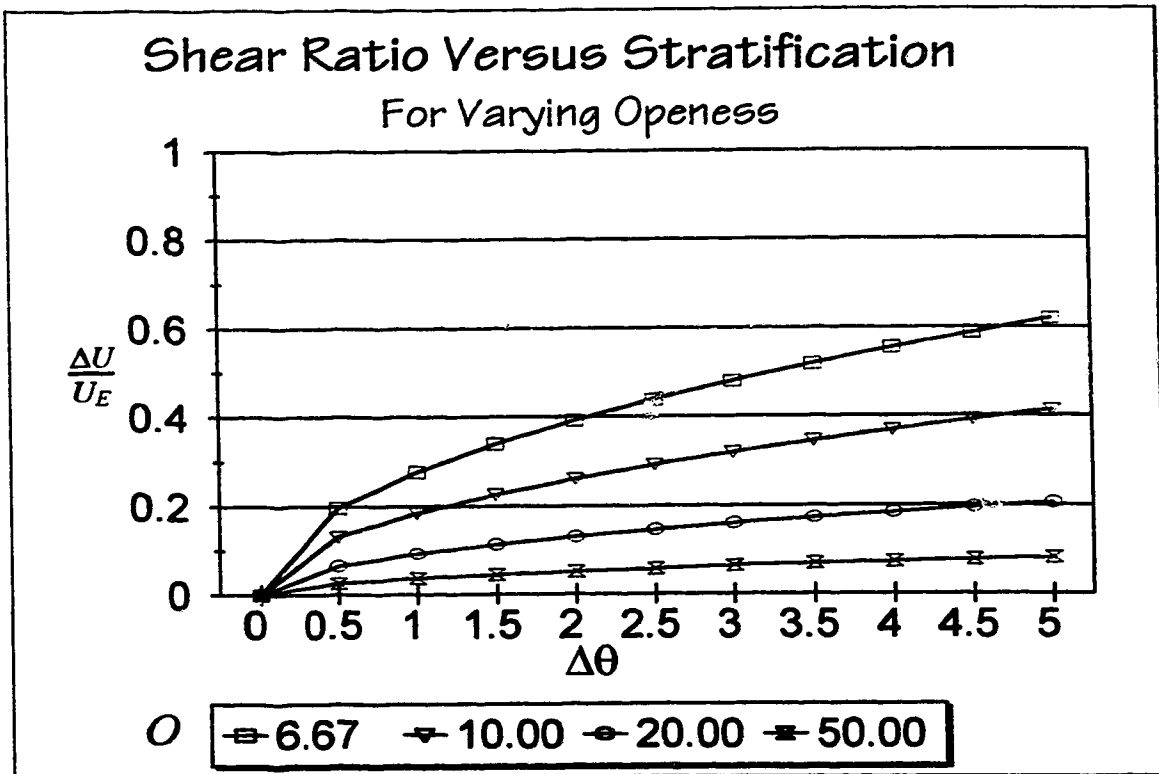


Figure (4.7) Shear ratio for varying stratification and openness (O) parameter. A ratio of zero corresponds to the shear (turbulence) driven valley wind equal to the external wind. A value of one implies the valley wind is not driven at all by shear with the external flow or the valley is entirely decoupled.

$$\frac{R_I^g}{O} = \frac{g \frac{\Delta\theta}{D} D}{\theta_E \left(\frac{\Delta U}{D}\right)^2 W_I} = \frac{gD^2(\Delta\theta)}{\theta_E(\Delta U)^2 W_I} \quad (4.14)$$

We have plotted the relationship of

$$\frac{\Delta U}{U_E} = \sqrt{\frac{gD^2\Delta\theta}{U_E^2 W_I \theta_E}} \quad (4.15)$$

to varying values of external wind, valley openness and stratification (Figures 4.7 and 4.8). This ratio will be zero when the valley wind is similar to the external wind and will be unity when the valley wind has no shear driven component from the external flow. The response is intuitively correct in that increasing stratification, decreasing external windspeed and decreasing openness of the valley

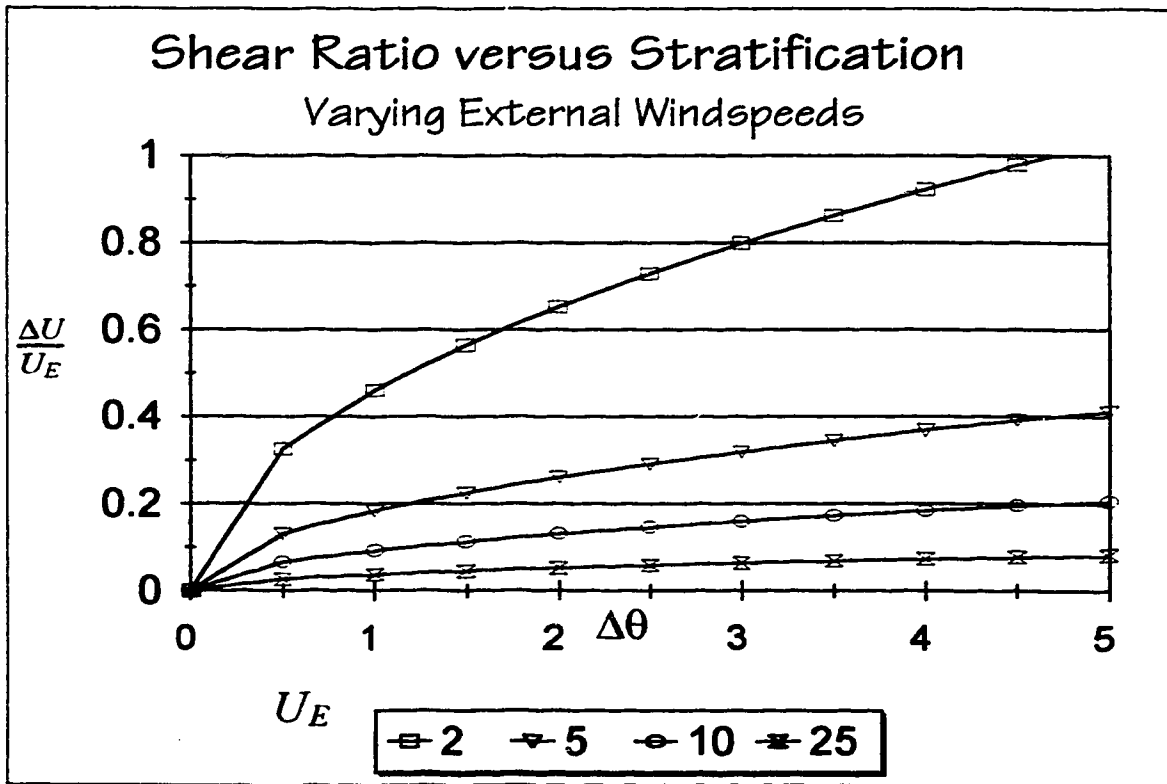


Figure (4.8) Shear driven flow for varying stratification with varying external windspeed. A ratio of zero implies that the valley wind is equal to the external wind. A value of one implies that the valley wind is not driven by shear or there is no shear coupling between the valley and external flow.

all lead to stronger decoupling. The magnitude of the ratio is arbitrary as was the definition of Equation 4.13, but the use of a scaling constant could make this a useful parameter for estimating the relative efficiency of shear interaction of a valley flow with the large-scale flow.

4.3 Radiational Influences on Drainage Flows

To this point we have used dimensional analysis to explore aspects of buoyant drainage flows, gravity wave interactions and shear driven flows, and we have seen some aspects of each flow. No clear parameter set has emerged to distinguish between the different classes of flow we consider relevant to our study. We now retain the principal influences which we have already explored and add the forcing mechanism of drainage flows; the turbulent kinematic heat flux to ground $\langle w'\theta' \rangle_G$.

Nocturnal longwave radiation causes the ground surface to cool below the temperature of the adjacent air. This results in a sensible heat transfer from the air to the ground, cooling the air. Turbulent mixing continues to mix warm air to the surface and mix cooler air from the surface through the airmass. This process transfers heat from the air to the ground where the energy continues to be emitted as longwave radiation. This heat flux is negative when the air is cooled (generally night-time) and positive when the air is heated by the ground (generally daytime).

We consider then, five variables of the flow; $\langle w'\theta' \rangle_G$, U_E , $\frac{\partial\theta}{\partial z}$, W_v , and D . From these variables we can form four ratios which, in combination, might allow us to discriminate between the possible flow classes we have described.

1. $F_R^2 = \frac{U_E^2}{D^2 \left(\frac{g}{\theta_0} \frac{\partial \theta}{\partial z} \right)}$: The Froude number becomes large under conditions of:

large U_E ; small D (i.e. shallow valley); or weakly stable stratification (small $\frac{\partial \theta}{\partial z}$). In each of these cases, or combinations thereof, the preceding dimensional analysis, and numerical or observational studies all indicate that the valley is not likely to be stagnant (decoupled from the flow).

F_R becomes small when: U_E is small; the valley depth, D , is large; or $\frac{\partial \theta}{\partial z}$ is large (i.e. strong stratification). Each of these cases is generally associated with stagnant conditions. Various values have been proposed for the critical Froude number (Bell and Thomson, 1980; Lee et al. 1987) but a value near unity seems a reasonable first guess (i.e. $F_R \leq 1$ implies a stagnant flow).

2. $O = \frac{W_V}{D}$; The openness parameter becomes large in a wide, shallow valley where stagnant conditions would be infrequent. A narrow deep valley has a small openness parameter and stagnation would be more frequent. A valley with a small O , would be more prone to having conditions where the wavelength of gravity waves would be similar to the valley width and hence gravity wave flushing would be more common than with a large O .

3. $B_{P(otential)} = \frac{\langle w'\theta' \rangle_G}{\theta_0 \sqrt{gW_V}}$; This parameter gives an indication of the potential for development of a buoyancy driven flow; essentially a ratio of turbulent vertical transport of heat to a heat advection scale (small for a steep slope and large for a shallow slope, with D assumed constant). Our primary interest is the nocturnal case so we assume that $\langle w'\theta' \rangle_G$ is always negative (i.e. the ground is cooling the adjacent air). $B_P \ll 0$ when the valley is narrow (i.e. a steep slope) and the turbulent heat flux is large. $B_P \approx 0$ when the valley is wide (i.e. a shallow slope) and/or $\langle w'\theta' \rangle_G$ is small.

4. $C_E = \frac{U_E^2}{gD}$, a ratio of the kinetic energy of the external flow to the energy required to climb (or descend) the ridge height (the square of an oceanography Froude number). This ratio will be small when there is a

deep valley and a light flow. As the flow increases or a shallower valley is considered, this value will become larger. Neglecting friction, the critical value is 1, when the kinetic energy of the external flow is sufficient to ascend (descend) the ridge.

If we return to the four idealised flow extremes of Figure (4.1), we can qualitatively estimate the corresponding region(s) of our 4-dimensional parameter space. See Table 4.1.

Flow Variables	Drainage Figure 4.1a	Gravity Wave Figure 4.1b	Shear Figure 4.1c	Wake Figure 4.1d
U_E	light	strong	strong	strong
W_V	small	non-specific	large	moderate
D	large	large	small	large
$\langle w'\theta' \rangle_G$	large negative	non-specific	non-specific	non-specific
$\frac{\partial \theta}{\partial z}$	non-specific	large positive	small	moderate
Dimensionless Parameters				
F_R	small	small	large	moderate
O	non-specific	non-specific	large	moderate
B_P	large	non-specific	non-specific	non-specific
C_E	small	moderate	large	moderate

Table 4.1. Summary of variables and discriminators for different flow regimes.

4.4 Conclusions

We have used dimensional analysis to explore the fundamental buoyancy equation, and gravity wave and shear interaction between the large scale flow and valley flow. From five fundamental variables we have constructed four dimensionless ratios which (might) allow discrimination between the idealised cases we considered.

**"The measure of a science... is its ability to predict."
(unknown)**

This chapter will briefly examine some approaches to numerical modelling of atmospheric flows in complex terrain and specifically in valleys.

5.1 Mass-Consistent Models of Flow in Complex Terrain

Even in the absence of other conservation equations, the continuity equation will ensure mass is conserved in a modelled wind field. If data are sparse, Pielke (1985) identifies four criteria which must be met to achieve realistic mass-consistent model simulations;

- (i) strong wind in the lower troposphere
- (ii) a strong inversion below the level of the highest terrain
- (iii) the layer below the inversion must be well mixed
- (iv) differential heating of the terrain is minimal

Dickerson (1978) used a mass-consistent (diagnostic) two-dimensional model to resolve the wind field in the San Francisco Bay area during summer and early fall. These seasons are dominated by an elevated inversion with a marine mixed layer below. There were about 40 surface weather stations in an area approximately 64 kilometres square. The calculations of mass flux in the mixed layer were consistent with a diverted flow around terrain obstacles. Sherman (1978) extended the work of Dickerson to three dimensions and included a pollutant dispersion calculation. Sherman found pollutant concentration errors of 2 to 50% of measured values.

Erasmus (1986a, 1986b) used a similar approach to examine the interaction of trade winds with the complex slopes of Oahu, Hawaii. His results showed good

agreement with observations, particularly in terms of ridge top amplification and cross-valley separations.

Mass-consistent models generally need a large number of observations or the physical conditions outlined above. This limits the applicability to interpolation of the wind field for a select group of cases.

5.2 Two-Dimensional Models

Stovel (1983) used a two-dimensional numerical flow model, with a simplified representation of the river valley at Edmonton, to examine drainage flows. A nocturnal drainage flow was generated by cooling the surface, and flow was calculated for up to 20 minutes of evolution. This model demonstrated the expected solenoidal features of a two-dimensional drainage flow and it captured some details of the flow. At the base of the valley the temperature change was mostly below 100 metres above the surface whereas at mid-slope the top of the modified layer was nearer 80 metres deep. Over the ridge the subsiding air from aloft exhibited slight adiabatic heating above 25 metres and fairly marked cooling below. Stovel ran her model with a steeper slope, and found that the flow reached a quasi-steady state earlier, but surprisingly, with a lower drainage speed. She also found that increasing stability of the atmosphere led to lower drainage speeds and achievement of a quasi-steady state sooner. Stovel's flow profiles showed a weak, near-surface drainage jet.

Wong (1985) extended the work of Stovel (1983) in the Edmonton river valley, using a more sophisticated model, with the specific objective of simulating

pollutant concentration. Wong found that a strong prevailing windspeed (2 m/s) at anemometer height (10 m) inhibited the formation of a drainage flow. The flow began to develop after the onset of nocturnal cooling more quickly under conditions of light wind (0.5 m/s) and continued to develop longer. Wong found that a steeper slope led to a stronger drainage flow, and that the height above ground of the low-level jet increased with increasing slope gradient.

Tang (1975) used a simple analytical model to examine cross-valley circulation. During nocturnal drainage in a gentle valley Tang found evidence of a circulation on the windward slope driven near the ground by drainage and above ground by the ambient flow. On the lee slope there was a general downslope motion. Tang also concluded that the interaction between a prevailing flow and one of thermal origin took place in the lowest 1000 metres above the slope.

Bell and Thomson (1980) examined valley ventilation under conditions of strongly stable thermal stratification and light cross valley winds with a two dimensional model (with Boussinesq approximation for an incompressible inviscid atmosphere). They used a Froude number as a discriminator between sweeping (where the large scale wind invades the valley) and stagnant (where the large scale wind has little interaction with the valley) flows,

$$F_R = \frac{u_r}{ND} \quad (5.1)$$

where u_r is the ridgetop windspeed, N the Brunt-Väisälä frequency $\left(\sqrt{\frac{g}{\theta_0} \frac{\partial \theta}{\partial z}}\right)$, and D the valley depth. A stagnant flow was observed below a critical Froude number of 1.3. Bell and Thomson suggested that the ratio of flow depth to valley depth must exceed 1.8 for the Froude number to reliably predict stagnant conditions.

McNider and Pielke (1984) used a hydrostatic model to examine the physics of the valley-plain wind and then applied the model to a valley where flow measurements had been made with a tether sonde. The first experiments they ran were two dimensional drainage flows in a valley 19 kilometres wide and 2 kilometres deep ($\theta = 9.5$). These flows showed a drainage jet about 8 metres above the slope. The drainage led to cooling of the valley, with a slightly warmer core of air remaining in the valley centre just above the surface. They discovered that in the valley the advective cooling dominated radiative effects as the cool air drained into the valley and hence stirred the air. The drainage developed quickly and reached a maximum after about 45 minutes, and gradually decreased to a steady state after about 7 hours. They note that the nature of the drainage flows leads to an upward turbulent transfer of momentum above the drainage maximum near the ground. They also point out that the drainage flow on a slope disturbs the distribution of potential temperature so that the layer near the surface is not necessarily as stable as it would be over flat terrain. The turbulence in this layer will tend to move the thermal profile toward an adiabatic shape.

Ye et al. (1990) investigated the impact of stability on nocturnal drainage flows using analytical and numerical models. This investigation showed the local atmospheric stability was dependent on the total cooling within the nocturnal boundary layer. Increased local atmospheric stability was found to be associated with stronger downslope flows, but the relationship did not extend to background or large scale stability. Ye et al. also found suggestions that for low slopes the drainage flow U_s is proportional to $\sqrt{\sin \alpha}$ where α is the slope angle.

5.3 Three-Dimensional Valley Flow Models

Egger (1987) used a low resolution model to examine the flow over the main massif and through the principal valleys of a range of mountains. The slope winds and flow through tributary valleys were considered as subgrid motions and parameterized. The valleys are represented as vertical channels in a cylinder, which represented the mountain massif. This study modelled the mean difference between terrain elevation but neglected valley slope as well as differential radiational characteristics along the valley. Thus the diurnal flow mechanism was the valley-plain radiational difference. The model exhibited the observed diurnal cycle of wind with daytime upslope and nocturnal downslope flow, driven by the pressure difference between the valley air versus the air over the plateau.

McNider and Pielke (1984) also ran their model in a three-dimensional mode, using an effectively infinite valley to the north end of the domain draining onto an infinite flat plain to the south. They found that the valley flow lagged the drainage flow down the side slopes, by about one hour. A slight asymmetry was observed in the flow, with a tendency of the flow field to turn to the right at the valley exit, attributed to Coriolis turning.

The model was also applied to a deep mountain valley to simulate available observations. There was good qualitative agreement, with a drainage flow developing downslope and evolving into an organised valley flow along the axis. However the model developed a deeper and slower flow layer than the observations. This may have been due to poor model resolution of the topography, and possible contamination by horizontal boundary effects.

Moore et al. (1987) used a dry, three-dimensional, meso-scale model to examine diurnal winds in the Southern San Joaquin Valley, near Bakersfield, California. This model used a Cartesian co-ordinate system and an interpolated three-dimensional temperature structure, constructed by matching surface values in the model with free atmosphere values from boundary conditions, rather than using explicitly predicted values. The slope drainage and mid-valley convergence for a valley cross-section were reproduced (solenoidal pattern). The vertical resolution was limited to 100 metres, hence low level jets were unresolved, or were, at best, underpredicted. This model demonstrates that even with the simplification of an interpolated thermal field, the essential features of a drainage flow in a valley can be numerically reproduced.

Whiteman and Doran (1993) used a version of the model of McNider and Pielke (1984), with a modified closure scheme (using the prognostic turbulent kinetic energy equation), to investigate interactions of nocturnal valley flows with external winds. They examined a broad valley in Tennessee with an openness ratio, $O \approx 60$. This valley exhibited strong evidence of pressure channelling, with winds predominantly observed along the valley axis, similar to the Rhine valley (Purves 1979) and Whitehorse. Whiteman and Doran demonstrated that the external pressure gradient dominates the flow in the valley if the geostrophic gradient implies free winds of 5 m/s second or greater; although the drainage flow contributes a small bias to the flow pattern. An external wind of 2 m/s allowed the valley drainage to develop largely independently of the external wind. They conclude that wide valleys will tend to be dominated by pressure channelling, due

to the relatively smaller effect of drainage flows or intra-valley pressure gradients from differential radiation (McKee and O'Neal, 1989). With strong external flows the downward transfer of momentum will have substantial effect, particularly in weakly stable thermal stratification.

Leone and Lee (1989) conducted a numerical simulation of the drainage flow in the Brush Creek valley using a finite element method with a non-hydrostatic model. They stipulated an atmosphere initially at rest, with a weakly stable (2K/km) stratification of the potential temperature. Cooling was introduced by specifying a constant downward surface heat flux. Drainage flow was observed to develop a low level jet down the slopes of the valley walls, which developed into a drainage jet directed along the valley axis. In fact there was a double jet maximum along the valley axis, with a lower level jet gradually weakening while the higher built in strength. It was hypothesised that the lower maximum is caused by the local drainage flow while the upper jet was a result of the mean valley flow, which continues to build during the simulation, and ultimately dominates the flow.

Yamada and Bunker (1989) also simulated a drainage flow in Brush creek focusing on a night with strong ambient wind (4m/s) and temperature gradients. Their model used a nested grid and a second order closure scheme. The observed wind maximum of about 5.7 m/s at a height of 220 metres above ground was reproduced, but the decrease to near zero by 500 metres above ground was not. The model runs did not adequately reflect the magnitude of cooling in the lowest

50 metres above ground. Yamada and Bunker used a variable roughness length over the model domain, based on a vegetation survey. A horizontal asymmetry in the flow was attributed to varying ground cover. Strong directional shear developed in the simulation, consistent with observed shears near the top of the drainage flow which nearly filled the valley for this case.

Doran (1990) used a non-hydrostatic model to simulate drainage conditions in a representation of Brush Creek valley ($O \approx 6$). Initially a weakly stable thermal structure was imposed (Brunt-Väisälä frequency, $N=0.004 \text{ s}^{-1}$), which developed as a surface heat flux was introduced, starting with -111 W/m^2 and diminishing to -25 W/m^2 over a period of four hours. The ambient wind speeds were varied in separate model runs, from 0.5 to 6 m/s with a constant angle of 60° to the valley axis.

At low ambient wind speeds, the down-valley drainage tended to fill the valley and develop stronger flows. Increasing ambient winds decreased both the depth and the magnitude of the drainage winds. With a fixed speed of 4 m/s the wind direction was varied from upvalley (0°) to a 60° angle across valley. When the ambient wind was upvalley, the drainage depth and strength were similar to a light wind cross-valley flow. As the direction moved through 10° to 60° there was a gradual decrease in strength but little overall change in depth. All cases with the ambient wind at any angle to the valley exhibited much less depth and overall weaker flow than an ambient wind upvalley. As the angle of the wind moves from parallel to the valley to perpendicular, the effective width of the deflecting obstacle (i.e., the ridge on the upstream side of the valley) decreases, as the path of the flow

approaches the most direct path across the ridge. This is proposed as a possible mechanism which would influence the wavelength of the induced gravity waves. Doran notes that the vertical velocity field over the valley is patchy with a complex pattern of upward and downward motion. He also notes that the Brush Creek studies cited the tributary flows as substantial contributors to the characteristics of the central valley flow.

5.4 Conclusions

Modelling and observations indicate that drainage flows have considerable variation in the first 500 metres above ground and particularly in the first 100 metres. This structure and its evolution will need to be resolved by a model used to simulate drainage flow. If the model is unable to explicitly resolve the structure, then the parameterization of the layer and the total heat and mass flux will need to be correctly represented.

The energy balance for the valley plays a significant role in the development and evolution of drainage flow. Many models assume a uniform radiation budget either in time or space. The complex variation of temperature through a valley suggests that this is a dangerous assumption. It seems critical that the surface energy balance be modelled properly with the longwave radiation balance correctly accounting for surface temperature, emissivity, and the sky view factor. The thermal structure which develops from the energy balance exerts enormous influence on the strength and structure of the drainage flow.

The advent of high speed computing has opened up the possibility of investigating atmospheric and specifically valley flows with a precision and economy not possible with observational or purely analytical methods. This powerful tool also has potential for misuse through excessive trust in its validity.

6

Numerical Experiments

"...since the machine-made forecasts are derived, at least in part, from idealised models, there will always be an unexplained residual which invites study. It is important, therefore, that the forecaster be conversant with the underlying theories, assumptions, and models. In particular, it is important that he be able to identify the "abnormal situation" when the idealised models ... are likely to be inadequate"

(Sverre Petterssen)

As a step to better understanding nocturnal drainage flows in general and valley drainage in particular, experiments were conducted with a numerical flow model. The model was initialised to match an idealised atmosphere, and run for several hours of nocturnal (radiational) surface cooling. It was anticipated that by exploring relatively simple physical configurations, insights might be gained which would be applicable to more complex situations.

The choice of a numerical model was between constructing and programming a simple one or two dimensional model, or using a more complex model package written by others. There are advantages and dis-advantages to both approaches, but the author was somewhat predisposed by previous experience as an operational meteorologist using synoptic scale models.

6.1 Numerical Experimental Method

Experimental investigations of fluid flow with numerical models fall in a spectrum between two extremes. One choice is to use a simple (non-atmospheric) model with well defined and understood simplifications. The limitations of the model are fairly obvious and the model will hopefully produce insights into a physical process within these constraints. In general the simplicity of the model

makes for computational economy and numerous variations can be explored. Simple models are applicable to a small class of problems and are illuminating for only specific portions of a flow, or specific influences on the flow.

At the other end of the scale are models which represent almost all aspects of real atmospheric flow and have complex parameterizations for unresolved portions and processes. Models of this sophistication are the work of numerous developers, and constructed by collecting simpler models. It would strain any single individual to consistently comprehend the processes within the model. This type of model is applicable to a wide range of flows, has a high computational expense, and tends to be used like a "black box".

The final decision was to proceed with a model which had exhibited skill in dealing with a wide range of scales and processes. The principal scale of our interest was to resolve flow, on the order of kilometres horizontally, and tens of metres in the vertical. The choice was made to use the Mesoscale Community Compressible Model (MC2) developed by Recherche en Prévision Numérique (RPN), a division of the Canadian Meteorological Centre (CMC) of Environment Canada (EC). This model has been used on a wide range of scales from synoptic development of mid-latitude cyclones (Tanguay et al , 1990), to a supersonic projectile through a domain the size of a coffee mug (with a modified version) This model is highly regarded internationally and has been anecdotally claimed as having contributed to Australia's win of the America's cup, by accurate prediction of near-shore breezes.

6.2 Overview of the Mesoscale Compressible Community Model (MC2)

MC2 is a nested regional model with lateral boundary conditions provided by a global or hemispheric model. The model can be used at all scales since it uses a fully elastic set of Euler equations with a semi-implicit, semi-Lagrangian integration scheme. The model is coded in accordance with standards at CMC and uses the standard physical parameterization routines in use for the synoptic scale models. A comprehensive description of the model is available in Bergeron et al. (1994).

As the name implies, MC2 is intended as a model to resolve mesoscale processes. This implies horizontal resolution on the order of kilometres and vertical resolution on the order of hundreds of metres. The preceding chapters on other valley studies suggest that this will not be entirely satisfactory since the surface layer and the lower boundary layer contain a good deal of the structure of interest in drainage flows. In its current form (Spring 1995), the first calculation level is fixed at 80 metres (Gal-Chen metres) above ground (to optimise performance of the physics package), with gradually increasing layer depths above. In the hope of eventually extending the current work to specific case studies with MC2, it was anticipated that the benefits of a model which can incorporate operational model output, would outweigh the disadvantage of limited resolution in the surface and lower boundary layer.

6.2.1 Model Equations and Co-ordinates

Euler equations form the basis of MC2, which in generalised co-ordinates are:

$$\frac{dU}{dt} = fV - K\frac{\partial S}{\partial X} - RT\frac{\partial q}{\partial X} + F_X \quad (6.1)$$

$$\frac{dV}{dt} = -fU - K\frac{\partial q}{\partial Y} + F_Y \quad (6.2)$$

$$\frac{dw}{dt} = -g - RT\frac{\partial q}{\partial z} + F_z \quad (6.3)$$

$$(1 - \alpha)\frac{dq}{dt} = -S\left(\frac{\partial U}{\partial X} + \frac{\partial V}{\partial Y}\right) - \frac{\partial w}{\partial z} + \frac{L}{T} \quad (6.4)$$

$$\frac{dT}{dt} = \alpha T\frac{dq}{dt} + L \quad (6.5)$$

$$\frac{dM}{dt} = E \quad (6.6)$$

$$\frac{dC}{dt} = B \quad (6.7)$$

U, V and w are the velocity components, q is a modified pressure co-ordinate

$\left(q = \ln\left(\frac{p}{p_0}\right)\right)$, $F_{X,Y,Z}$ are sources or sinks of momentum corresponding to their subscript, $\alpha = \frac{R}{C_p}$, S is the metric map projection term, L represents heat sources or sinks, M is specific humidity, E represents sources or sinks of vapour, C is liquid water content and B is sources or sinks of liquid water.

MC2 uses a transformed vertical co-ordinate, Z, which is a monotonic function of the geometric co-ordinate z to incorporate topography into the model.

Z is based on the Gal-Chen co-ordinate system where

$$\zeta(X, Y, z) = \left[\frac{z - h_0(X, Y)}{H - h_0(X, Y)} \right] H \quad (6.8)$$

which is the height in Gal-Chen units and $h_0(X, Y)$ is the topography height

function. At the ground level, $Z=0$ is terrain following, whereas at the top of the

model atmosphere $Z=H$, corresponds to a constant z. MC2 uses a hybrid of the

Gal-Chen co-ordinate obtained by stretching or compressing the Gal-Chen

co-ordinate vertically. This results in a co-ordinate

$$Z = Z(\zeta(X, Y, z)) \quad (6.9)$$

which allows variable spacing of the vertical grid to apply maximum resolution in the area of interest.

Spatial discretization uses a staggered grid in the horizontal and vertical. In the vertical, even index levels are called momentum levels and carry the variables U, V and q' (departure of modified pressure from hydrostatic). Intermediate levels are called thermodynamic levels and carry w (z co-ordinate), W (Z co-ordinate), T' (temperature departure from a constant), M , and C .

6.2.2 Pre-processor Module

Geophysical data and boundary conditions are prepared for the time integration by a pre-processor program (PILMC2). This program incorporates the climatic fields of soil moisture, land-sea mask, albedo and other geophysical parameters into boundary files for the model. The primary purpose of this module is to determine the vertical placement of the computational levels and vertically interpolate the boundary data fields provided by larger-scale models or analysis. A list of switches in a control file, determines how PILMC2 prepares the fields for integration. Topographic information, for example, can be excluded or included.

6.2.3 Integration Module

The main module of the program (MC2) integrates in time, the number of prescribed time steps from the pre-processor. The integration can be preceded by a dynamic initialisation in which the model is stepped forward and backward in time a number of time-steps to bring the model toward dynamic balance. In this process there is no consideration of unresolved scales or processes (physics).

The integration can be performed with any of several advection schemes, and in a hydrostatic or non-hydrostatic mode. The model can be run without physical parameterizations, with simple parameterizations, or with a complete package of physics for unresolved scales and processes. The horizontal diffusion coefficient can be specified, as well as the size of the nesting zone.

6.2.4 Model Physics

MC2 uses the same physics package as the Regional Finite Element (RFE) Model and the Canadian Spectral Model. This set of parameterizations is typical of modern medium range models, and balances the best available algorithms for unresolved processes against computational expense. A full description is available in Mailhot (1994) and only the portions of particular interest to the following cases will be highlighted briefly.

The turbulent vertical diffusion is handled with a one and one half order gradient transfer model (as described in Chapter 3). The physics package solves for the turbulent kinetic energy, E , and then

$$K_{\psi} = \frac{c\lambda\sqrt{E}}{\phi_{\psi}} \quad (6.10)$$

where c is a constant and λ is determined by

$$\lambda = \min [k(z + z_0), \lambda_e] \quad (6.11)$$

where k is von Karman's constant (0.4), z_0 is the roughness length and λ_e is the asymptotic value for large z (200 metres). The stability functions for equation

6.11 are, for the unstable case (Ri less than 0)

$$\phi_M^2 = \phi_T = (1 - 20Ri)^{-0.5} \quad (6.12)$$

and for the stable case (Ri greater than 0)

$$\phi_M = \phi_T = 1 + 5Ri \quad (6.13)$$

The Richardson number is the gradient form

$$Ri = \frac{g}{\theta_v} \frac{\frac{\partial \theta_v}{\partial z}}{\left(\frac{\partial u}{\partial z}\right)^2 + \left(\frac{\partial v}{\partial z}\right)^2} \quad (6.14)$$

where θ_v is the virtual potential temperature. There is no horizontal turbulent diffusion.

The surface layer treatment is based on Monin-Obukhov similarity theory and is assumed to have quasi-constant fluxes with height. In this layer Equation (6.10) can be simplified to an equilibrium form

$$K_\psi = \frac{\lambda u_*}{\phi_\psi} \quad (6.15)$$

so that turbulent kinetic energy (E) is not considered. Boundary fluxes are modelled by the bulk parameterization:

$$-\langle w'\psi' \rangle = C_\psi u_* (\psi_a - \psi_S) \quad (6.16)$$

where the subscript "a" implies the top of the surface layer and the subscript S implies the surface value. C is based on the bulk Richardson number for the surface layer

$$Ri_B = \frac{g}{\theta_{vS}} \frac{\theta_{va} - \theta_{vS}}{u_a^2 + u_w^2} z_a \quad (6.17)$$

and in the stable case ($Ri_B > 0$) the transfer coefficient becomes

$$C_\psi = \frac{k}{\ln \frac{z_a + z_0}{z_0} (1 + 5Ri_B)} \quad (6.18)$$

The surface layer is arbitrarily set to the height of the first active level in the model, which for MC2 is 80 (Gal-Chen) metres deep.

Surface budgets of heat and moisture were simplified in the experimental runs by setting the atmosphere to be very dry, the model running times to darkness hours, and moisture processes off. Gravity wave drag, moist convective processes

and resolved condensation also were turned off. This left clear skies, and no cloud was "generated" by the physics package.

Dynamic forcing during model runs was nocturnal surface radiative cooling, driven by an excess of outward longwave radiation over incoming. Two longwave schemes are available in the physics package; we used the more complex and computationally intensive Garand type scheme, updated every 30 minutes of integration time. This scheme uses complex emission and absorption balance, for numerous wavelength bands based on water vapour, carbon dioxide, ozone and cloud. There is no consideration of topographic effects, such as a radiating surface which is not horizontal, or sky view, where a steep walled valley or canyon would receive radiation back from other ground surfaces. A detailed description of this radiation scheme is available in Garand and Mailhot (1990).

6.2.5 Nesting and Boundary Conditions

The prescription of boundary conditions is accomplished in essentially three different ways for MC2. The surface conditions of model skin temperature, albedo, roughness length, etc. are defined from climate values, or measured (or modelled) values. These are written to arrays which correspond to computational points for use in model calculations.

Horizontal boundaries require as a minimum, starting and ending values for the fundamental model variables of velocity, temperature, moisture and geopotential heights of pressure surfaces, which are then interpolated between prescription times by the pre-processor. A horizontal nesting scheme addresses

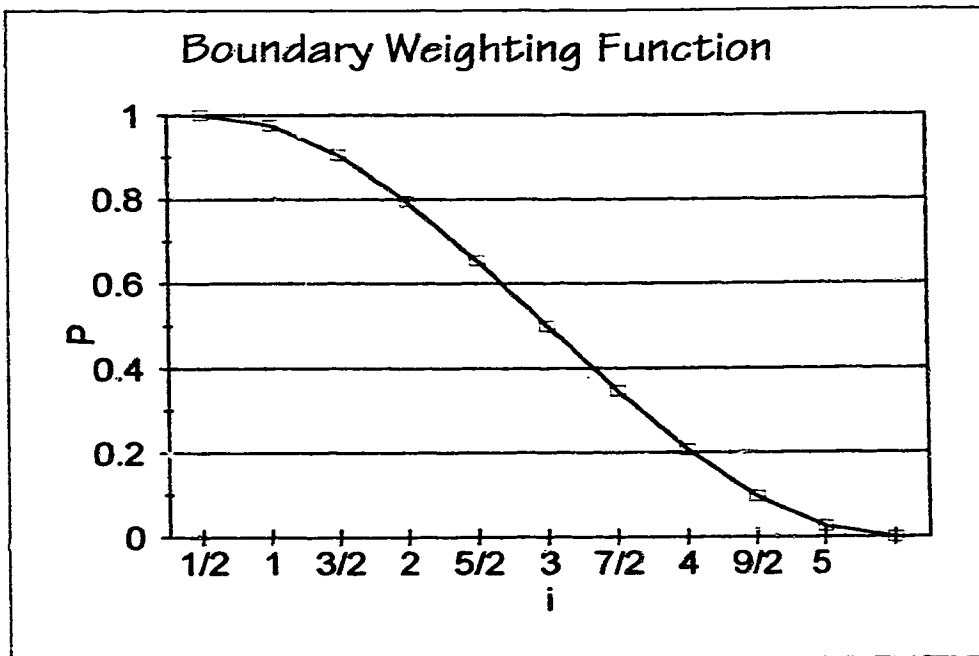


Figure (6.1) Weighting function for variables from boundary and interior points where i is the gridpoint distance from the boundary.

the risk of abruptly shocking the model with boundary conditions, and to minimize boundary reflection of model values. In this scheme values at interior points near the boundaries are spatially filtered, using a weighting function to ensure a smooth transition to the external boundary values (Figure 6.1). This leaves a zone around the outside of the model domain with values blended from external conditions and internal model calculations.

A similar scheme is implemented at the model top: a sponge layer, or a vertical nesting layer, can be defined, in which external values are gradually blended into the model. This is particularly important where there may be vertical propagation of energy to the model lid such as gravity waves.

6.2.6 Post-Processing of Data

MC2 includes a post-processing module which converts the model values into a file format for further analysis and field viewing. The data can be output, either interpolated onto pressure levels, or directly on calculation surfaces (Gal Chen levels). Data was extracted for the experiments onto 15 defined pressure levels and the 25 Gal-Chen levels. The file format is compatible with a field viewer developed at RPN called XREC (Rêver En Couleurs), which enables viewing of horizontal grids of data, vertical data profiles and vertical cross-sections. The fields can be displayed with contours or colours to represent the data.

The MC2 distribution also comes with a library of functions to allow extraction and manipulation of data values or fields from the files. The output files for the model runs were large (on the order of 30 Megabytes) and so these utilities facilitated analysis of the enormous volumes of data.

6.2.7 Summary

This brief overview of MC2 does not do justice to its sophistication or complexity. We have generally assumed that the developers have made scientifically justifiable choices of structure, equations and parameterizations. This study has made no attempt to critique the methods of the model, and investigation of its structure has been focused on gaining sufficient understanding to correctly interpret results.

6.3 Drainage Flow Experiments

Experiments were conducted with MC2 using an idealised atmosphere over a flat plain, and in one of a series of sinusoidal valleys. The model was initially run with a horizontal grid spacing of 10 kilometres and a model top at 12000 metres, to provide boundary conditions for a nested run of the model. The final run was nested with a horizontal grid spacing of 2500 metres and a model lid at 6000 metres. The computational grid was 68 X 68 points, with 25 vertical calculation levels distributed automatically through the vertical domain.

6.3.1 Idealised Atmosphere

A program was written to generate an idealised atmosphere for use as initial and boundary conditions for the model (10 km grid spacing), with imposed

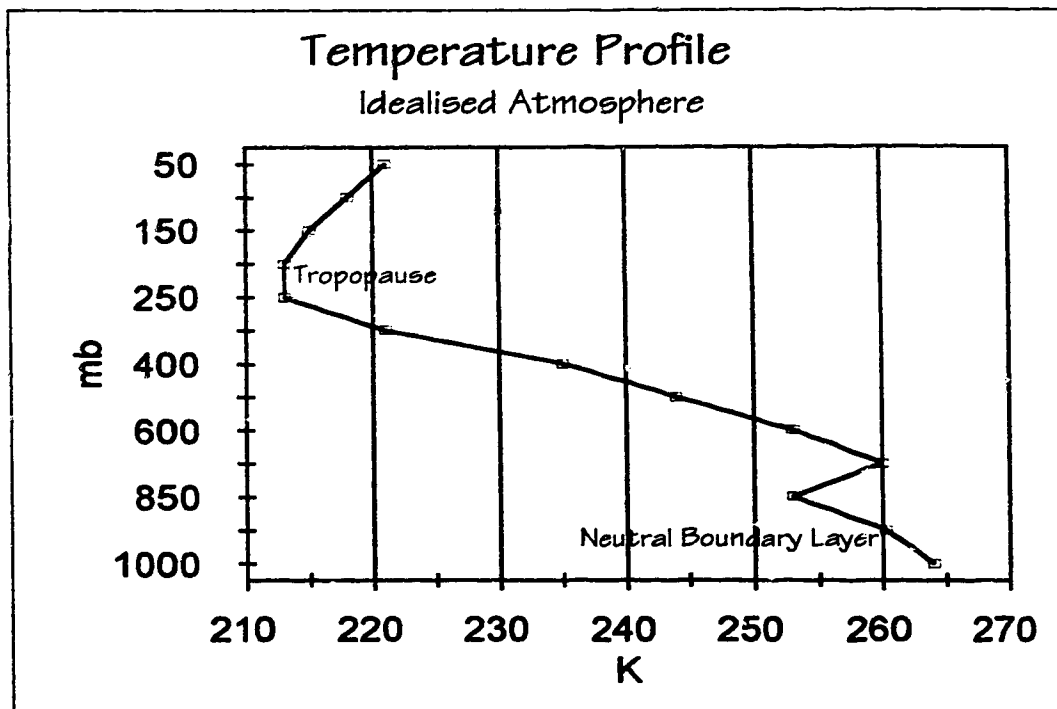


Figure (6.2) Temperature profile for idealised atmosphere at Southern point.

thermal stratification and pressure gradients. The idealised atmosphere began with a horizontally-uniform wind field defined by

$$\frac{U}{U_{850}} = \left\{ \begin{array}{ll} \left(\frac{1000-p}{150} \right)^{\frac{1}{7}} & p \geq 850 \\ 1 & p < 850 \end{array} \right\} \quad (6.19)$$

where U_{850} is an imposed wind at 850 mb (4 knots) and p is the pressure level for which winds are calculated. The V component was set to 0.0 m/s. From this field of wind velocities, the geopotential heights were calculated for the southernmost gridpoints, using an imposed thermal structure with a neutral boundary layer and typical winter profile above (Figure 6.2). The geopotential heights were calculated as

$$Z = \frac{-R\langle T \rangle}{g} \left(\ln \frac{p}{p_0} \right) \quad (6.20)$$

where p_0 is the surface pressure, p is the pressure level at Z , and $\langle T \rangle$ is the average potential temperature in the layer. The average temperature is a pressure weighted mean

$$\langle T \rangle \equiv \frac{\int_{p_0}^p T(p) d \ln p}{\int_{p_0}^p d \ln p} \quad (6.21)$$

The geopotential heights in the remainder of the grid were calculated from the geostrophic wind equation

$$U_g = \frac{g \nabla Z}{f} \quad (6.22)$$

Since U_g is given, the relation can be rearranged to

$$Z = Z_0 - \left(\frac{U_g f \Delta y}{g} \right) \quad (6.23)$$

where Z_0 is the height one grid length (Δy) south of the point in question. The temperatures across the grid were adjusted to account for the northward decrease in Z .

The other boundary conditions of the model were imposed uniformly over the domain. The values were chosen by selecting typical values over Yukon from a February synoptic scale model analysis (summarised in Table 6.1).

Parameter	Assigned Value	Unit	Typical Range
Albedo	0.7	none	0.0-1.0
Deep Soil Temperature	258	K	
Dew Point Depression	30	K	
Ice Cover	0	none	0.0-1.0
Land Sea Mask	0.96	none	0.0-1.0
Launching Height	40	m	
Sea Surface Temperature	253	K	
Snow Cover	1.0.	none	0.0-1.0
Soil Moisture Available	1	none	0.0-1.0
Surface Temperature	256	K	
Topography	0	m	
Roughness Length	0.4	ln(m)	

Table 6.1 Summary of boundary values used for idealised atmosphere simulations with MC2.

The goal of the experiments was to use a complex model to simulate simple meteorological situations. The first step was to simulate the development of a

nocturnal boundary layer in a horizontally homogeneous atmosphere, over a quasi-infinite flat plain.

6.3.2 Development of a Nocturnal Boundary Layer over a Flat Plain

The development of the nocturnal boundary layer has been examined using a one-space-dimensional prognostic model by Delage (1974):

$$\frac{\partial u}{\partial t} = fv + \frac{\partial}{\partial z} K \frac{\partial u}{\partial z} \quad (6.24)$$

$$\frac{\partial v}{\partial t} = f(u_G - u) + \frac{\partial}{\partial z} K \frac{\partial v}{\partial z} \quad (6.25)$$

$$\frac{\partial \theta}{\partial t} = \frac{\partial}{\partial z} K \frac{\partial \theta}{\partial z} \quad (6.26)$$

with $V_G=0$ and u_G specified. K was assumed to be

$$K = l\sqrt{cE} \quad (6.27)$$

where l is the mixing length (stability corrected in the manner of Blackadar), c is a proportionality constant (ratio of shear stress to TKE at equilibrium) and E is the turbulent kinetic energy. The Delage model was driven by imposed cooling of the ground. The results exhibited a dependence on the Rossby number

$$R_o = \frac{U_G}{z_0 f} \quad (6.28)$$

where z_0 is the roughness length. The second ratio which was influential was

$$D = \frac{g\theta_s}{\bar{\theta}U_G f} \quad (6.29)$$

where θ_s is a scaling potential temperature and $\bar{\theta}$ is the mean absolute potential temperature. Delage found that the night-time temperature inversion developed steadily with increasing time (Figure 6.3). A quasi-equilibrium state was reached when mixing became sufficiently suppressed that further cooling was inhibited by reduced TKE (Figure 6.5). During the development of the nocturnal BL the TKE

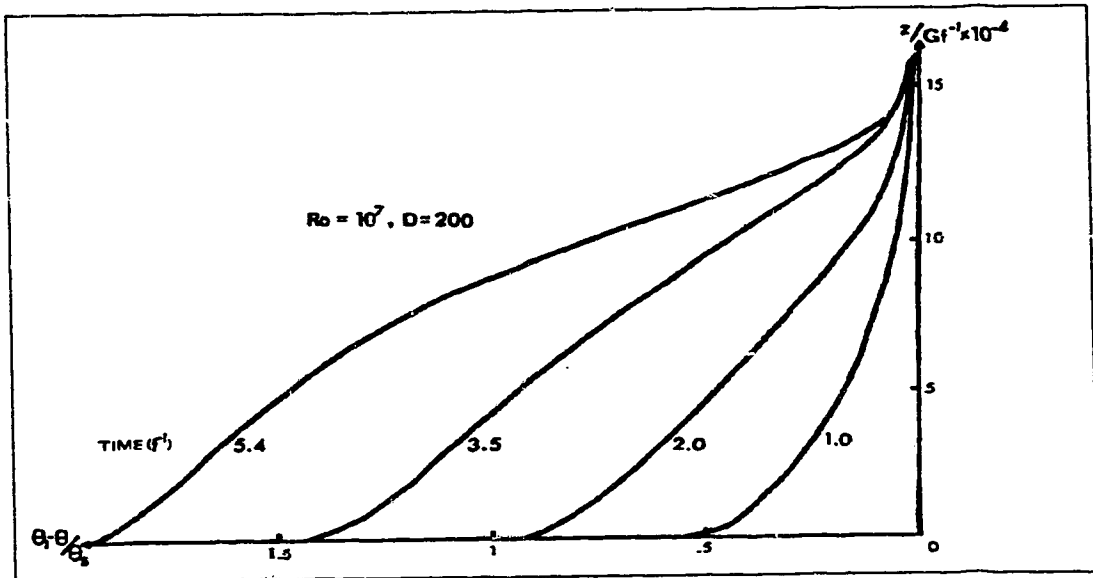


Figure (6.3) Profiles of θ at various times during the development of a nocturnal boundary layer over a flat plain. Here G is the geostrophic wind, and for θ the subscript s denotes a scaling value and the overbar denotes the mean absolute potential temperature. (After Delage 1974)

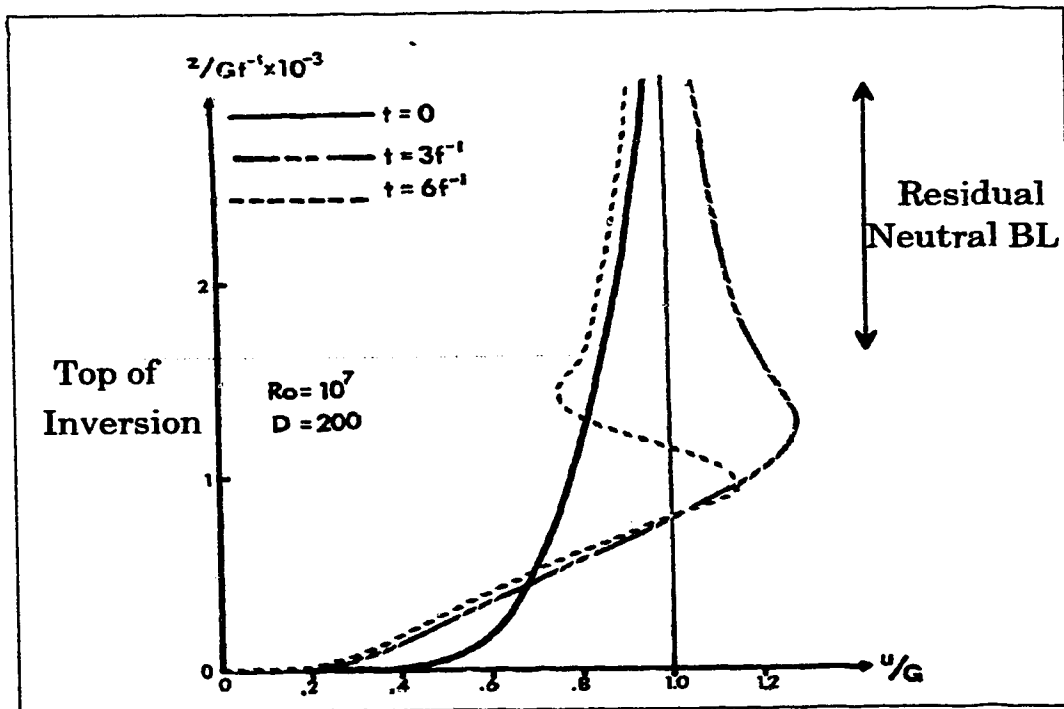


Figure (6.4) Wind Structure at three different times. Here G is the geostrophic wind. The wind accelerates above ground eventually developing into a shallow jet with a distinct speed minimum above. After Delage (1974)

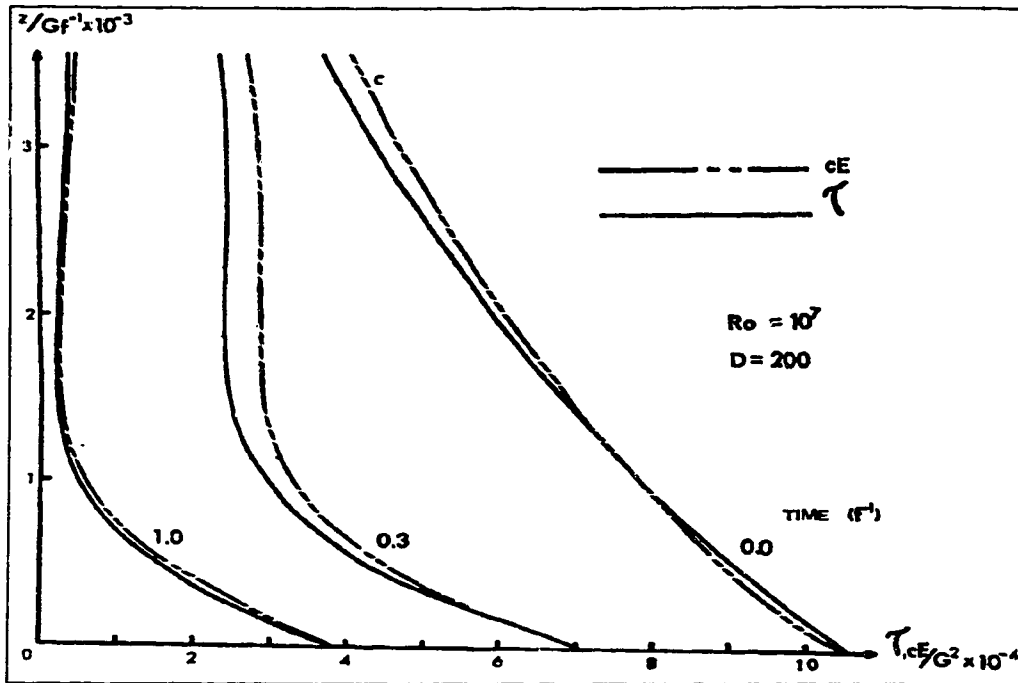


Figure (6.5) Vertical profiles of turbulent energy and shear stress at different times. Here G is the geostrophic wind and E is the turbulent kinetic energy. As time progresses the TKE is suppressed by increasing stability with the highest values near the surface. After Delage (1974)

and hence shear stress gradually decreased. The wind responded by becoming light near the surface, and developing a nocturnal jet near the top of the nocturnal BL (Figure 6.4).

Delage conducted his simulations under an assumption of a steady ground cooling rate, and steady-state external conditions, which he recognises as rare. Comparisons with observational data were qualitatively good and agreed well in terms of evolution over time. Delage concluded that explicit inclusion of radiation through a realistic surface energy balance should improve the results. He further concluded that the nocturnal Atmospheric Boundary Layer (ABL) structure cannot be described by a diagnostic model.

6.3.3 Development of a Nocturnal Boundary Layer with MC2

MC2 was used to simulate three hours of development of a nocturnal boundary layer over a flat plain, starting from the atmosphere described in Section 6.3.1. The model was run both with and without dynamic initialisation, with similar results. The timestep for the 10 km grid length was 120 seconds and was reduced to 30 seconds for the 2.5 kilometre grid.

The enormous volume of data from this simulation was examined for some essential features that could be compared with the work of Deige. The data were analysed by displaying model fields using XREC as well as averaging the values over a 8 X 8 grid of points located near the model center, to get horizontally averaged values remote from the boundaries. In general only averaged values will be discussed. At each pressure level the fields of temperature (data file pointer TT), u (UU),v (VV),w (WZ), geopotential height (GZ) and unresolved turbulent kinetic energy (TK) were averaged and standard deviations calculated. The temperature field was converted to potential temperature (θ). The standard deviation values permitted calculation of a spatially resolved large eddy TKE.

$$TKE_{R(resolved)} = \frac{1}{2} \sqrt{\sigma_u^2 + \sigma_v^2 + \sigma_w^2} \quad (6.30)$$

It must be emphasised that with a grid size of 2500 metres, only very large scale structures are resolved. These data were imported into a spreadsheet for further analysis and display.

Under the imposed conditions of a dry atmosphere and neglecting heat transfer to the ground the surface heat flux is approximately equal to the net infrared radiation at the ground.

$$Q_{H_0} \approx Q_* < 0 \quad (6.31)$$

The net infrared radiation

$$Q_* = L \downarrow - L \uparrow \quad (6.32)$$

is parameterized by the physics package. At $t=0$, $Q_* \approx -110 \text{ Wm}^{-2}$, while by $t=3$ hours, $Q_* \approx -85 \text{ Wm}^{-2}$. The surface temperature and hence outgoing longwave flux density ($L \uparrow$) is spatially constant throughout the domain, but air temperature decreases northward resulting in reduced incoming longwave flux density ($L \downarrow$).

This results in slightly greater net radiative losses over the northern portions of the domain. Over time the net radiation decreases everywhere, and tends toward a more uniform field across the domain. Sustained values on the order of $Q_* \approx -100 \text{ Wm}^{-2}$, are high compared to values some investigators have imposed

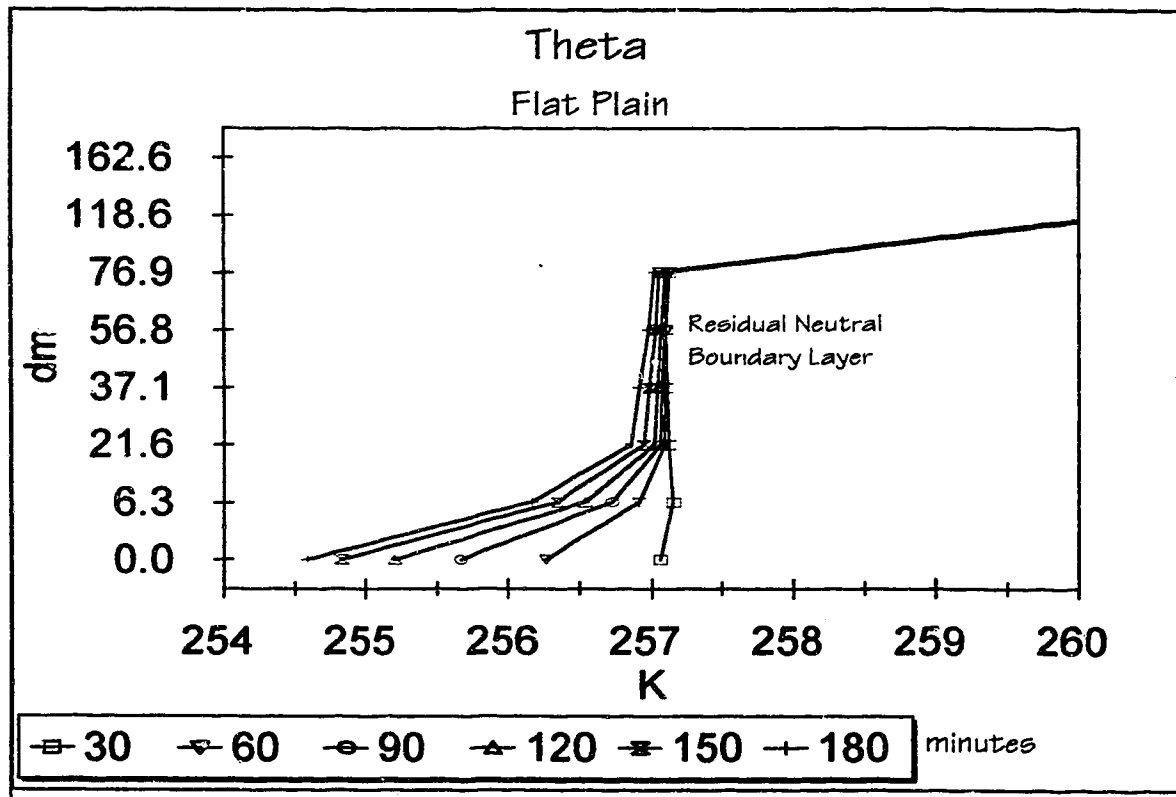


Figure (6.6) Evolution of the potential temperature profiles over a flat plain showing developing ground-based inversion into a residual neutral layer from nocturnal boundary layer simulation with MC2.

on models, such as Doran (1990) who, for a summer time event, started with $Q_* = 111 Wm^{-2}$ and decreased the value to $Q_* = 25 Wm^{-2}$ over four hours.

The development of the temperature profile with time, agrees qualitatively with Delage (Figure 6.6). The overall trend of cooling a layer near the ground while keeping a residual neutral boundary layer nearly unchanged is consistent with Delage. The rate of change of the potential temperature in the boundary layer decreases with time (i.e. $\frac{\partial \partial \theta}{\partial t} < 0$) which is also consistent with Delage. The increasing stability will tend to suppress turbulent mixing in the lower levels, hence decreasing the efficiency of cooling.

The spatially averaged wind profile (Figure 6.7) somewhat resembles the pattern of Delage. Due to lack of resolution, MC2 eclipses the region of strong

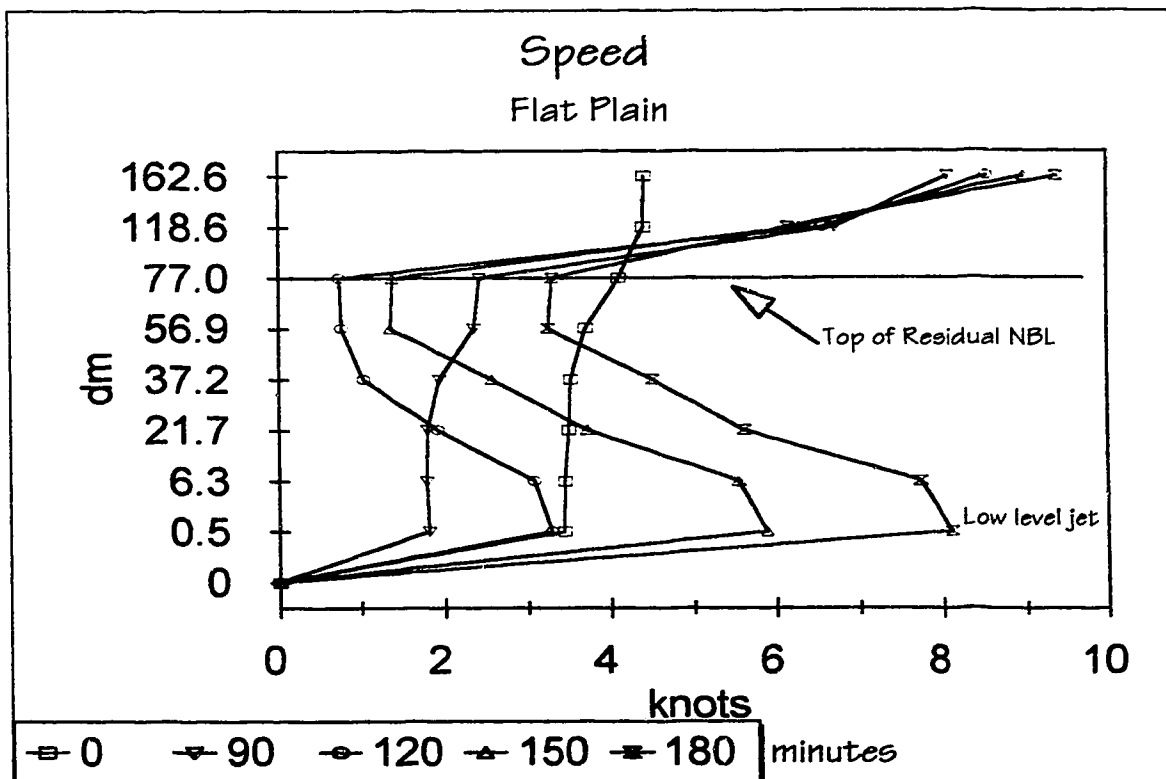


Figure (6.7) Spatially averaged wind speed over a flat plain from nocturnal boundary layer simulation with MC2. Indications of a low level jet are shown at anemometer height (5 m) with a probable stronger value unresolved above 0.5 dm.

shear below 80 metres. For the purpose of unscaling the Delage height, assuming a geostrophic wind near 10 m/s; the low level jet of Delage's model, should be located near 80 metres above ground. Since the first active calculation level in MC2 occurs near this level, it is not possible to accurately resolve the height of the MC2 jet. The magnitude of the averaged wind in this lower layer is consistent with a stronger unresolved jet.

The gradients in cooling rates across the domain translated into an increasing surface pressure gradient so that by the end of the integration a moderate gradient had developed. After three hours of integration, at 850 mb

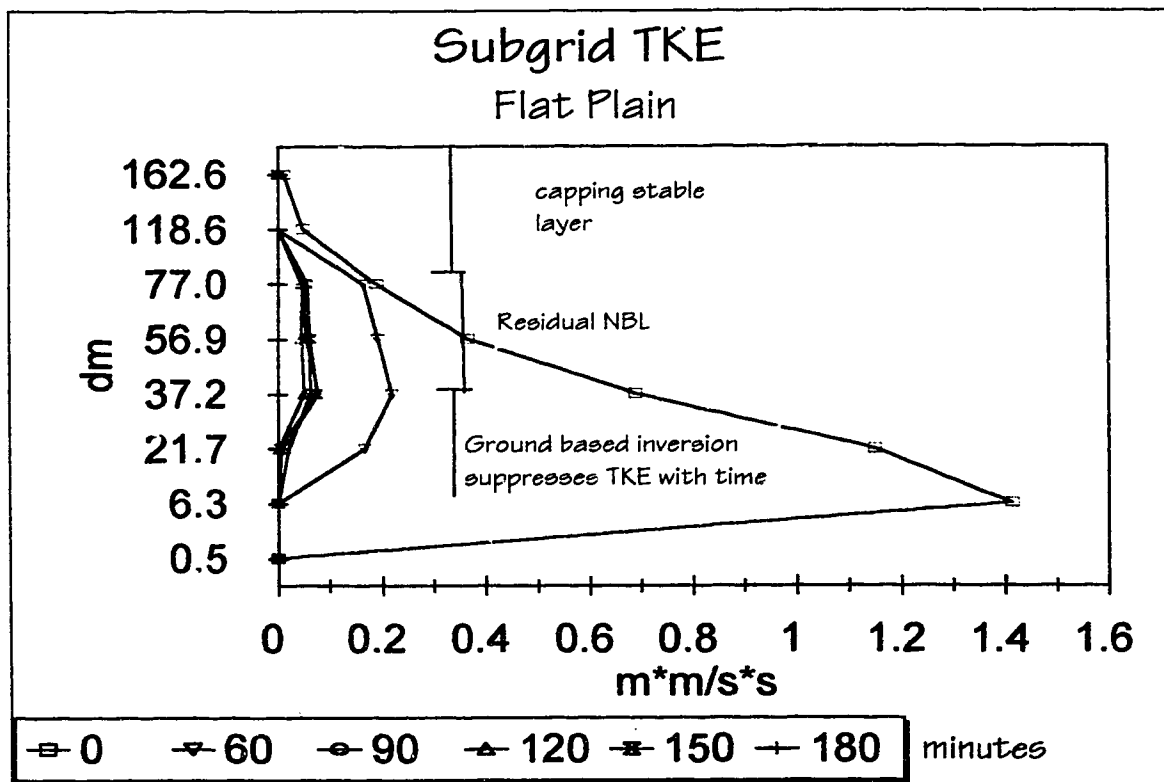


Figure (6.8) Sub-grid Turbulent Kinetic Energy (TKE) from the physics package for MC2. The model does not calculate TKE at or below the first calculation level (80m).

(about 1180 metres above ground) the gradient remains light with a geostrophic wind of about one (1) knot from 221°. This is understood to have amplified the anemometer level flow (0.5 dm)

The other field to consider is the turbulent kinetic energy (TKE) which Delage deduced. The unresolved TKE (Figure 6.8) is provided by the physics package, but TKE is not used in the surface layer by the physics, and hence TKE values are not calculated or stored for the first two levels. The overall trend of the unresolved TKE is to decrease sharply within the growing inversion, with lagging reduction in the residual neutral layer aloft.

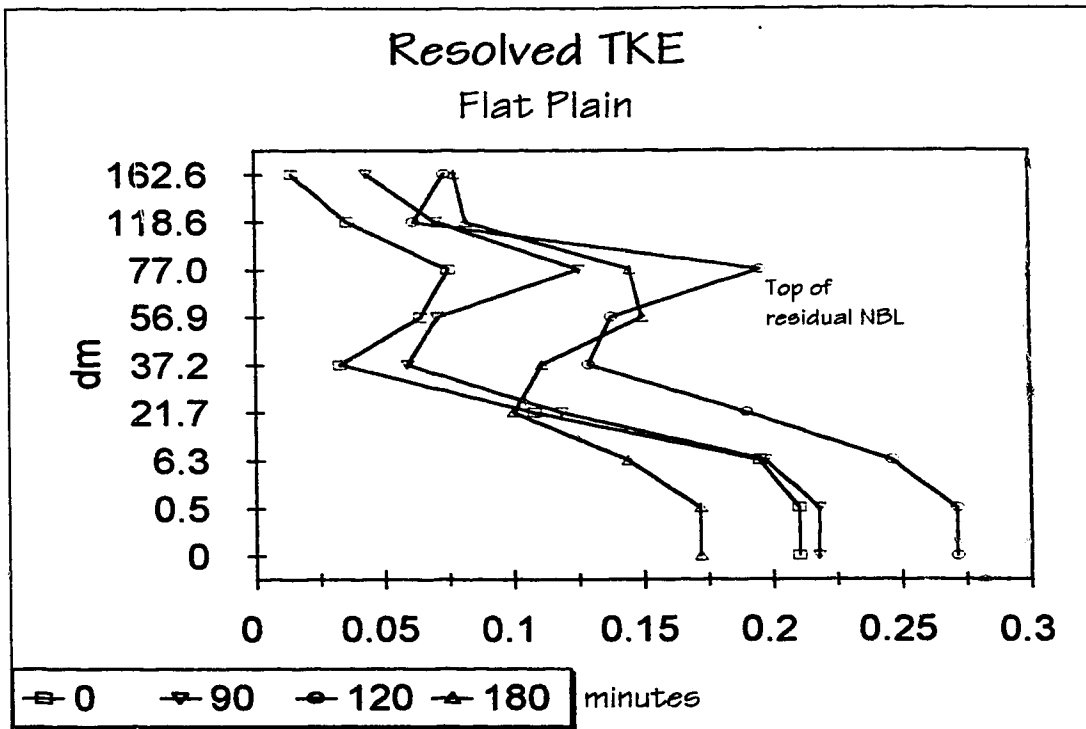


Figure (6.9) Spatially resolved "meso-eddy" TKE from MC2 nocturnal boundary layer simulations for a flat plain.

The spatially resolved "meso-eddy" TKE (Figure 6.9) was extracted from the data from MC2 as described above. The resolved TKE exhibits the highest values in the near ground layer in keeping with the expected pattern. There is little change in the low level TKE for the first 90 minutes and then an increase till 120 minutes. This is understood as the balance between increasing stability and accelerating low level windspeed in response to the increasing pressure gradient. Over the next 60 minutes the low level TKE decreases.

The study of an NBL with MC2 was intended for comparison with the work of Delage (1974). The developing horizontal pressure gradient and varying net surface radiation, contravene Delage's assumption of horizontal equilibrium. The change in radiation with time would have been an acceptable variant and should have generated a similar boundary layer to Delage. However the developing pressure gradient near the surface altered the flow in the low layers, so that significant differences from the results of Delage are to be expected.

This simulation has also demonstrated that it is not easy to set up a simple, physically reasonable situation with horizontal uniformity on a very large spatial scale. As an example, the imposition of a constant surface temperature across the field, while varying the air temperature, was unrealistic. A nocturnal BL simulation might be better performed by finding an actual meteorological case where there is persistent light flow, little atmospheric moisture and little change in large-scale conditions over time. The atmosphere tends toward a natural balance and a realistic model, such as MC2, will tend to adjust the numerical atmosphere

toward this balance. A real data set for use as boundary conditions would ensure that any results would only come from model representation of physical processes and not the attempts of the model to balance artificially imposed conditions. This also raises a warning that further variations to the boundary conditions might be fraught with hazard.

6.3.4 Development of the Nocturnal Boundary Layer in a Valley with MC2

Further complexities were introduced to MC2 to simulate the development of a nocturnal boundary layer in an infinite sinusoidal valley. The atmosphere was initialised as for the flat plain case, but a series of sinusoidal valleys were introduced as topography to the boundary files, for the 10 km grid spacing. The valleys were 113 kilometres wide at the ridge ($W_v = 113$ km) with a depth (ridge-trough) of 2400 metres. The surface (ground) temperature field was altered with elevation (at a similar rate to air temperature), and to reflect the northward decrease in air temperature. The initial conditions and some descriptive dimensionless ratios are presented in Table 6.2. Based on our discussion in Chapter 4, we would expect this flow to be stagnant, with no gravity waves and a drainage flow weaker than that observed in Brush Creek studies.

The high resolution run of the model, with a grid spacing of 2500 metres, covered slightly more than one pair of ridges and the intervening valley, with a timestep of 10 seconds (the timestep for the 10 kilometre grid length was 120 seconds).

	Idealised Valley	Brush Creek (Doran 1990)
W_v	113 kilometres	4 kilometres
D	2400 metres	700 metres
U_E	2.2 m/s (4 knots)	2 m/s
θ_0	273 K	assumed 273 K
$\frac{\partial \theta}{\partial z}$	9.88×10^{-3} K/m	4.5×10^{-4} K/m
$\langle w'\theta' \rangle_G$	-1.8×10^{-2} mK/s	-1.1×10^{-1} mK/s (initially)
$O = \frac{W_v}{D}$	47	5.7
$TAF = \frac{W_v D}{A_{\text{valley section}}}$	2	2
$F_R = \frac{U_E}{D \sqrt{\frac{g}{\theta_0} \frac{\partial \theta}{\partial z}}}$	0.05	0.7
$B_P = \frac{\langle w'\theta' \rangle_G}{\theta_0 \sqrt{gH_v}}$	-6.3×10^{-8}	-2.0×10^{-5}
$C_E = \frac{U_E^2}{gD}$	1.7×10^{-4}	5.8×10^{-4}

Table 6.2 Summary of initial variables and dimensionless parameters for MC2 simulation of nocturnal boundary layer in a sinusoidal valley. Values used by Doran (1990) in his simulation of a strong drainage case are presented for comparison.

Data were stored at 30 minute intervals over the four hour integration.

This produced an enormous volume of data which was processed in a similar manner to the flat plain case, seeking indications of a drainage flow; development of an along valley jet and variable cooling rates according to valley location. Five locations across the valley were selected for evaluation of the flow (ridges, mid-slope and valley bottom).

The averaged values (calculated from a sample of 75 grid points characterising the domain; narrow in x long in y) for U and W, exhibited

$\frac{\sigma_{U,V}}{U,V} \approx 1 - 3$. This is indicative of a highly variable flow along the y-axis, consistent with our anticipation of a strong three-dimensional component to valley flows. Further examination of some data indicated that the vertical interpolation scheme used to extract data on set pressure levels, produced averaged values of wind for anemometer height that obscured the structure the model had resolved. This prompted further processing of the data and output files were generated using the (25) calculation levels (Gal-Chen levels).

Gal-Chen heights above ground vary according to the underlying terrain and height above the terrain (equation 2.55). For the 80 G-C (Gal-Chen) metre level, the actual height above ground is; at the ridge top (2400 metres) 48 metres above ground; at the mid point (1200 metres) 64 metres above ground; and 80 metres at valley centre.

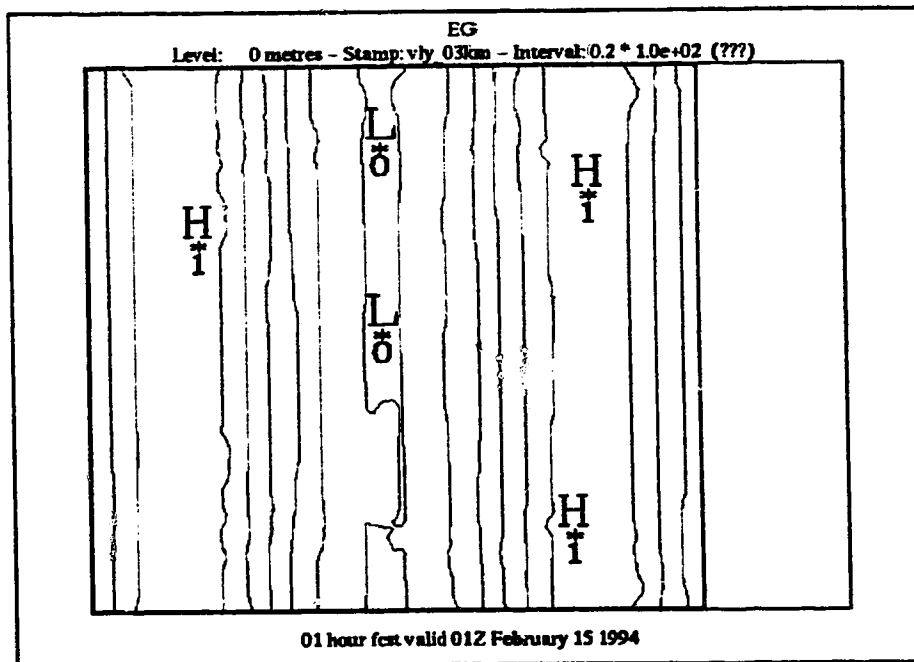


Figure (6.10) Model net infrared radiation at the surface (X 10 W/m²) over sinusoidal valley from nocturnal simulation with MC2.

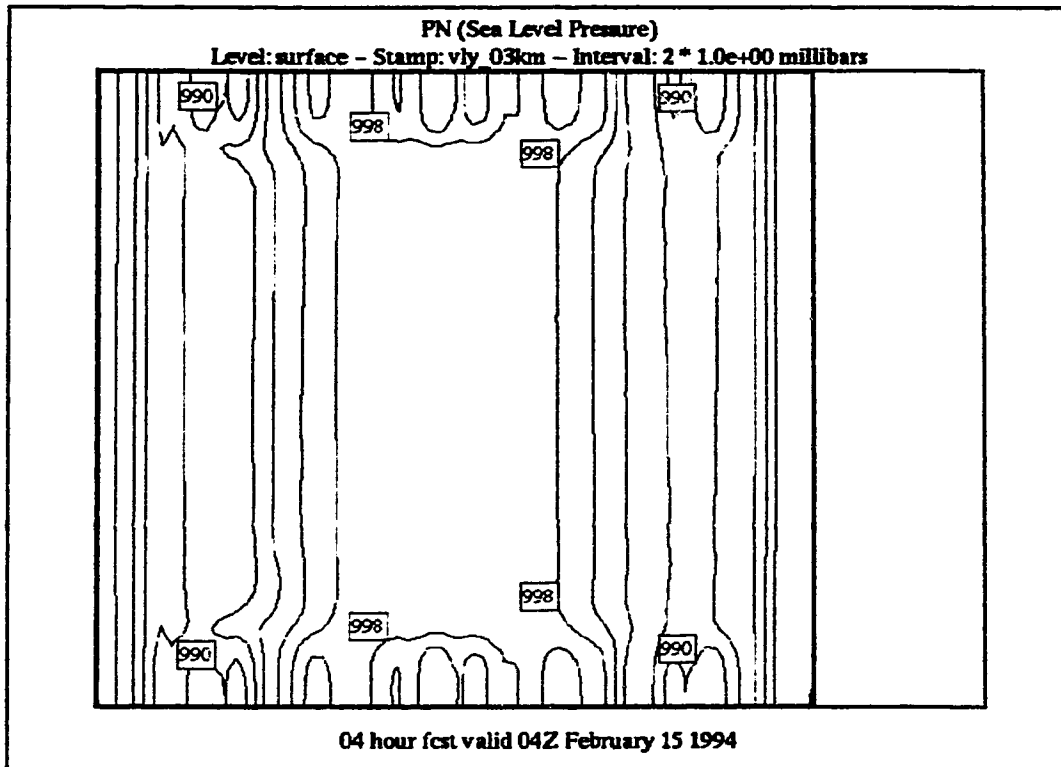


Figure (6.11) Mean sea level pressure from nocturnal valley simulation. Pressure is in millibars. The geostrophic gradient from ridge top to valley centre is on the order of 70 m/s.

The net surface infrared radiation after one hour of integration (Figure 6.10) showed values around 100 W/m^2 (i.e. heat gain) along the ridges and about -18 W/m^2 in the valley. This diminishes slightly with time and by four hours the ridges show values near 70 W/m^2 and the valley bottom is nearer -16 W/m^2 . Thus the numerical flow has been subjected to net radiational cooling at the ground in the valley centre but has received a substantial net gain along the ridges.

This result is surprising since a cloud free, night-time situation with light flow was simulated. Re-examination of the imposed boundary conditions revealed that the imposed ground temperature was inconsistent with the vertical temperature profile. The ground temperature was assumed to decrease linearly

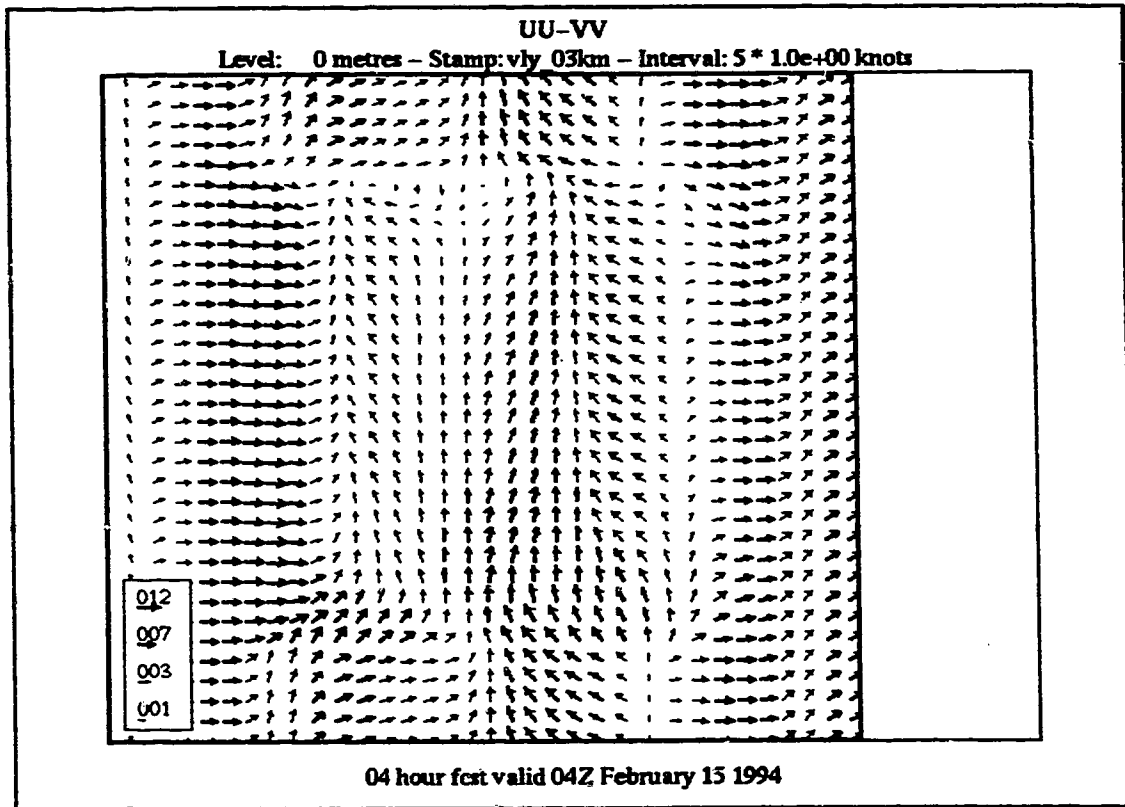


Figure (6.12.) Anemometer height (5m) wind for nocturnal valley simulation with MC2. Location of ridges denoted by R and valley by V.

from the valley bottom to the ridge, whereas the air temperature was neutrally buoyant near the surface with an inversion layer above. This resulted in a deep layer of air above the valley floor which was warmer than the ground temperature.

The simulation began with a nearly uniform mean sea level (MSL) pressure field but over the simulation the pressure fell less in the valley, than along the ridges, and by four hours there is a strong gradient (Figure 6.11). This gradient is likely a result of the air-ground temperature difference and may also be partly an artefact of the method of reduction to sea level. The existence of an uphill pressure gradient at the ground caused winds at the lowest calculation level

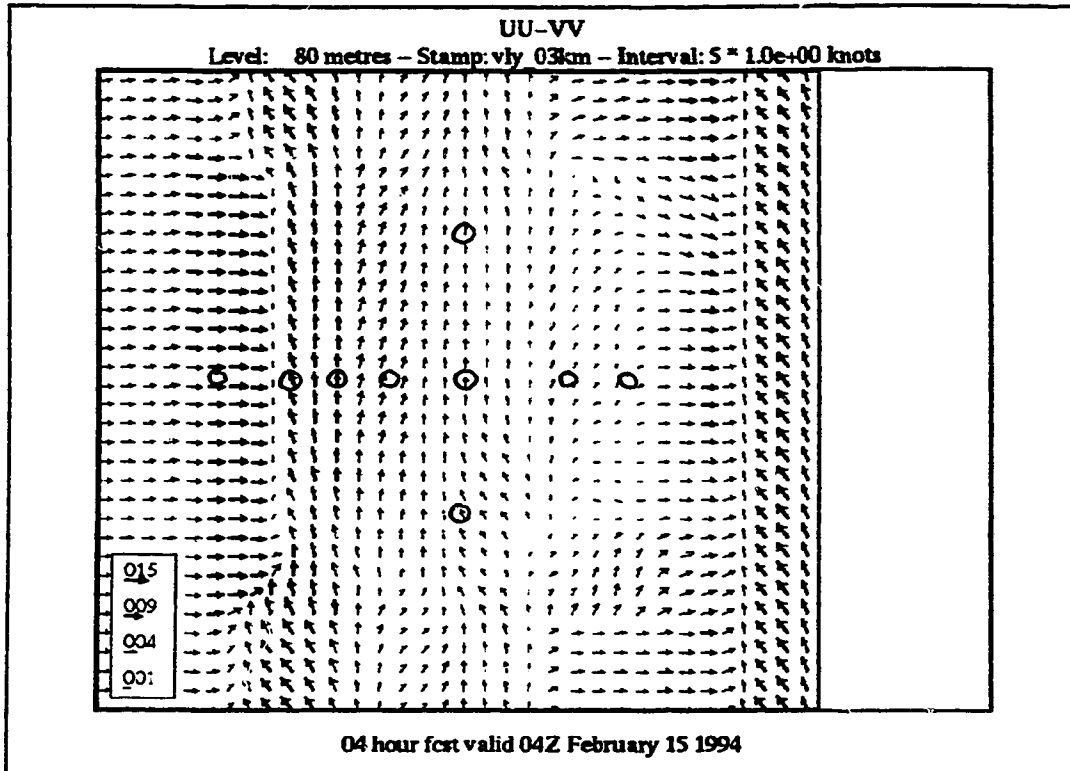


Figure (6.13) Winds at the first calculation level of the model in the nocturnal valley simulation. The first level is 80 G-G metres which is 48 metres above the ground at ridgetop, 64 metres at mid-slope and 80 metres in the valley centre. Circles denote locations of vertical wind profiles shown in Figures (6.14-6.22).

(anemometer height; 5 metres) shown in Figure (6.12), to blow upslope at some points along both sides of the valley, nearly at right angles to the isobars (Figure 6.11). As a result, at this level we do not consistently see the drainage flow expected but rather, a pressure influenced flow which is likely an artefact of our manipulation of the boundary and initial conditions. The winds at the 80 G-C metre calculation level (Figure 6.13) exhibit similar variations with both upslope and downslope flow, of similar or slightly smaller magnitude than at the surface.

Vertical profiles of the U component at points across the valley are shown in figures (6.14 - 6.19) (profile locations are identified on Figure 6.13 by circles).

The shear, at some locations, between the surface and 80 G-C metres is physically

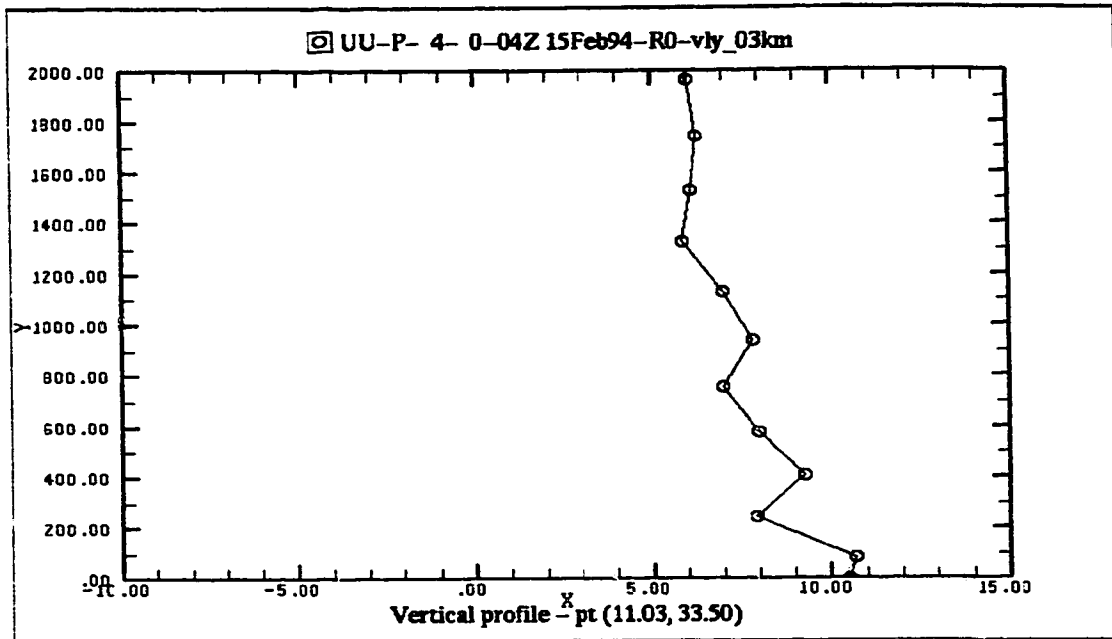


Figure (6.14) Vertical profile of U component at West ridgetop from nocturnal valley simulation after four hours of integration. Height is in Gal-Chen metres and speed is in knots. ($X=0$; $Z_0=2400$ metres)

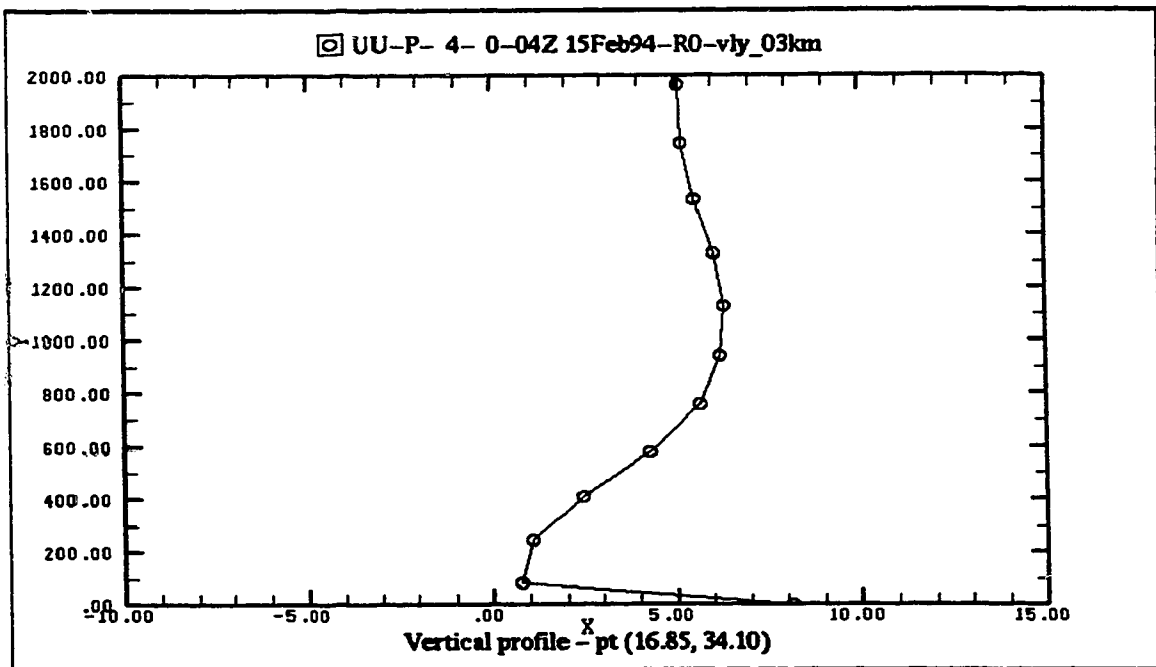


Figure (6.15) Vertical profile of U component on West slope from nocturnal valley simulation after four hours of integration. Height is in Gal-Chen metres and speed is in knots ($X=15$ kilometres; $Z_0=1800$ metres)

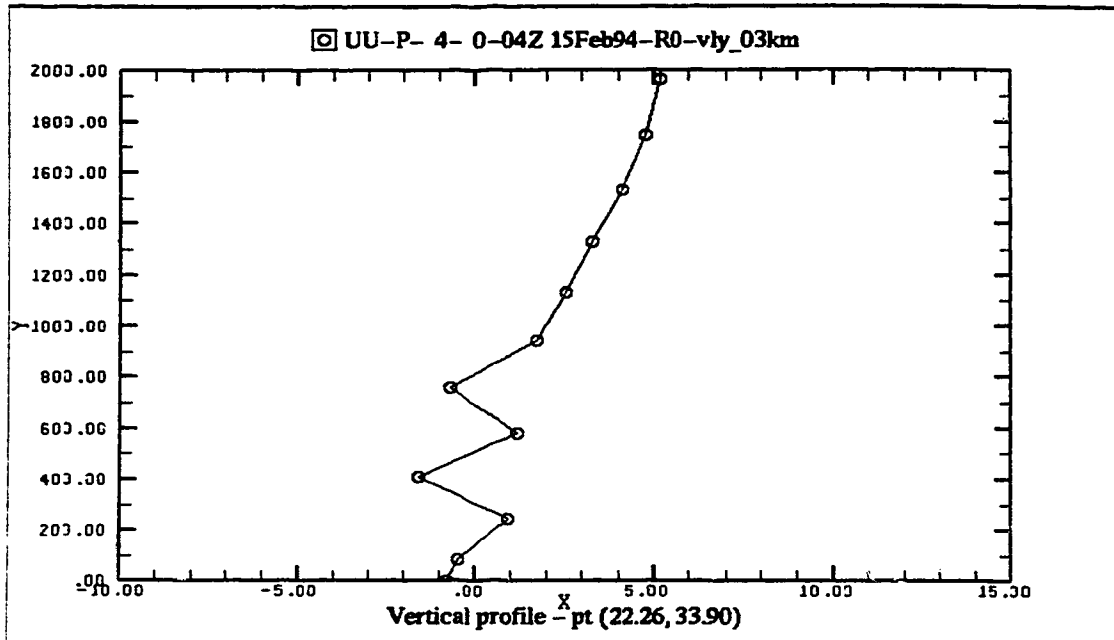


Figure (6.16) Vertical profile of U component middle of West slope from nocturnal valley simulation after four hours of integration. Height is in Gal-Chen metres and speed is in knots ($X=27.5$ kilometres; $Z_r=1200$ metres)

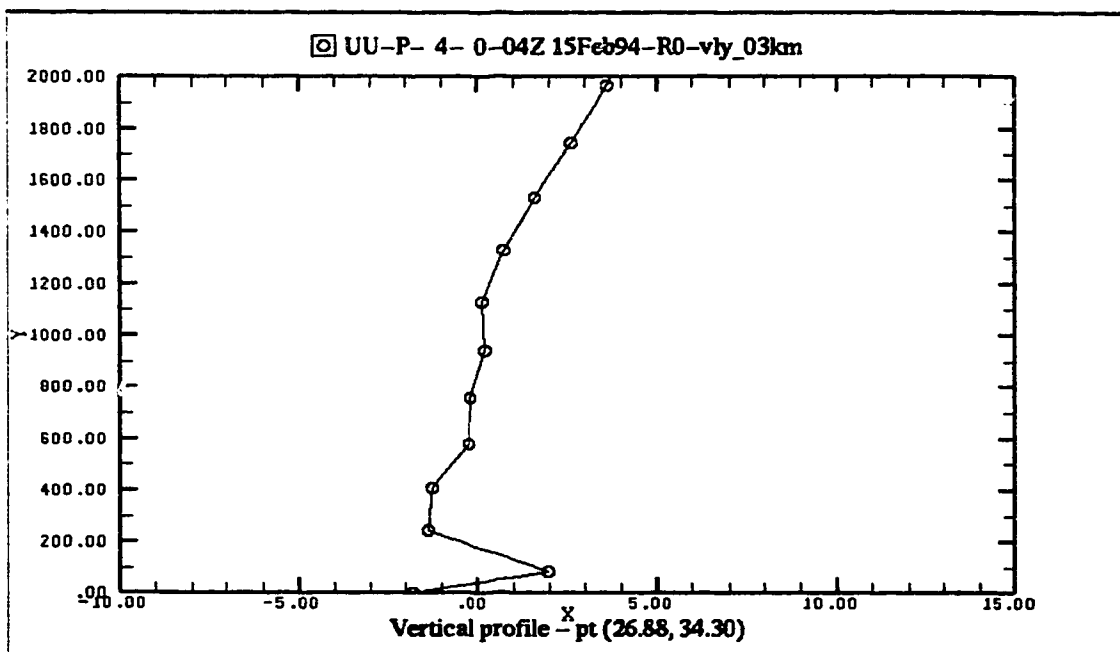


Figure (6.17) Vertical profile of U component on West slope from nocturnal valley simulation after four hours of integration. Height is in Gal-Chen metres and speed is in knots ($X=40$ kilometres; $Z_0=600$ metres)

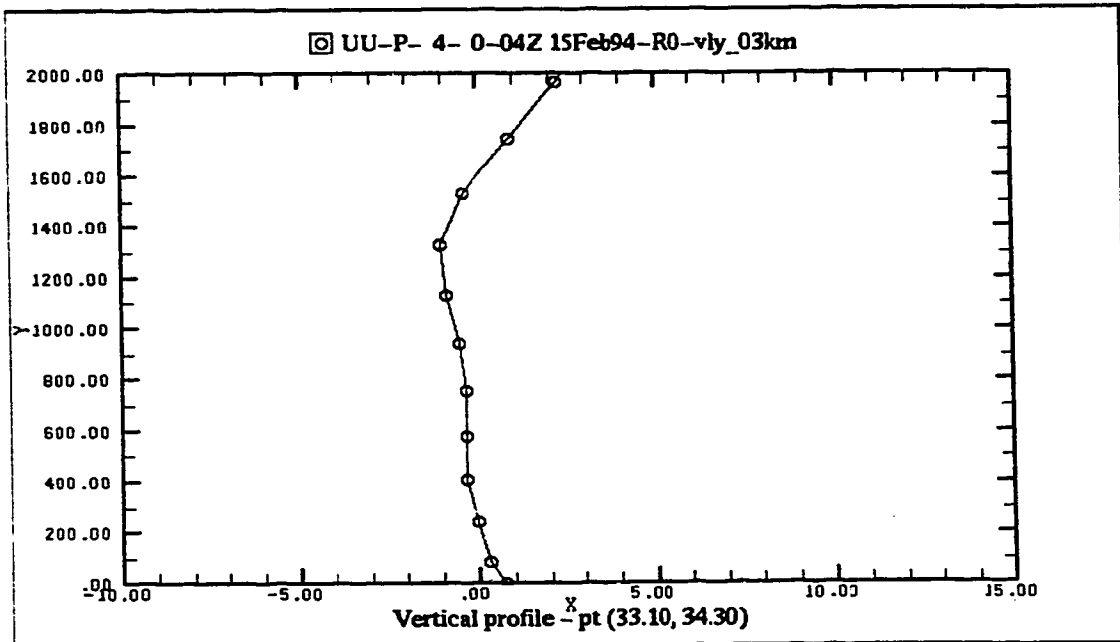


Figure (6.18) Vertical profile of U component at valley centre from nocturnal valley simulation after four hours of integration. Height is in Gal-Chen metres and speed is in knots (X=55 kilometres; $Z_0=0$)

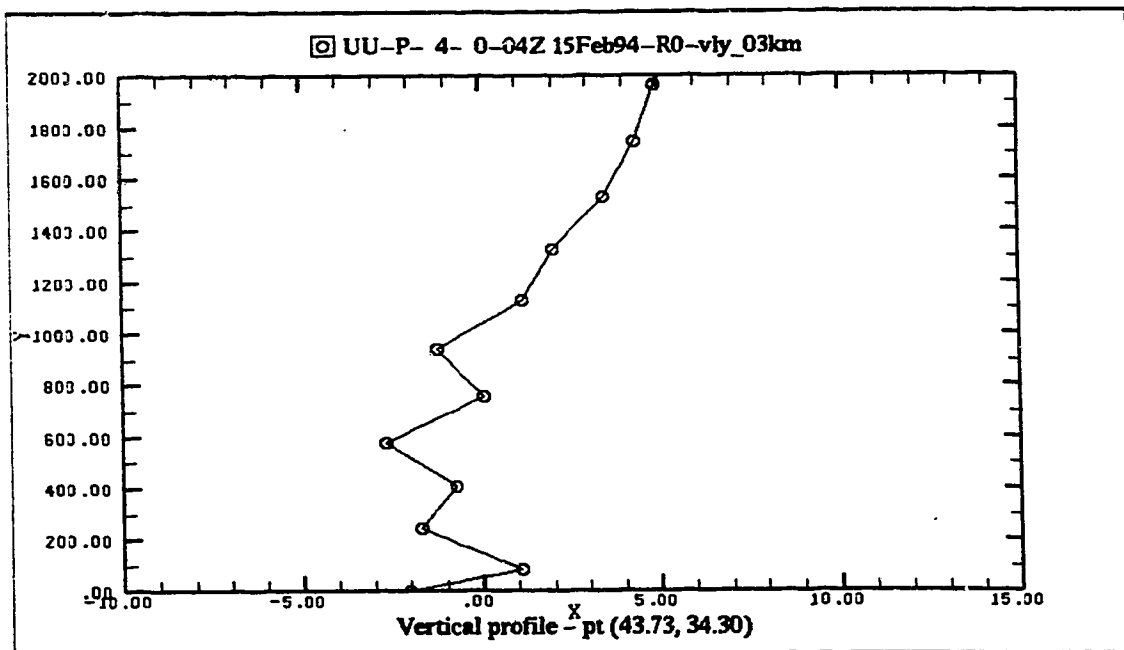


Figure (6.19) Vertical profile of U component on East slope from nocturnal valley simulation after four hours of integration. Height is in Gal-Chen metres and speed is in knots (X=82.5 kilometres; $Z_0=1200$ metres)

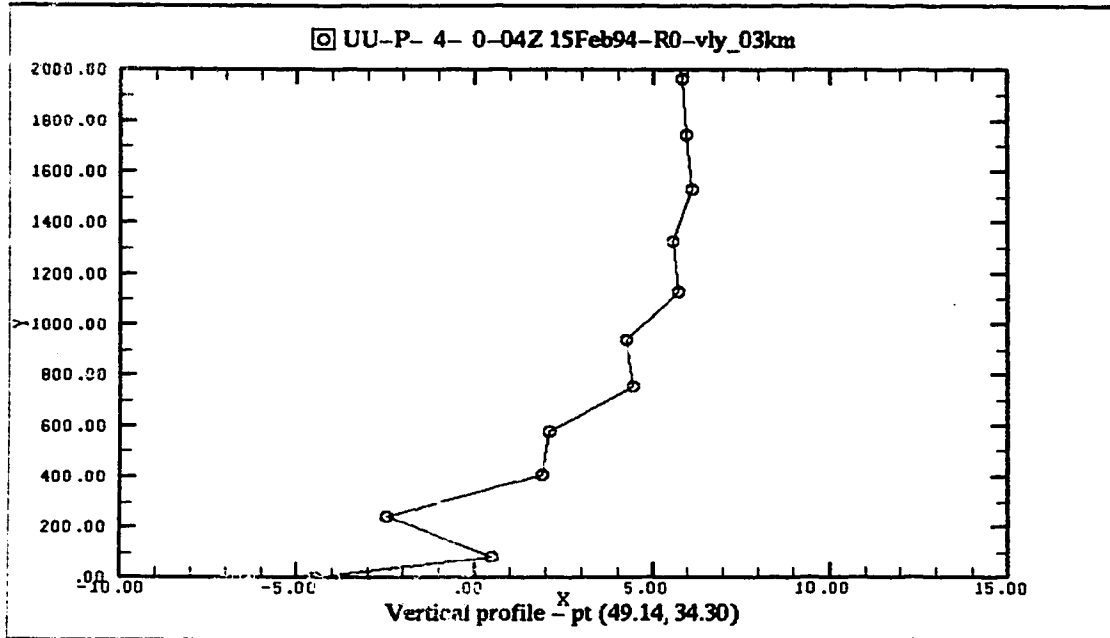


Figure (6.20) Vertical profile of U component on East slope from nocturnal valley simulation after four hours of integration. Height is in Gal-Chen metres and speed is in knots. (X=95 kilometres; Z₀=1800 metres)

unrealistic and believed erroneous as a result of the model MSL pressure gradient (and resultant wind). This shear may have contaminated the character of the drainage jet due to turbulent momentum transport, and certainly alters the model treatment of the surface layer (equations 6.16 to 6.18). We will consider the flow structure in a qualitative manner since we lack confidence in the quantitative validity of the data, and will focus our discussion on the first 240 G-C metres.

At the West ridge we can see a local windspeed maximum at 80 G-C metres, which is due to acceleration of the flow over the ridge. Downhill from the ridgetop at 1800 metres elevation (Figure 6.14), a developing drainage jet shows up at anemometer height but not the 80 G-C metre level. Model resolution does

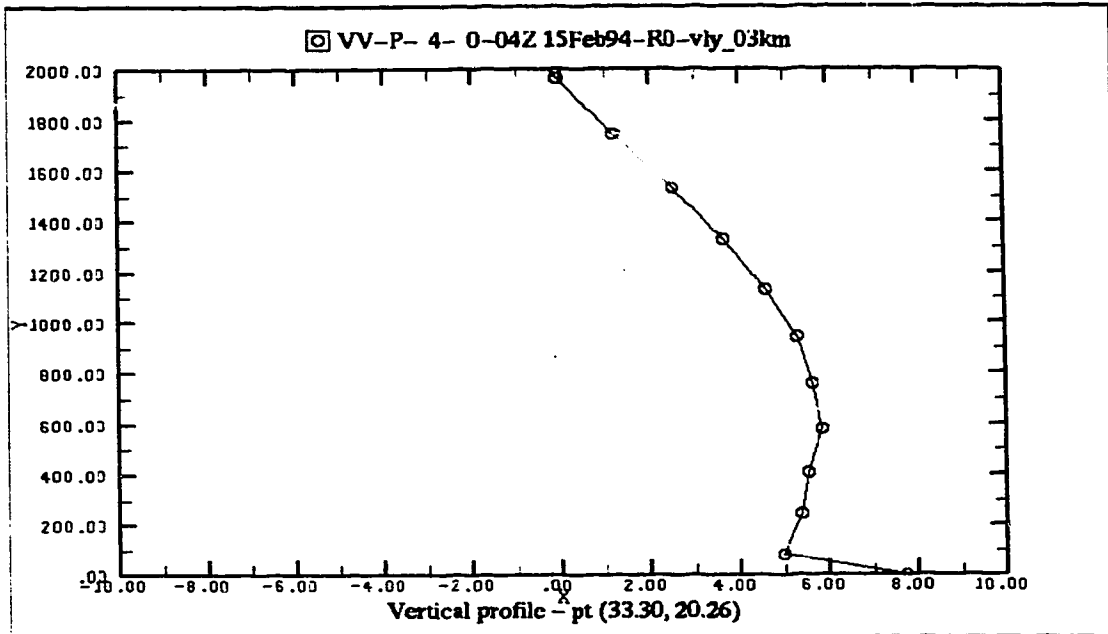


Figure (6.21) V component from southern point at valley centre from nocturnal valley simulation. Vertical co-ordinate is Gal-Chen metres (identical to geopotential metres at valley centre) and the horizontal co-ordinate is knots, positive northward. At four hours of integration.

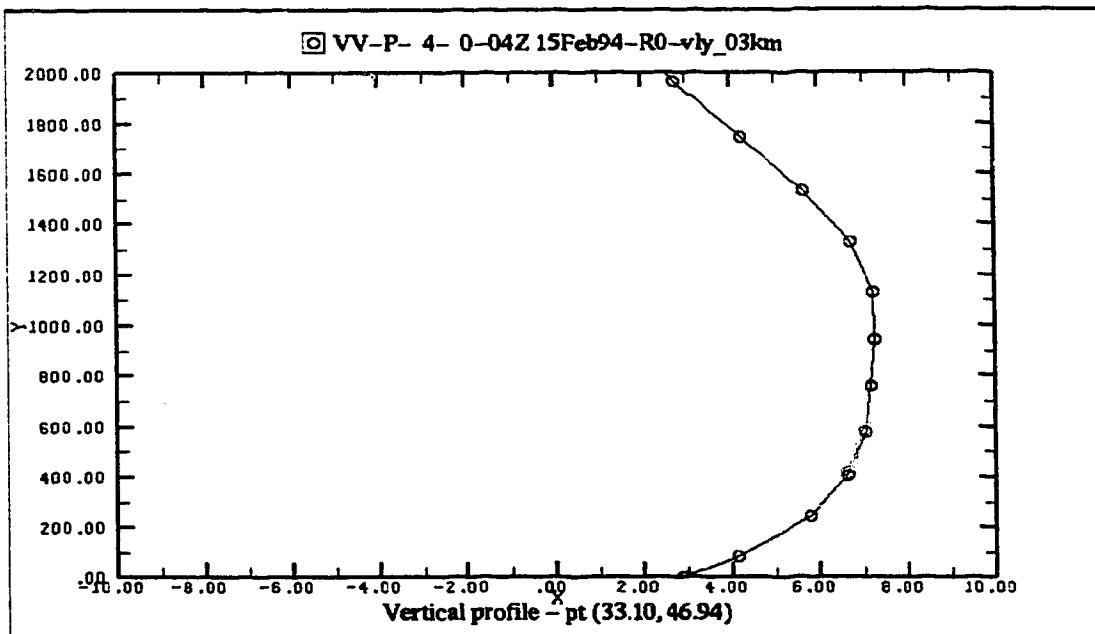


Figure (6.22) V component from northern point at valley centre from nocturnal valley simulation. Vertical co-ordinate is Gal-Chen metres (identical to geopotential metres at valley centre) and the horizontal co-ordinate is knots, positive northward. At four hours of integration.

not allow reliable inference for the exact height, although near the surface is consistent with observations (Defant 1949 and others). Further downslope, at an elevation of 1200 metres (Figure 6.16) the flow near ground is weakly upslope. An oscillation in the strength is evident between 240 and 1000 G-C metres. At the 600 metre elevation point (Figure 6.17) a downslope maximum is evident at 80 G-C metres as we enter the region of the valley with net radiational heat loss. At valley centre (Figure 6.18) the flow is near zero, consistent with a region of horizontal convergence of opposing drainage flows.

The East slope seems to have a slightly better defined drainage and we can see a weak downslope (drainage) jet at the mid-point (1200 metres) of the slope. Near the East ridge (Figure 6.20) the drainage is weaker than the West slope at that height with more variation in the flow strength above 80 G-C metres.

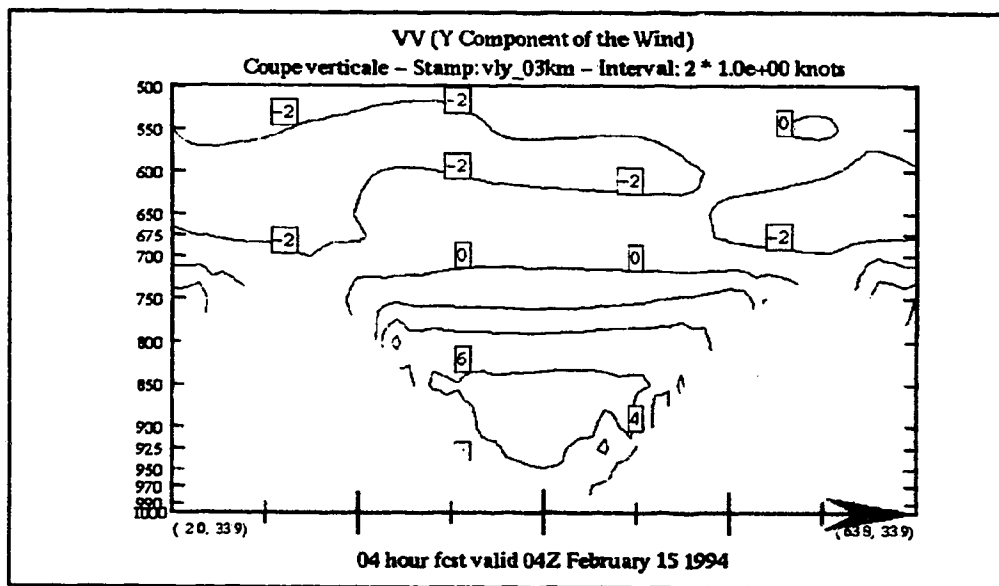


Figure (6.23) V component cross section at mid-point in valley from nocturnal valley simulation. Vertical co-ordinate is millibars and the contours are isotachs at 2 knot intervals; positive into the page. At four hours of integration.

The V component at the valley center (Figure 6.21, 6.22) reveals a deep, well developed, along valley flow (South) which increases in intensity northward (i.e. along the flow) with a maximum speed near 1200 metres in the north and nearer 600 metres in the south. The southern point also exhibits a near surface jet with the strongest flow at anemometer level. This may be a double jet structure where the low level flow dissipates toward the north and is dominated by the deep flow. The core of winds is large and somewhat elevated in comparison with other observed and modelled flows.

Observations in Brush Creek by Doran et al (1989) and Shinn et al (1989) found evidence which suggested a meandering along-valley jet during drainage flow. We examined the profiles at numerous points along and near the valley centre, but found no conclusive evidence either for or against meandering of the jet indicated in Figures (6.21, 6.22). A cross section of the valley with isotachs (Figure 6.23) demonstrates a broad core of along-valley winds, approximately centred in the valley East to West.

The strength of the along-valley flow is somewhat surprising considering this valley is level, effectively infinite, and completely uniform in the y direction. Part of the forcing for this valley flow may lie in the pressure gradient of the nesting grid which had slightly lower pressure over the north portion of the domain. The local pressure gradient (Figure 6.11) has similar (slightly lower) pressure at both ends.

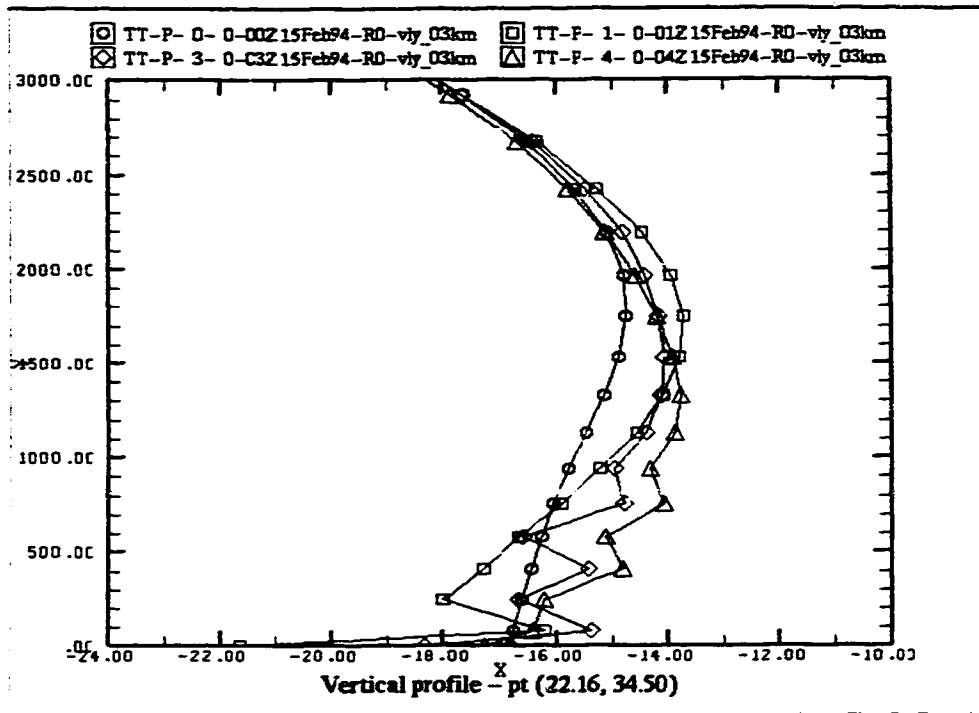


Figure (6.24) Temperature Profiles at Mid-point on West Slope. Height is in G-C metres and temperature is in °C. The circle is for t=0 minutes, the square is for t=60, the diamond is for t=180, and the triangle is for t=240.

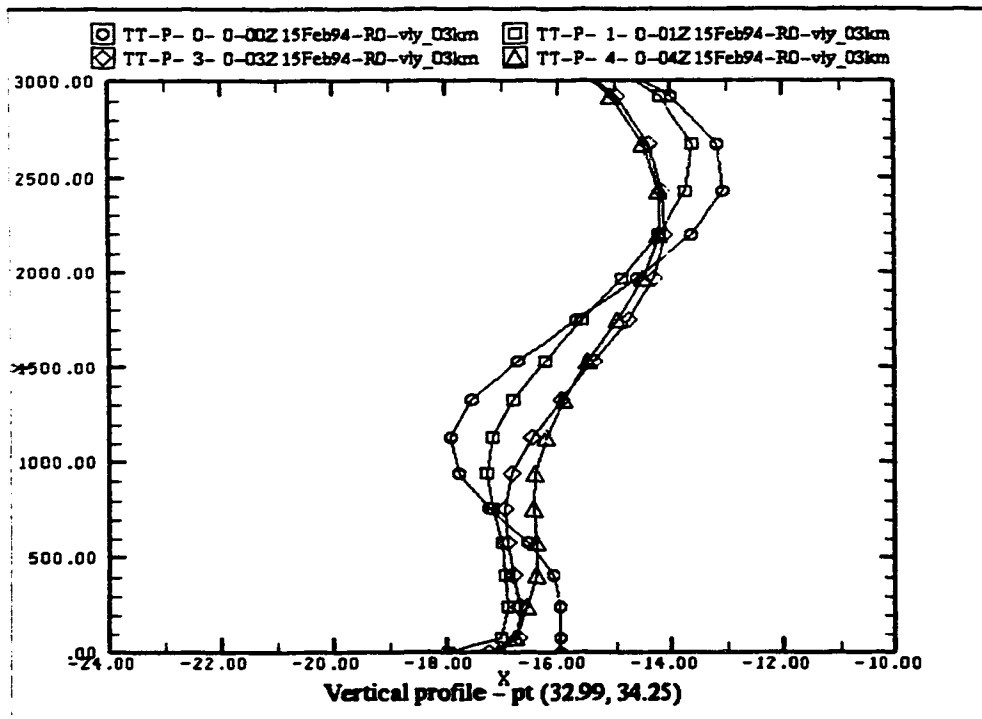


Figure (6.25) Temperature Profiles at Valley Centre. Height is in G-C metres and temperature is in °C. The circle is for t=0 minutes, the square is for t=60, the diamond is for t=180, and the triangle is for t=240.

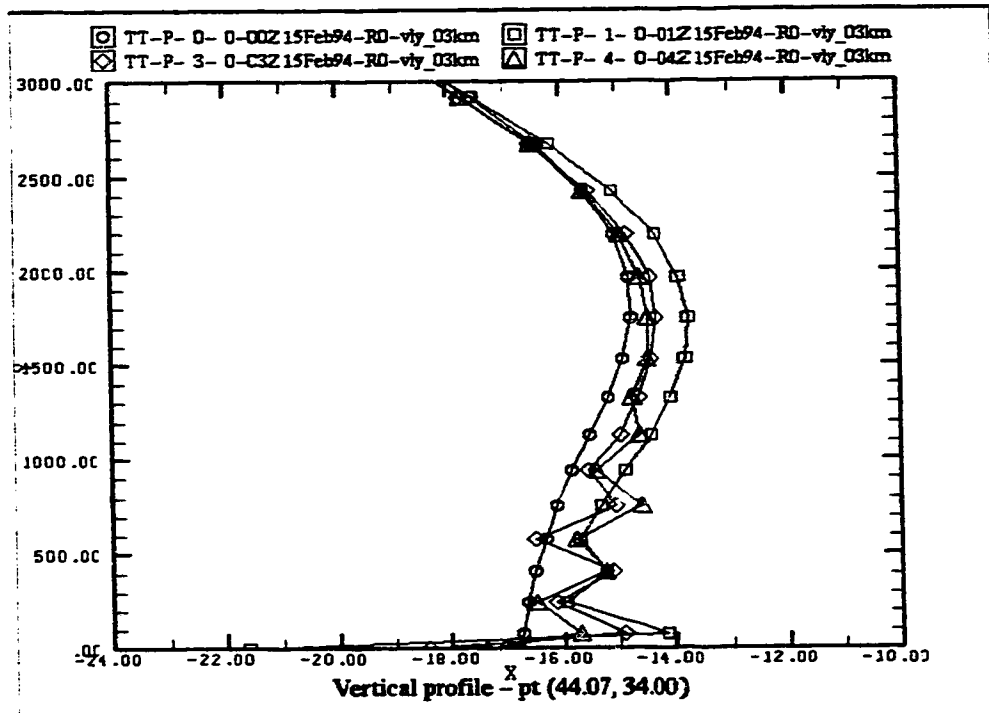


Figure (6.26) Temperature Profiles at Mid-point on East Slope. Height is in G-C metres and temperature is in °C. The circle is for t=0 minutes, the square is for t=60, the diamond is for t=180, and the triangle is for t=240.

Temperature profiles at three points across the valley (at similar points to the wind profiles) are shown in figures (6.24 to 6.26). On both slopes, the first 60 minutes exhibit marked cooling near the surface with warming aloft. The next 180 minutes of simulation increase the air temperatures near the surface and generally decrease the warming in the higher levels. At the valley center the temperature in the lowest calculation levels drops initially and then gradually warms. The levels below the inversion layer show warming through the simulation, while the inversion layer above, exhibits cooling.

The development of the temperature profiles is consistent with a sensible transfer of heat through turbulent mixing between layers and between the ground and air. The cooling at the valley bottom suggests that there is a radiational heat

loss, but the magnitude of the temperature change at mid-slope implies that for most of the valley longwave radiational heat loss is swamped by sensible transfer. This is attributed to the initialisation of the surface (ground) temperature and the difference that resulted over the higher terrain, between the air and ground temperature. The net effect on all profiles was an increase in stability during the simulation

6.4 Conclusions

The numerical experiments using MC2 to study nocturnal boundary layers over a flat plain, and a sinusoidal valley have been a mixture of frustration and reward. The consistent development by MC2 of flow features which are well documented in the literature, gives a measure of confidence that, given a more realistic initialisation and boundary-conditions, and higher resolution, MC2 would probably provide sound predictions. The fact that our simulations were accomplished using excessively simplistic, and in fact unrealistic, boundary conditions is particularly noteworthy. We conclude that to apply a comprehensive atmospheric model to simulate these idealised flows, requires a more realistic set of initial and boundary conditions. This might be accomplished by seeking out real cases which have characteristics similar to those of interest. The uncontrolled atmospheric complications, which creep into this type of simulation (e.g. movements of a far-off frontal systems or temperature advection aloft), might have less impact than initial conditions which are dynamically inconsistent.

The elegance and relative simplicity of two dimensional simulations makes them attractive and they certainly have considerable merit. However, excessive confidence in two dimensional models, for three dimension decision making, may be hazardous. Our model simulations have shown strongly three-dimensional valley flows, where there is substantial structure (flow inhomogeneity) in the third dimension.

"The wind blows where it wishes and you hear the sound of it, but do not know where it comes from and where it is going..." (John 3:8a, New American Standard Version)

7.1 Goals of the Study

Our goal, in this study, was to learn about conditions that lead to poor dispersion of wood smoke pollutants at Whitehorse. Our analysis of the character of woodsmoke pollutants gave us confidence that the primary influence was dispersion. This allowed us to narrow our focus to the investigation of small scale flow in a valley and seek some understanding of the influences on valley winds.

7.2 Original Hypothesis

Our original hypothesis was that the poorest dispersion in a valley (hence highest pollutant levels) occurred under conditions of light external flow, a dry atmosphere (i.e. no cloud and little vapour), and during nocturnal radiational cooling (which would enhance the stabilising stratification). We then focused on drainage flows, and influences that might alter or overwhelm drainage.

7.3 Summary of Nocturnal Evolution

We found that an initially adiabatic nocturnal boundary layer over a flat plain developed a strongly stable layer through radiational cooling. This stability lead to decreasing wind and turbulence and eventually suppressed further cooling.

This evolution does not hold for nocturnal valley environments and studies indicated that nocturnal cooling tended to generate flows. These flows develop as a result of slope drainage; valley-plain pressure differences; and perhaps even from intra-valley pressure gradients that arise from varying radiational geometry and

surface emissivity and/or heat capacity. This nocturnal drainage tended to reduce the stratification and maintained mixing and advection in the valley.

We have also seen that the effectiveness of the nocturnal drainage flow is strongly influenced by large scale atmospheric parameters. The distribution and quantity of water (vapour and liquid) alters the radiational balance in the valley and contributes heat through phase change processes (latent heat). External flow across a valley and large scale stratification determine the potential and effectiveness for interaction with the valley flow. Large scale pressure gradient along a valley will "swamp" drainage effects and impose externally driven flow. Even adjacent geographical features can alter the flow through physical blockage or as a heat source/sink (e.g. lakes, oceans or glaciers)

We have been able to derive a set of dimensionless parameters which, given appropriate calibration, might be able to distinguish between valley flows which are "stagnant" (i.e. isolated from the large scale flow) and those that are driven by forcing external to the valley. In a given "stagnant" valley, we should be able to quantify the strength of the drainage.

7.4 Implications of Nocturnal Evolution

When we look back to our original hypothesis, we identified conditions that will generally lead to decoupling of the valley from the large scale flow. We have found evidence that this decoupling does not necessarily imply that the valley will be stagnant, but will frequently be accompanied by the development of drainage along the slopes; along valley flow; and given appropriate geometry, a

valley-plain flow. The magnitude of drainage flows observed and modelled indicate that dispersion should be quite effective (at least within the valley) during a strong drainage flow.

If we return to the original problem, the question remains; what are the criteria for poor dispersion and consequent high pollutant levels at Whitehorse? It seems probable that "folk wisdom" that anticipates wood smoke problems under clear skies and light winds contains some truth. However if conditions lead to strong drainage flows these are likely to be sufficient to mitigate high levels of TSP (at least until the whole valley is filled with pollutants).

7.5 Directions for Further Investigation

Further investigation at Whitehorse specifically, and valleys in general, should be directed toward identification of conditions where external influences allow the valley to be decoupled from the large scale flow, but are not conducive to development of drainage flows. One possible configuration in a valley is light ambient flow, strong stratification and a layer of moisture near the ground (cloud or vapour) sufficient to impair radiative cooling. It is certainly conceivable that a layer of smoke might also be an impairment to radiational efficiency.

We specifically recommend that further investigation at Whitehorse should commence with a statistical study seeking correlations between wind (speed and direction) and temperature structure, with total suspended particulate based solely on the data from the monitoring site in Riverdale subdivision. An established

relation can then be investigated in terms of external effects such as radiation, and large scale influences such as pressure gradient, stratification and flow.

Numerical modelling of specific cases might also be illuminating, but, in time and resources, is not the most economical approach to establishing a causal relationship. The unique geometry of the valley may preclude usable statistical correlations and require numerical simulation of events and non-events (expected high TSP did not occur).

7.6 Revised Hypothesis

Our new hypothesis for further investigation is; high pollutant levels will occur under conditions that lead to decoupling of a valley from the large scale flow, but where strong drainage flows do not develop. These are most likely to occur under light external flow; strong stratification; and with some inhibition to drainage. The inhibition to drainage may be geometrical configuration of the valley; a layer of moisture to inhibit radiation or perhaps even a large scale counterbalancing pressure gradient.

7.7 Summary

Our investigation and analysis holds the promise that relatively simple relations can be established for influences on dispersion at Whitehorse in particular and valleys in general. We have laid the foundation for understanding valley flows and have identified an appropriate direction for further study.

Bibliography

- A. Lanfranco and Associates. (1985) *Emission Monitoring Survey of Woodchip Boiler Exhausts. Pelly Crossing, Yukon.* for Government of Yukon. Energy and Mines Branch. Whitehorse Yukon. 19 pp.
- Albert, Jaques. (1982) *Channeled winds in Juan de Fuca Strait: An Empirical Verificiation.* Pacific Region Technical Notes 82-014. Pacific Weather Centre, Vancouver.
- Allwine, K. J. (1982) Assessment of the Long-Range Transport of Residential Woodstove Fine Particulate Emissions for two Future United States Energy Scenarios. *Proceedings 1981 International Conference on Residential Solid Fuels. Environmental Impacts and Solutions.* Oregon Graduate Center. Beaverton
- Allwine, K. Jerry, Lamb, Brian K., and Eskridge, Robert (1992) Wintertime Dispersion in a Mountainous Basin at Roanoke, Virginia: Tracer Study. *Journal of Applied Meteorology* Volume 31 Number 11 pp1295-1311
- Allwine, K. Jerry (1993) Atmospheric Dispersion and Tracer Ventilation in a Deep Mountain Valley. *Journal of Applied Meteorology* Volume 32 Number 6. pp1017-1037
- Angle, R. P. and Sakiyama, S. K. (1991) *Plume Dispersion in Alberta* Standards and Approvals Division, Alberta Environment. Edmonton.
- Bader, David C. and Whiteman, C. David. (1989) Numerical Simulation of Cross-Valley Plume Dispersion during Morning Transition Period. *Journal of Applied Meteorology* Volume 28 Number 7. pp652-664.
- Banta, R. and Cotton, W.R (1981) An Analysis of the Structure of Local Wind Systems in a Broad Mountain Basin *Journal of Applied Meteorology* Volume 20 Number 11 pp 1255-1266
- Barnett, Stockton G., and Shea, Damien (1982) Effects of Woodstove Design and Operation on Condensable Particulate Emissions. *Proceedings 1981 International Conference on Residential Solid Fuels. Environmental Impacts and Solutions.* Oregon Graduate Center. Beaverton

- Barr, Sumner and Orgill, Montiem (1989) Influence of External Meteorology on Nocturnal Drainage Winds. *Journal of Applied Meteorology* Volume 28 Number 6. pp497-517.
- Bell, Robert C. and Thomson, Rory O. R. Y. (1980) Valley ventilation by cross winds. *Journal of Fluid Mechanics* Volume 96. pp 757-767.
- Bergeron, Guy, Laprise, Rene and Caya, Daniel (1994) *Formulation of the Mesoscale Compressible Community (MC2) model*. Cooperative Centre for Research in Mesometeorology. Dorval
- Black, Thomas L. (1987) A Comparison of Key Forecast Variables Derived from Isentropic and Sigma Coordinante Regional Models. *Monthly Weather Review* Volume 115 pp 3097-3114
- Bleck, Rainer and Benjamin, Stanley G. (1993) Regional Weather Prediction with a Model Combining Terrain-following and Isentropic Coordinates. Part I: Model Description. *Monthly Weather Review* Volume 121 pp 1770-1785.
- Bossert, James E., Sheaffer, John D. and Reiter, Elmar R. (1989) Aspects of Regional-Scale Flows in Mountainous Terrain. *Journal of Applied Meteorology* Volume 28 Number 7. pp590-601.
- Carlson, James H. (1982) Residential Wood Combution in Missoula, Montana: An Overview of its Air Pollution Contributions, Health Effects and Proposed REgulatory Solutions. *Proceedings 1981 International Conference on Residential Solid Fuels. Environmental Impacts and Solutions*. Oregon Graduate Center. Beaverton
- Carruthers, D. J. and Hunt, J. C. R. (1990) Fluid Mechanics of Airflow over Hills: Turbulence, Fluxes and Waves in the Boundary Layer. in *Atmospheric processes over Complex Terrain*. Editor: William Blumen. American Meteorological Society. Boston.
- Chartier, Yves (1992) *An intorduction to RPN standard files*. Recherche Prévision Numérique, Atmospheric Environment Service. Dorval
- Chartier, Yves (1994) *XREC (Rêver En Couleurs) User Guide*. Recherche Prévision Numérique, Atmospheric Environment Service. Dorval

- Clarke, Ken. (1974) *A Note on the Energy Balance at Whitehorse for heating and cooling under clear skies*. Unpublished technical note. Yukon Weather Centre. Whitehorse.
- Clements, William E., Archuleta, John A. and Hoard, Donald E. (1989) Mean Structure of the Nocturnal Drainage Flow in a Deep Valley. *Journal of Applied Meteorology* Volume 28 Number 6. pp457-462.
- Cooper, John A., Frazier, Clifton A. and Pritchett, Lyle C. (1984) *Characterization of Air Quality Impacts from Residential Wood Combustion in Juneau and Fairbanks, Alaska. Volume I and II*. NEA Inc Beaverton
- Coulter, R. L., Orgill, Monte and Porch, William. (1989) Tributary Fluxes into Brush Creek Valley. *Journal of Applied Meteorology* Volume 28 Number 7. pp555-568.
- DeCesar, Richard T. and Cooper, John A. (1982) The Quantitative Impact of Residential Wood Combustion and Other Vegetative Burning Sources on the Air Quality in Medford, Oregon. *Proceedings 1981 International Conference on Residential Solid Fuels. Environmental Impacts and Solutions*. Oregon Graduate Center. Beaverton
- Defant, F. (1949) A Theory of Slope Winds, Along with Remarks on the Theory of Mountain Winds and Valley Winds. in *Alpine Meteorology: Translations of Classic Contributions by A. Wagner, E. Ekhardt and F. Defant*. Edited by C. David Whiteman and Ekkehard Dreiseitl. PNL-5141/ASCOT-84-3. Pacific Northwest Laboratory, Richland Washington, 121 pp.
- Delage, Yves (1974) A Numerical Study of the Nocturnal Atmospheric Boundary Layer. *Quarterly Journal of the Royal Meteorological Society*. Volume 100 Number 425. pp351-364.
- Desgagne, Michel, Benoit, Robert and Chartier, Yves (1994) *The Mesoscale Compressible Community Model (MC2) User's Manual*. Recherche En Prévision Numérique, Atmospheric Environment Service. Dorval

- Detering, H. W. and Etling D. (1985) Application of the E - Turbulence Model to the Atmospheric Boundary Layer. *Boundary Layer Meteorology*. Volume 33 Number. pp113-133.
- di Cenzo, C. S. (1979) *A Numerical Study of Temperature in an Urban Valley Using a Radiative-Conductive Model*. unpublished M.Sc. Thesis University of Alberta 159pp.
- Dickerson, Marvin H. (1978) MASCON-A Mass Consistent Atmospheric Flux Model for Regions with Complex Terrain. *Journal of Applied Meteorology*. Volume 17 Number 3. pp241-253.
- Doran, J. C., Wesely, M. L., McMillen, R. T. and Neff, W. D. (1989) Measurements of Turbulent Heat and Momentum Fluxes in a Mountain Valley. *Journal of Applied Meteorology* Volume 28 Number 6. pp438-444.
- Doran, J.C. (1990) The Effects of Ambient Winds on Valley Drainage Winds *Boundary-Layer Meteorology* Volume 51 pp 177-189.
- Doran J.C, Horst, T. W. and Whiteman, C. D. (1990) The Development and Structure of Nocturnal Slope Winds in a Simple Valley. *Boundary-Layer Meteorology* Volume 52 Numbers 1-2 pp 41-68.
- Durrant, Dale R. (1986) Mountain Waves. *Mesoscale Meteorology and Forecasting*. American Meteorological Society. Boston
- Duykerke, P. G. (1988) Application of the E - Turbulence Closure Model to the Neutral and Stable Atmospheric Boundary Layer. *Journal of the Atmospheric Sciences*. Volume 45 Number 5. pp865-880.
- Egger, J. (1987) Valley Winds and the Diurnal Circulation over Plateaus. *Monthly Weather Review*. Volume 115 Number 10. pp 2177-2186.
- Ekhart, E. (1944) Contributions to Alpine Meteorology in *Alpine Meteorology: Translations of Classic Contributions by A. Wagner, E. Ekhart and F. Defant*. Edited by C. David Whiteman and Ekkehard Dreiseitl. PNL-5141/ASCOT-84-3. Pacific Northwest Laboratory, Richland Washington, 121 pp.

- Ekhart, E. (1948) On the Thermal Structure of the Mountain Atmosphere in *Alpine Meteorology: Translations of Classic Contributions by A. Wagner, E. Ekhart and F. Defant*. Edited by C. David Whiteman and Ekkehard Dreiseitl. PNL-5141/ASCOT-84-3. Pacific Northwest Laboratory, Richland Washington, 121 pp.
- Ellenton, G. (1985) *Atmospheric Modelling to Determine the Effect of Incremental Woodsmoke Emissions of the Air Quality in Whitehorse, Yukon*. for Government of Yukon contract No. 23906-1-3. 64 pp.
- Environment Canada (1982a) *Canadian Climate Normals 1951-1980 Temperature and Precipitation: The North - Y. T. and N. W. T.* Canadian Climate Program, Toronto. UDC:551.582(712)
- Environment Canada (1982b) *Canadian Climate Normals 1951-1980 Wind*. Canadian Climate Program, Toronto. UDC:551.582.2(71)
- Erasmus, D. Andre (1986) A Model for Objective Simulation of Boundary-Layer Winds in an area of Complex Terrain. *Journal of Climate and Applied Meteorology*. Volume 25 Number 12. pp 1832-1841.
- Erasmus, D. Andre (1986) A Comparison of Simulated and Observed Boundary-Layer Winds in an Area of Complex Terrain. *Journal of Climate and Applied Meteorology*. Volume 25 Number 12. pp 1832-1841.
- Fleagle, Robert G. (1950) A Theory of Air Drainage *Journal of Meteorology* Volume 7 pp 227-232.
- Fritschen, Leo J. and Simpson, James R. (1989) Surface Energy Radiation Balance Systems: General Description and Improvements. *Journal of Applied Meteorology* Volume 28 Number 7. pp680-689.
- Garand, L., and Mailhot, J. (1990) The influence of infrared radiation on numerical weather forecasts. Proceedings of the Seventh Conference on Atmospheric Radiation, July 23-27 1990, San Francisco, U.S.A. *American Meteorological Society*. J146-J151.
- Garrat, J. R. (1992) *The Atmospheric Boundary Layer*. Cambridge University Press. Cambridge

- Grainger, Clive and Meroney, Robert N. (1993) Dispersion in an Open-Cut Coal Mine in Stably Stratified Flow *Boundary-Layer Meteorology* Volume 63 Numbers 1-2. pp 117-140.
- Gudiksen, Paul H. (1989) Categorization of Nocturnal Drainage Flows within the Bush Creek Valley and the Variability of Sigma Theta in Complex Terrain. *Journal of Applied Meteorology* Volume 28 Number 6. pp 489-495.
- Gudiksen, Paul H. and Shearer, Donald L. (1989) The Dispersion of Atmospheric Tracers in Nocturnal Drainage Flows. *Journal of Applied Meteorology* Volume 28 Number 7. pp602-608.
- Higgs, Robert. (1990) *A Statistical Approach to Channelled Winds at CFB Comox*. Canadian Forces Weather Service Technical Note 1-90. Ottawa.
- Holton, James R. (1979) *An Introduction to Dynamic Meteorology* Academic Press. New York.
- Hooke, William H. (1986) Gravity Waves. *Mesoscale Meteorology and Forecasting*. American Meteorological Society. Boston
- Hunt, Julian C.R., Snyder, William H., and Lawson, Robert E. Jr (1978) *Flow Structure and Turbulent Diffusion around a Three-Dimensional Hill. Part I: Flow Structure* Environmental Sciences Research Laboratory, Office of Research and Development. United States Environmental Protection Agency. Research Triangle Park.
- Hunt, J.C.R. and Snyder, W.H. Experiments on stably and neutrally stratified flow over a model three-dimensional hill. *Journal of Fluid Mechanics* Volume 96 pp 671-704.
- Jackson, P.S. and Hunt, J. C. R. (1975) Turbulent wind flow over a low hill. *Quarterly Journal of the Royal Meteorological Society*. Volume 101. pp929-955.
- Jacobs, Philip and Bunch, Snowden. (1982) Health Costs of Residential Wood Combustion. *Proceedings 1981 International Conference on Residential Solid Fuels. Environmental Impacts and Solutions*. Oregon Graduate Center. Beaverton.

- Jaffe, S. (1958) Effect of prevailing wind on the valley wind regime at anemometer level, preliminary report on valley wind studies in Vermont.
AFCRC-TR-58-29, Air Force Cambridge Research Laboratory, 32 pp.
- Kao, S. K. (1982) An Analytical Solution for Three-Dimensional Flows in the Atmospheric Boundary Layer over Terrain. *Journal of Applied Meteorology* Volume 20 Number 4 pp 386-390
- Kau, W. S., Lee, H. N. and Kao, S. K. (1982) A Statistical Model for Wind Prediction at a Mountain and Valley Station Near Anderson Creek California. *Journal of Applied Meteorology*. Volume 21 Number 1. pp18-21.
- Kowalczyk, John F., Bosserman, Peter B., and Tombleson, Barbara (1982) Particulate Emissions from New Low Emission Wood Stove Designs Measured by EPA Method V. *Proceedings 1981 International Conference on Residential Solid Fuels. Environmental Impacts and Solutions*. Oregon Graduate Center. Beaverton.
- Lange, Rolf. (1989) Transferability of a Three-Dimensional Air Quality Model between Two Different Sites in Complex Terrain. *Journal of Applied Meteorology* Volume 28 Number 7. pp665-679
- Lee, J. T. and Barr, Sumner. (1981) *Wind Tunnel Studies of Flow Channeling in Valleys*. in Proceedings of Second Conference on Mountain Meteorology. American Meteorological Society. Boston.
- Lee, J. T., Lawson, R. E. Jr., and Marsh, G. L. (1987) Flow Visualization Experiments on Stably Stratified Flow over Ridges and Valleys. *Meteorology and Atmospheric Physics* Volume 37. pp183-194.
- Leone, John M. and Lee, Robert L. (1989) Numerical Simulation of Drainage Flow in Brush Creek, Colorado. *Journal of Applied Meteorology* Volume 28 Number 6. pp530-542.
- Mailhot, Jocelyn (1994) *The Regional Finite-Element (RFE) Model Scientific Description - Part 2: Physics*. Recherche En Prévision Numérique, Atmospheric Environment Service. Dorval

- McCandless, R. (1984) *Impact of Residential Wood Combustion on Measured Particulate and PAH Concentrations in Whitehorse Yukon*. presented at 77th Annual Meeting of the Air Pollution Control Association. 15pp.
- McKee, Thomas B. and O'Neal, Robert D. (1989) The Role of Valley Geometry and Energy Budget in the Formation of Nocturnal Valley Winds. *Journal of Applied Meteorology* Volume 28 Number 6. pp445-456.
- McNider, Richard T. and Pielke, Roger A. (1984) Numerical Simulation of Slope and Mountain Flows. *Journal of Climate and Applied Meteorology* Volume 23 Number 10 pp 1441-1453.
- Mickle, R. E., Salmon, J. R. and Taylor, P. A. (1984) *Kettles Hill '84: Velocity Profile Measurements over a Low Hill*. Atmospheric Environment Service Report. AQRB-84-012-L.
- Moore, Gary E., Daly, Christopher and Liu, Mei-Kao (1987) Modelling of Mountain-Valley Wind Fields in the Southern San Joaquin Valley, California. *Journal of Climate and Applied Meteorology*. Volume 25 Number 9. pp1230-1242.
- Morris, Gregory (1982) Health Effects of Residential Wood Combustion; The Implications of Environmental Stochasticity. *Proceedings 1981 International Conference on Residential Solid Fuels. Environmental Impacts and Solutions*. Oregon Graduate Center. Beaverton.
- Muhlbaier, Jean L (1982) A Characterization of Emissions for Wood-Burning Fireplaces. *Proceedings 1981 International Conference on Residential Solid Fuels. Environmental Impacts and Solutions*. Oregon Graduate Center. Beaverton.
- Nappo, Carmen J., Rao, K. Shankar and Herwehe, Jerold A. (1989) Pollutant Transport and Diffusion in Katabatic Flows. *Journal of Applied Meteorology* Volume 28 Number 7. pp617-625.
- NEA Inc. (1984) *Characterization of Air Quality Impacts from Residential Wood Combustion in Juneau and Fairbanks, Alaska. Vol I and II* for

- State of Alaska, Department of Environmental Conservation. 53 pp and 43 pp.
- Neff, W. D. and King, C. W. (1989) The Accumulation and Pooling of Drainage Flows in a Large Basin. *Journal of Applied Meteorology* Volume 28 Number 6. pp518-529.
- Overland, James E. and Walter, Bernard A. Jr. (1981) Gap Winds in the Strait of Juan de Fuca. *Monthly Weather Review*. Volume 109 Number 10. pp2221-2233.
- Orgill, Montie M. (1989) Early Morning Ventilation of a Gaseous Tracer from a Mountain Valley. *Journal of Applied Meteorology* Volume 28 Number 7. pp636-651.
- Patnakar, Suhas V. (1980) *Numerical Heat Transfer and Fluid Flow*. Hemisphere Publishing Corporation. Washington.
- Patankar, Suhas V. (1981) A Calculation Procedure for Two-dimensional Elliptic Situations. *Numerical Heat Transfer*. Volume 4. pp408-425.
- Pielke, R. A. (1985) The Use of Mesoscale Numerical Models to Assess Wind Distribution and Boundary-Layer Structure in Complex Terrain. *Boundary Layer Meteorology*. Volume 31. pp217-231.
- Pierrehumbert, R.T. and Wyman, B. (1985) Upstream Effects of Mesoscale Mountains *Journal of the Atmospheric Sciences* Volume 42 Number 10 pp 977-1003.
- Porch, William M., Fritz, Richard B., Coulter, Richard L and Gudiksen, Paul H. (1989) Tributary, Valley and Sidewall Air Flow Interactions in a Deep Valley. *Journal of Applied Meteorology* Volume 28 Number 7. pp578-589.
- Post, M. J. and Neff, W. D (1986) Doppler Lidar Measurements of Winds in a Narrow Mountain Valley. *Bulletin of the American Meteorological Society* Volume 67 Number 3 pp 275-281

- Purves, M. A. (1979) *The Relationship between Surface and Geostrophic Winds at Baden-Sollengen, West Germany*. Technical Memorandum 868. Environment Canada.
- Rajaratnam, N. (1987) *Engineering Fluid Mechanics* Department of Civil Engineering, University of Alberta Edmonton. Unpublished Course Notes.
- Rogers, R. R. (1979) *A Short Course in Cloud Physics* Pergamon Press, Toronto.
- Schlichting, Herman (1970) *Boundary-Layer Theory* Seventh Edition. Mcgraw-Hill Inc. New York. 817 pp.
- SENES Consultants Limited (1983) *Pollution from Woodstoves in Riverdale, Yukon Territory* for Environment Canada Contract No. KE145-3-0331
- Sherman Christine A. (1978) A Mass-Consistent Model for Wind Fields over Complex Terrain. *Journal of Applied Meteorology*. Volume 17 Number 3. pp312-319.
- Shinn, J. H., Cederwall, R. T., Gouveia, F. J. and Chapman, K. R. (1989) Micrometeorology of Slope Flows in a Tributary Canyon during the 1984 ASCOT Experiment. *Journal of Applied Meteorology* Volume 28 Number 7. pp569-577
- Simons, Carl A., Christiansen, Paul D., Pritchett, Lyle C., and Beyerman, Glenn A. (1987) *Whitehorse Efficient Woodheat Demonstration* OMNI Environmental Services Inc. Beaverton. 112 pp.
- Stovel, Leslie D. (1983) *A Two-dimensional Numerical Model of Airflow within a small Urban Valley*. Unpublished M.Sc thesis University of Alberta 163pp.
- Stuart, R. Ambury (1983) *The Impact of Residential Wood Burning on Urban Air Quality in Canada*. for Renewable Energy Division of Energy, Mines and Resources. 94 pp.
- Tanguay, Monique, Robert, Andre and Laprise, Rene (1990) A Semi-Implicit Semi-Lagrangian Fully Compressible Regional Forecast Model. *Monthly Weather Review* Volume 118 Number 10 pp 1970-1980.

- Taylor, P. A. (1977) Some Numerical Studies of Surface Boundary-Layer Flows Above Gentle Topography. *Boundary-Layer Meteorology* Volume 11 Number 4 pp 439-466.
- Taylor, P. A. and Teunissen, H. W. (1987) The Askervein Hill Project: Overview and Background Data. *Boundary-Layer Meteorology*. Volume 39 Number 1/2. pp15-40.
- Tyson, P. D. and Preston-Whyte, R. A. (1972) Observations of Regional Topographically-Induced Wind Systems in Natal. *Journal of Applied Meteorology* Volume 11 Number 4 pp 643-650.
- Wagner, A. (1938) Theory and Observation of Periodic Mountain Winds. in *Alpine Meteorology: Translations of Classic Contributions by A. Wagner, E. Ekhart and F. Defant*. Edited by C. David Whiteman and Ekkehard Dreiseitl. PNL-5141/ASCOT-84-3. Pacific Northwest Laboratory, Richland Washington, 121 pp.
- Wahl, H. E., Fraser, D. B., Harvey, R.C. and Maxwell, J.B. (1987) *Climate of Yukon*. Canadian Government Publishing Centre, Ottawa.
- Weisman, Morris L. and Klemp, Joseph B. (1986) Characteristics of Isolated Convective Storms. *Mesoscale Meteorology and Forecasting*. American Meteorological Society. Boston
- Wetzel, Peter J. (1982) Toward Parameterization of the Stable Boundary Layer *Journal of Applied Meteorology* Volume 21 Number 1 pp 7-13.
- Whiteman, C. David and Barr, Sumner (1986) Atmospheric Mass Transport by Along-Valley Wind Systems in a Deep Colorado Valley *Journal of Climate and Applied Meteorology* Volume 25 Number 9 pp1205-1212.
- Whiteman, C. David (1989) Morning Transition Tracer Experiments in a Deep Narrow Valley. *Journal of Applied Meteorology* Volume 28 Number 7. pp626-635.
- Whiteman, C. David (1990) Observations of thermally developed wind systems in mountainous terrain. *Atmospheric Processes over Complex Terrain*,

- Meteorological Monographs*. Number 45. American Meteorological Society. Boston pp 5-42.
- Whiteman, C. David and Doran J. Christopher (1993) The Relationship between Overlying Synoptic-Scale Flows and Winds within a Valley. *Journal of Applied Meteorology* Volume 32 Number 11 pp 1669-1682
- Wong, Raymond (1985) *A Valley Drainage Wind and Dispersion Model*. unpublished PhD dissertation University of Alberta pp.237.
- Yamada, T. (1983) Simulations of Nocturnal Drainage Flows by a q^2 Turbulence Closure Model. *Journal of the Atmospheric Sciences* Volume 40 Number 1 pp 91-106.
- Yamada, T. and Bunker, S. (1989) A Numerical Study of Nocturnal Drainage Flows with Strong Wind and Temperature Gradients. *Journal of Applied Meteorology*. Volume 28 Number 7. pp545-551.
- Ye, Z.J., Garratt, J.R., Segal, M., and Pielke, R.A. (1990) On the Impact of Atmospheric Thermal Stability on the Characteristics of Nocturnal Downslope Flows. *Boundary Layer Meteorology* Volume 51 pp77-97.